The cyanobacterial circadian clock

Four different phosphorylated forms of KaiC assure
the performance of the core oscillator

D I S S E R T A T I O N

zur Erlangung des akademischen Grades

Dr. Rer. Nat.
im Fach Biologie

eingereicht an der
Mathematisch-Naturwissenschaftlichen Fakultät I
Humboldt-Universität zu Berlin

von
Dipl.-Phys. Christian Brettschneider

Präsident der Humboldt-Universität zu Berlin:
Prof. Dr. Jan-Hendrik Olbertz

Dekan der Mathematisch-Naturwissenschaftlichen Fakultät I:
Prof. Dr. Andreas Herrmann

Gutachter:
1. Prof. Dr. Markus Kollmann
2. Prof. Dr. Hanspeter Herzel
3. Prof. Dr. Mark Byrne

eingereicht am: 24. 3. 2011
Tag der mündlichen Prüfung: 8. 8. 2011

Abstract

Biological activities in cyanobacteria are coordinated by an internal clock. The rhythm of the cyanobacterium *Synechococcus elongatus* PCC 7942 originates from the *kai* gene cluster and its corresponding proteins. In a test tube, the proteins KaiA, KaiB and KaiC form complexes of various stoichiometry and the average phosphorylation level of KaiC exhibits robust circadian oscillations in the presence of ATP. The characteristic cycle of individual KaiC proteins is determined by phosphorylation of serine 431 and threonine 432. Differently phosphorylated KaiC synchronize due to an interaction with KaiA and KaiB. However, the details of this interaction are unknown. Here, I quantitatively investigate the experimentally observed characteristic phosphorylation cycle of the KaiABC clockwork using mathematical modeling. I thereby predict the binding properties of KaiA to both KaiC and KaiBC complexes by analyzing the two most important experimental constraints for the model. In order to reproduce the KaiB-induced dephosphorylation of KaiC a highly non-linear feedback loop has been identified. This feedback originates from KaiBC complexes, which are exclusively phosphorylated at the serine residue. The observed robustness of the KaiC phosphorylation level to concerted changes of the total protein concentrations demands an inclusion of two KaiC binding sites to KaiA in the mathematical model. Besides the formation of KaiAC complexes enhancing the autophosphorylation activity of KaiC, the model accounts for a KaiC binding site, which constantly sequestrates a large fraction of free KaiA. These theoretical predictions have been confirmed by the novel method of native mass spectrometry,

which was applied in collaboration with the Heck laboratory.

The mathematical model elucidates the mechanism by which the circadian clock satisfies three defining principles. First, the highly non-linear feedback loop assures a rapid and punctual switch to dephosphorylation which is essential for a precise period of approximately 24 h (free-running rhythm). Second, the dissociation of the protein complexes increases with increasing temperatures. These perturbations induce opposing phase shifts, which exactly compensate during one period (temperature compensation). Third, a shifted external rhythm of low and high temperature affects only a part of the three compensating phase perturbations, which leads to phase shifts (phase entrainment).

An *in silico* evolution analysis shows that the existing second phosphorylatable residue of KaiC is not necessary for the existence of sustained oscillations but provides an evolutionary benefit. The analysis demonstrates that the distribution of four phosphorylated states of KaiC is optimized in order for the organism to uniquely distinguish between dusk and dawn. Consequently, this thesis emphasizes the importance of the four phosphorylated states of KaiC, which assure the outstanding performance of the core oscillator.

Zusammenfassung

Cyanobakterien zählen zu den ältesten Lebewesen auf der Erde. Diese Bakterien, auch Blaualgen genannt, trugen wesentlich zur Sauerstoffanreicherung der Erde bei, da sie eine ausgeprägte Fähigkeit zur Photosynthese besitzen. Der produzierte Sauerstoff der Photosynthese hemmt jedoch eine weitere Aktivität von Cyanobakterien, die Stickstofffixierung. Um die Hemmung zu vermeiden, werden diese Aktivitäten zeitlich getrennt und optimal dem täglichen Hell-Dunkel-Rhythmus angepasst. Ein evolutionärer Vorteil wird erzielt, wenn der Organismus diesen Rhythmus antizipiert und sich darauf vorbereitet. Aus diesem Grund haben Cyanobakterien eine innere Uhr entwickelt, deren Rhythmus zirkadian ist, „zirka diem“ bedeutet „ungefähr ein Tag“.

Cyanobakterien der Spezies *Synechococcus elongatus* PCC 7942 haben sich als Modellorganismus etabliert, weil in ihnen die ersten bakteriellen zirkadianen Oszillationen auf molekularer Ebene entdeckt worden sind. Ihre zirkadiane Uhr entspringt dreier, auf der DNS beieinanderliegenden, Gene (*kaiA, kaiB, kaiC*) und ihrer dazugehörigen Proteine. Phosphorylierte KaiC-Proteine üben eine Rückkopplung auf die Transkription von *kaiB* und *kaiC* aus, wodurch die Aktivität des *kaiBC*-Promotors zirkadian oszilliert. Eines der wichtigsten Experimente der letzten Jahre hat gezeigt, dass dieser Transkriptions-Translations-Oszillator mit einem weiteren Oszillator gekoppelt ist, der nicht von Transkription und Translation abhängt. Das Experiment des Kondo Labors rekonstruiert zirkadiane Oszillationen mit nur drei Proteinen KaiA, KaiB, KaiC und ATP. Die Proteine bilden Komplexe verschiede-

ner Stoichiometrie, die durchschnittliche Phosphorylierung des Proteins KaiC zeigt stabile Oszillationen mit einer zirkadianen Periode. Da ein Entfernen von einem der Proteine zum Verlust der Oszillationen führt, wird dieser Post-Translations-Oszillator auch als Kernoszillator bezeichnet.

Der Phosphorylierungszyklus von KaiC wird bestimmt durch fortlaufende Phosphorylierung und Dephosphorylierung an zwei Positionen des Proteins, den Aminosäuren Serin 431 und Threonin 432. Die Phase des Kernoszillators kann an der Verteilung der vier Phosphorylierungszustände (nicht-, serin-, threonin- und doppeltphosphoryliert) abgelesen werden. KaiC wechselwirkt mit KaiA und KaiB, damit verschieden phosphorylierte KaiC synchronisieren und die Uhr über mehrere Tage konstante Oszillationen zeigt. Die Details dieser Wechselwirkung sind jedoch unbekannt. In dieser Dissertation erstelle ich ein mathematisches Modell des Kernoszillators und simuliere die vorliegenden Experimente des O'Shea Labors. Die Simulation reproduziert den KaiC Phosphorylierungszyklus der Uhr quantitativ. Um die wichtigsten experimentellen Nebenbedingungen zu erfüllen, muss das theoretische Modell zwei molekulare Eigenschaften von KaiC berücksichtigen, wodurch ich wichtige Vorhersagen treffe.

Die erste Nebenbedingung ist durch die Robustheit des Systems gegeben. Die KaiC-Phosphorylierung ändert sich nicht, wenn die Gesamtkonzentrationen der drei Proteine in gleicher Weise variiert werden. Um diese Bedingung zu erfüllen, muss das Modell zwei verschiedenartige Komplexe von KaiA und KaiC berücksichtigen. Zusätzlich zu einem KaiAC Komplex, der die Autophosphorylierung von KaiC unterstützt, muss KaiC den größten Teil von KaiA unabhängig vom Phosphorylierungszu-

stand sequestrieren. Diese zweite Bindestelle ist meine erste theoretische Vorhersage. Die zweite Nebenbedingung ist durch das Übergangsverhalten nach Hinzugabe von KaiB gegeben. KaiB induziert eine Dephosphorylierung von KaiC, die abhängig vom Phosphorylierungsniveau ist. Ein Umschalten zwischen phosphoylierendem und dephosphorylierendem KaiC ist deshalb nur in bestimmten Zeitfenstern möglich. Um die gemessenen Zeitfenster in der Simulation zu reproduzieren, postuliere ich im Modell, dass sechsfach Serin phosphorylierte KaiBC Komplexe KaiA inaktivieren. Diese hochgradig nichtlineare Rückkopplung ist meine zweite theoretische Vorhersage.

Die beiden Vorhersagen werden anschließend experimentell überprüft. Hierfür werden aufgereinigte Kai-Proteine mit ATP gemischt. Proben an ausgewählten Zeitpunkten werden mit der nativen Massenspektrometrie untersucht. Diese ist eine neuartige Methode, die es erlaubt, intakte Proteinkomplexe zu untersuchen. Die Spektren bestätigen sowohl die zweite KaiAC-Bindestelle als auch die nichtlineare Rückkopplung.

Das mathematische Modell erlaubt es außerdem, die drei definierenden Prinzipien von zirkadianen Uhren für den Kernoszillator zu erklären. Erstens sichern konstante Phosphorylierungs- und Dephosphorylierungsraten von KaiC und ein pünktliches Umschalten zwischen beiden Phasen den Freilauf des Oszillators. Dieser Freilauf bewirkt, dass die zirkadiane Uhr auch unter konstanten Bedingungen, vor allem gleichbleibenden Lichtverhältnissen, weiterlaufen kann. Zweitens muss die Periodendauer des Oszillators zu unterschiedlichen äußeren Bedingungen erhalten bleiben (Temperaturkompensation). Diese Bedingung wird realisiert, indem temperaturabhängige Dissoziationskonstanten

von KaiAC und KaiBC Komplexen Phasenverschiebungen erzeugen, die sich gegenseitig kompensieren. Drittens muss die Phase des Oszillators sich dem Tagesrhythmus anpassen können. Diese Anpassung folgt aus einem äußeren Warm-Kalt-Rhythmus, der die drei temperaturabhängigen Phasenverschiebungen nur zum Teil einschaltet und damit die Kompensation verhindert.

Eine *in silico* Evolutionsanalyse zeigt, dass eine zweite phosphorylierbare Aminosäure einen evolutionären Vorteil bringt und die Verteilung der Phosphorylierungszustände optimiert ist, um eindeutig die Zeit zu bestimmen. Das Ergebnis weist darauf hin, dass diese Verteilung die physiologisch wichtige Ausgangsgröße der Uhr ist und die vier Phosphorylierungszustände die Funktionen der zirkadianen Uhr von Cyanobakterien sichern.

Contents

1 Introduction

All mammals possess a biological clock with a period adapted to earth rotation. The existence of this rhythm is apparent if we artificially illuminate or darken our environment. Even when the external conditions of light and temperature do not correspond to the day and night rhythm, we fall asleep in a daily rhythm. Such regular activities of humans, which have been studied in bunker experiments (Aschoff and Pohl, 1978), are coordinated by an internal clock. The clock approximates the external rhythm of sunlight and thereby allows the body to anticipate daily activities, such as the sleep-wake cycle and metabolism. For this reason, our organism is able to prepare the day by increasing the blood pressure and the body temperature before waking up. As such preparations provide an evolutionary advantage, humans and other higher organisms have developed an internal clock. Clocks allow plants to spread their leaves before they get light and photosynthesis can start. They allow predator animals to anticipate food availability and to prepare for the time of hunt (Albrecht, 2003).

As cyanobacteria are simple unicellular organisms, scientists believed for a long time that they did not possess an internal clock but simply react to different external conditions such as light and temperature. The research group of Prof. Huang, however, observed that cyanobacteria exhibit circadian

rhythms of nitrogen fixation (Grobbelaar et al., 1986). Their observation has motivated many scientists to further study circadian clocks in cyanobacteria. Cyanobacteria have become a model organism for analyzing the molecular components of biological clocks inside the cell because a complex interaction with multiple oscillators can be excluded in a unicellular organism. Moreover, cyanobacteria help us studying the evolution of circadian clocks, as they are one of the oldest organisms on earth known to possess an internal clock. In the following years, Takao Kondo and his collaborators Carl Johnson and Susan Golden have focused on the species *Synechococcus elongatus* PCC 7942 in order to analyze the clock of cyanobacteria on a molecular level because it is genetically tractable (Kondo et al., 1993). They have integrated bacterial luciferase into the genome of *S. elongatus* in order to visualize promoter activities. Using this methodology, the Kondo lab has shown that the gene expression is coordinated in a daily rhythm. A mutation analysis further demonstrates that this rhythm originates from the complex interaction between the *kai* gene cluster of the DNA and the corresponding Kai proteins (Ishiura et al., 1998).

Like a wrist watch, the internal clock must fulfill three defining features -- that are all properties which define a biological clock. The first defining feature of the clock is a free-running period of approximately 24 h under constant environmental conditions. We therefore speak of circadian clocks, "circa diem" means "approximately a day". As internal clocks coordinate daily repeating environmental patterns within the organism, a perfectly stable circadian oscillator, which naturally averages over short-term fluctuations, makes important contributions to its fitness. Second, the period must remain stable across the physiological temperature range despite the high sensitivity

of biochemical reaction rates to changes in temperature. This defining feature of the biological oscillator is known as temperature compensation. However, a deficiency arises as the phase of any biochemical oscillator cannot be perfectly robust against intracellular perturbations. Moreover, organisms might move into zones with shifted rhythms of light and temperature. Therefore, the third defining feature of circadian oscillators is the ability to reset its phase and to entrain to a rhythmic external zeitgeber, e.g. light or temperature.

In one of the most important recent experiments, the Kondo laboratory determined a simple core oscillator (Nakajima et al., 2005). Although this oscillator is deprived of its cellular environment, it still conforms to the three defining features. In a test tube, the proteins KaiA, KaiB and KaiC form complexes of various stoichiometry and the average phosphorylation level of KaiC exhibits robust circadian oscillations in the presence of ATP. The phase of the oscillator is displayed by four phosphorylated states, which originate from two phosphorylatable amino acids of KaiC, serine 431 and threonine 432 (Nishiwaki et al., 2007). Moreover, KaiC proteins form hexamers throughout the circadian cycle (Mori et al., 2002). In order to achieve constant oscillations of the average KaiC phosphorylation level, differently phosphorylated KaiC synchronize. Both inactivation of KaiA (Rust et al., 2007) and monomer exchange of KaiC hexamers (Kageyama et al., 2006) have been suggested to induce synchronization. Although these two experimental properties have been investigated extensively, the details of the synchronization mechanism are still unknown. Consequently, we lack a deeper understanding of the three defining features.

In this thesis, I investigate the synchronization mechanism of KaiC phos-

phorylation. The starting point is the following hypothesis: The dissociation constants of the KaiABC complexes crucially depend on the phosphorylated state of KaiC hexamers. This novel hypothesis allows to quantitatively reproduce the experimentally observed characteristic phosphorylation cycle of the KaiABC core oscillator using mathematical modeling. The model is based on the distribution of phosphorylated forms of KaiC monomers, the phosphoform distribution. The theoretical predictions of the modeling approach are analyzed by native mass spectrometry, which is applied in collaboration with the Heck laboratory. This is a novel methodology, which has only recently been developed (Heck, 2008). I employ these theoretical and experimental results to describe the mechanism of the three defining features.

Although the phosphoform distribution characterizes best the phase of the KaiABC clock, it is unknown whether it represents the physiologically relevant output. I therefore follow the hypothesis that two phosphorylation sites of KaiC provide an evolutionary advantage in comparison to a single phosphorylated KaiC and that the phosphoform distribution is optimized for clearly indicating the circadian time. This hypothesis is analyzed by an *in silico* evolutionary approach.

The questions adressed in this thesis and the methodologies have been discussed and established in collaboration with my mentor Markus Kollmann. The experimental results have been generated together with Stefanie Hertel (Lab of Ilka Axmann, Humboldt Universität zu Berlin) and Rebecca Rose (Lab of Albert Heck, Utrecht University). The results of chapter 3 and 4 have been published in Molecular Systems Biology (Brettschneider et al., 2010).

1.1 Background

The ability of organisms to adapt to rapidly changing environments is a fundamental property of life. Living systems can respond to stress conditions, such as temperature changes and starvation, in a highly effective manner. Such environmental changes occur randomly and organisms cannot prepare for them in advance. In contrast, daily and annual rhythms are determined by the planetary movement of the earth, see Figure 1.1, and are thus predictable. The rotation of the earth generates rhythms of light and temperature, which can be anticipated. Many organisms therefore have developed an internal clock by which they can approximate the twenty-four hour day and night cycle in the absence of external stimuli. Consequently, the internal clock coordinates the daily activities. Moreover, there is evidence that even annual rhythms of organisms such as hibernation are coordinated by internal clocks (Gwinner, 1977; Gwinner and Dittami, 1990).

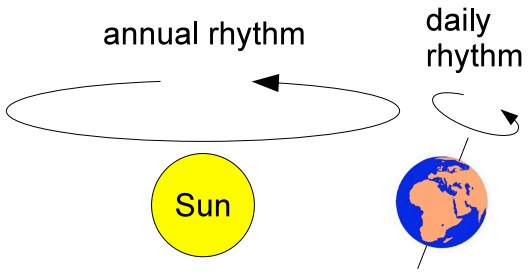

Figure 1.1: The movement and the rotation of the earth generate continuous rhythms of sun light intensity which can be anticipated.

The concept of an internal rhythm has been described first in 1729 by

the French astronomer Jean Jacques d'Ortous de Mairan. He observed a heliotrope plant in constant darkness continuously opening and closing its leaves. His work marks the beginning of chronobiology, which describes the interaction between the circadian clock and the physiology of an organism. The Swiss botanist Augustin-Pyrame de Candolle first investigated the principle of phase entrainment in the mid 1830's. Instead of observing the movement of plant leaves in darkness, he analyzed its rhythm in artificial light. He thereby made two important observations. Although plants display a circadian period in sunlight, they have a reduced period of approximately 22.5 h under constant illumination. Moreover, if the plant is exposed to a shifted rhythm of light, it adapts to the new external rhythm after a transient period. Thus, he successfully identified two defining characteristics of a circadian clock. It must have a free-running rhythm of approximately 24 h and it must be capable of resetting its phase in response to an environmental input. The third defining feature of circadian clocks is the ability for temperature compensation. This has been observed later in populations of bees (Wahl, 1931), fiddler crabs (Brown and Webb, 1948) and drosophila (Pittendrigh, 1954). The period of the internal oscillator thereby remains constant. The amplitude, however, may vary a little.

A jet lag illustrates the free-running rhythm and the ability for entrainment of human circadian clocks. When we humans are exposed to a phase shifted night- and day cycle, our free-running rhythm does not adapt to the external rhythm immediately. After a few days, our rhythm eventually is entrained by the shifted external phase. The circadian clock of humans has been systematically studied in bunker experiments by Jürgen Aschoff (Aschoff et al., 1967; Aschoff, 1969; Aschoff and Wever, 1976). In the

absence of any external zeitgebers, the volunteers, living inside the bunker for several weeks, displayed various free-running rhythms. It has been shown that humans have a slightly longer period ($\sim 25h$) on average. The experiments further revealed that without external stimuli the sleep-wake rhythms dissociated from temperature cycles. Aschoff concluded that humans possess a weakly connected multioscillatory system, which is composed of virtually as many clocks as there are cells. The question arises how light can achieve phase coherence in cells of opaque organisms. The coherence originates from the hierachical architecture of the mammalian timing system. The photic information from the retina synchronizes the neurons of the suprachiasmatic nucleus (SCN), the central pacemaker. The SCN cells then transmit its rhythmic information to cells in different brain regions and peripheral organs (Albrecht, 2003). A minor part of mammalian cells is additionally entrained by different zeitgebers, such as temperature. There is an interesting discussion about how much regular rhythms of food uptake and metabolism, which are coordinated by the clock, may in turn entrain the mammalian clock (Tu and McKnight, 2006).

In order to understand the different intracellular mechanisms of circadian clocks, researchers have examined several organisms like insects and plants. The rhythms of insects have been first discribed by Konopka in *Drosophila pseudoobscura* and *Drosophila melanogaster*. The first clock gene identified was *period (per)* (Konopka and Benzer, 1971). The core clock mechanism is believed to consist of a transcription-translation oscillator. The feedback loop, which is necessary to induce oscillations, is defined by the actions of the proteins CLOCK (CLK) and CYCLE (CYC), the mRNAs *period (per)* and *timeless (tim)*, and PER and TIM proteins. The cells of most tissues in

the adult fly have clocks that run independently. The dominant pacemaker for behavioral rhythms is within the lateral neuron cells. The mechanism of entrainment involves a light-promoted turnover of the TIM protein to reset the clock. The circadian clock of plants has been extensively studied in *Arabidopsis thaliana* (Harmer et al., 2001). Its circadian rhythms rely on a negative feedback loop oscillator with additional levels of post-transcriptional and post-transational regulation. The identification of its molecular components has been illustrated by the promoter activity of the clock-controlled gene LHCB fused to the firefly LUCIFERASE (LUC). The central oscillator can be entrained by light and temperature cycles. Two classes of photoreceptors, phytochromes (PHY) and cryptochromes (CRY) are responsible for a light-driven entrainment.

1.2 The cyanobacterium *Synechococcus elongatus* serves as a model organism for bacterial circadian clocks

Internal rhythms of cyanobacteria have been observed first by (Grobbelaar et al., 1986). They could show that *Synechococcus* RF-1 displays rhythms of nitrogen fixation under continuous illumination.

In the following, the research group of Kondo has established *Synechococcus elongatus* PCC 7942 as a model organism for circadian rhythms in prokaryotes. They have shown that the promoter activity of a specific reporter strain satisfies the defining features (Kondo et al., 1993). The promoter activity thereby complies with certain biochemical constraints, which are schematically illustrated in Figure 1.2.

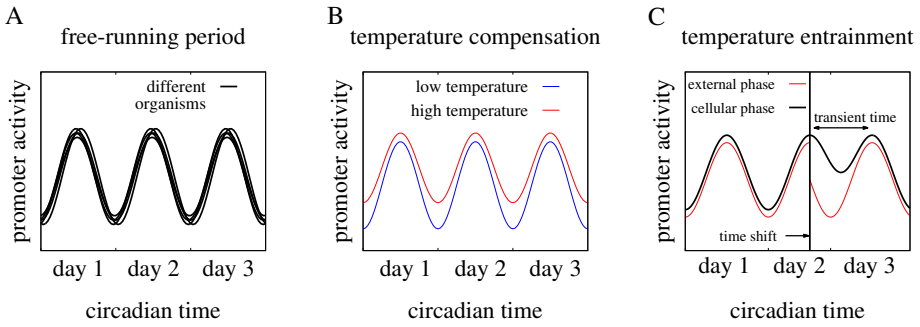

Figure 1.2: The defining features can be translated into molecular constraints. A) A constant free-running and circadian period causes the promoter activities of different cyanobacteria to oscillate synchronously. B) The period of the oscillations must be temperature-compensated, while the amplitude and the shape of the oscillations may vary a little. C) When the phase entrains to a shifted external rhythm, a transient time can be observed.

As the existence of the circadian clock is assured, the clock handle, which indicates the circadian time, and its regulatory components have to be identified. A simple candidate for this clock handle is the specific activity of a single promoter or the concentration of a particular protein, which oscillate in a circadian rhythm. A promoter trap experiment, however, has revealed that the transcription of almost all genes is coordinated in a circadian rhythm (Liu et al., 1995). Besides the components that represent the clock handle, an enhanced set of genes and proteins is expected to regulate period and amplitude of the oscillator. Therefore, all genes of the cyanobacterial DNA must be examined if they undergo circadian rhythms. This has been realized by inserting parts of the DNA library into clock mutants that show no circadian oscillations or an arrhythmic behavior (Ishiura et al., 1998). According to their experiments the circadian rhythm of gene expression is controlled by three genes *kaiA*, *kaiB* and *kaiC*. Translated KaiABC proteins

interact and further regulate the *kaiBC* promoter (P*kaiBC*). KaiC thereby induces a negative feedback on P*kaiBC* whereas KaiA stimulates P*kaiBC* promoter activity, see Figure 1.3. This feedback loop causes the clock genes to oscillate in a circadian period. In relation to the Goodwin oscillator (Goodwin, 1965), a transcription-translation-oscillator (TTO) has been suggested to describe the core clock of cyanobacteria (Ishiura et al., 1998).

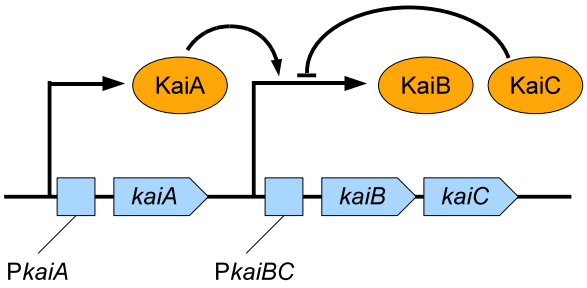

Figure 1.3: Schematic view of the Transcription-Translation Oscillator (TTO). Protein KaiA stimulates the activity of the *kaiBC* promoter (P*kaiBC*), KaiB and KaiC induce a negative feedback on their expression.

The TTO-hypothesis has evoked the prediction that the total amount of the KaiC protein indicates the circadian time of the clock and therefore represents the clock handle. The prediction has been supported by the experimental observation that an overexpression of KaiC at low concentrations induces a phase resetting (Xu et al., 2000). However, the level of KaiC protein is not sufficient for describing the circadian phase. Although the total amount of KaiC proteins naturally decreases during cell division,

the circadian phase is exactly transferred to the daughter cell for several generations (Mihalcescu et al., 2004). This is an indication that a second quantity must oscillate and coordinate circadian activities, independently of the total protein concentrations. In succession, Tomita et al. have discovered that the ratio of KaiC phosphorylation displays a circadian rhythm and that the oscillations do not depend on the translational feedback (Tomita et al., 2005). Moreover, the phosphorylation oscillator has been decoupled from translation by reconstituting robust circadian oscillations *in vitro* (Nakajima et al., 2005), calling into question the initial hypothesis that the core oscillator is described by a TTO.

These experiments have shown that cyanobacteria possess a second post-translational oscillator (PTO) beside the TTO. The phase of the PTO is based on the ratio of phosphorylated KaiC. The oscillations are accompanied by a formation of KaiAC complexes in a low phosphorylated state and of KaiBC complexes in a highly phosphorylated state (Kageyama et al., 2003; Kitayama et al., 2003), see Figure 1.4. The oscillations of phosphorylated KaiC are temperature compensated and they entrain to rhythmic temperature changes (Yoshida et al., 2009). The question arises if these two oscillators both are necessary for the coordination of circadian activities or if the independently running PTO is the core oscillator while the TTO is simply a side-effect.

(Kitayama et al., 2008) suggested that both oscillators are necessary for the coordination of circadian activites. Although KaiC was kept constant in a hyperphosphorylated state, temperature compensated oscillations have been measured. However, these oscillations do not persistently oscillate in a circadian period but show damped oscillations with a period of approximately 48 hours. This is in contrast to the defining feature of a circadian free-

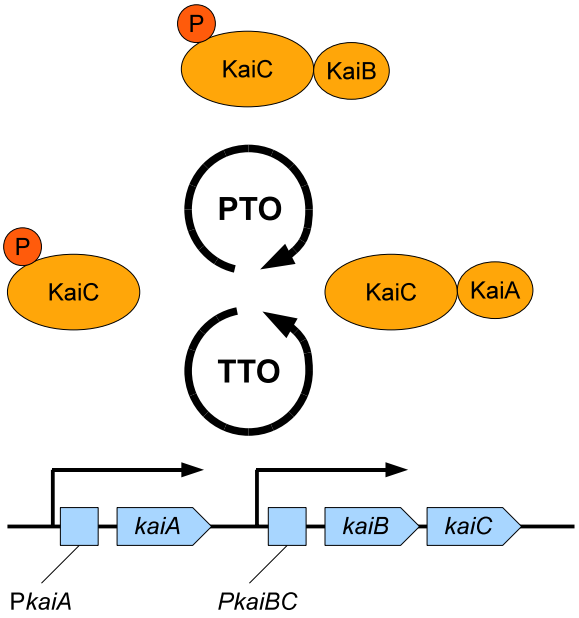

Figure 1.4: Both a Transcription-Translation Oscillator (TTO) and a Post-translational oscillator (PTO) have been observed in cyanobacteria. The PTO displays oscillations of phosphorylated KaiC. The phosphorylated form of KaiC negatively regulates P*kaiBC*, which drives the TTO.

running oscillator, suggesting that the TTO does not serve as a regulator for circadian activites. Consequently, the TTO has been identified as a slave oscillator, while the PTO is the core pacemaker (Qin et al., 2010). Zwicker et al. stress the dysfunction of a PTO when the cell doubling time drops below the 24h period (Zwicker et al., 2010). They conclude that the TTO is necessary in conditions of high growth rates. These conclusions allowed me to analyze the different oscillators and their connections separately.

1.3 Biochemical properties determine the phase of the *in vitro* core clock

The basic biochemical properties of KaiABC assembly and phosphorylation are analyzed with various methodologies. Structural analyses have elucidated that each KaiC protein consists of an N-terminal (CI) and a C-terminal (CII) half, which results in a double-doghnut shaped hexamer, see Figure (Mori et al., 2002). The N-terminal is responsible for the formation of hexamers (Mori et al., 2002), which show a rapid exchange of monomers at the early dephosphorylation stage (Ito et al., 2007; Kageyama et al., 2006; Mori et al., 2007). KaiA and KaiB both bind exclusively to the C-terminal of the KaiC hexamer. The three proteins form various complexes (Pattanayek et al., 2006, 2008) to modify the phosphorylation dynamics (Hayashi et al., 2006). The KaiC proteins form hexamers (Mori et al., 2002), and can autophosphorylate (Nishiwaki et al., 2000) and autodephosphorylate (Xu et al., 2003) at the residues serine 431 (S431) and threonine 432 (T432) (Nishiwaki et al., 2004; Xu et al., 2004). KaiA proteins form stable dimers (Ye et al., 2004; Uzumaki et al., 2004) and enhance autophosphorylation activity of KaiC (Iwasaki et al., 2002), whereas KaiB oligomers attenuate the activity of KaiA (Xu et al., 2003). The circadian rhythm of KaiC phosphorylation is dominated by the subsequent modifications of the two residues S431 and T432 from unphosphorylated (U), threonine phosphorylated (T) to both residues phosphorylated (D), and dephosphorylation via the serine phosphorylated state (S) to the unphosphorylated form (Nishiwaki et al., 2007; Rust et al., 2007), see Figure 1.5.

Besides its kinase and phosphatase activity, KaiC has a weak but stable in-

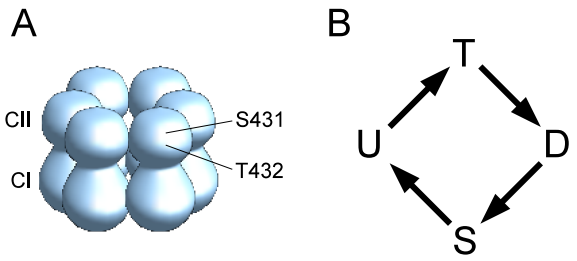

Figure 1.5: A) A double-doughnut shaped KaiC hexamer contains an N-terminal (CI) and a C-terminal (CII). B) On the C-terminal (CII) subsequent phosphorylations cause the characteristic phosphorylation cycle.

trinsic ATPase activity which is superimposed by assembly and disassembly rhythms of various KaiABC complexes (Mori et al., 2007). All three activities display a circadian rhythm when KaiA and KaiB is added to KaiC (Terauchi et al., 2007; Mori et al., 2007). The rhythms of KaiC phosphorylation and of ATPase activity are temperature compensated (Tomita et al., 2005; Terauchi et al., 2007; Murakami et al., 2008). The ATPase activity displays a simple oscillatory rhythm, whereas the phosphorylation dynamics passes through multiple states and the Kai proteins form complexes with various stoichiometries. A further simplification of the phosphorylation based oscillator has been proposed by introducing the ATPase activity as a fundamental time keeper (Terauchi et al., 2007).

As shown in experiments, the three different activities depend on each other. The phosphorylation of KaiC modulates the ATPase activity (Terauchi et al., 2007), which likely induces structural conformational changes (Mori et al., 2002) that in turn determine the phosphorylation activity (Kim et al., 2008). Consequently, there is no fundamental time keeping activity, which

operates independently of other biochemical reactions and therefore assures the oscillatory behavior of the clock. Although a fundamental time keeper could not be identified, the experiments show which activity can serve as a clock handle. The ATPase activity cannot fully determine the circadian time because a medial ATPase activity (approximately 20 ATP are hydrolized per day per KaiC) can either increase or decrease (Terauchi et al., 2007). The complex formation dynamics of the Kai proteins is described by three different complexes, KaiAC, KaiBC and KaiABC, which oscillate during the day. Each circadian time thereby shows a different distribution of the complexes (Mori et al., 2007). In principle, this distribution could serve as a clock handle, because it fully determines the circadian time. The observed oscillations, however, are too small with respect to the total concentration of KaiC proteins.

The third candidate for a clock handle is the phosphorylation activity. It fully characterizes the circadian phase, as has been determined by the O'Shea lab (Rust et al., 2007). Equally phosphorylated KaiC mixtures start to phosphorylate or to dephosphorylate, which only depends on their S-KaiC to T-KaiC ratio. In the following, I test the assumption that the phosphoform distribution fully determines the circadian time and therefore represents the clock handle.

1.4 Models of the oscillator illustrate the mechanism of the *in vitro* core clock

In this thesis, I investigate the molecular interactions between the Kai proteins in order to obtain a deeper understanding of the clock mechanism.

The main approach is to generate a quantitative model of the *in vitro* clock. Modeling biological processes is an additional technique beside experimental observations, which helps to understand the underlying mechanism and to organize the data into a logical framework. The mathematical model allows us to reliably predict the development of the complex biological system and to explain the molecular mechanism of the three defining features. The first defining feature, a free-running rhythm in constant conditions, is fulfilled in the KaiABC oscillator because it follows a robust intrinsic trajectory after different initial conditions (Rust et al., 2007). It also returns to the same trajectory after small perturbations, such as temporal temperature changes (Yoshida et al., 2009). This robust behavior demands a limit-cycle oscillator as a model for circadian clocks (Dunlap et al., 2004). The limit-cycle oscillator must fulfill several experimental constraints of the KaiABC system.

In the first modeling approaches, multiple phosphorylation steps of the KaiC hexamers were included. Clusters of phosphorylated KaiC hexamers thereby induce an irreversible switch to dephosphorylation which assures the phosphorylation cycle (Emberly and Wingreen, 2006). In another approach, different Kai protein complexes lead to a 6-dimensional state space (Mehra et al., 2006). The phosphorylation cycle of individual KaiC hexamers is assured by the formation of KaiABC complexes, initiating the dephosphorylation process. In both cases, an interaction of two hexamers or more synchronize the phosphorylation levels. Emberly et al. introduced a monomer exchange rate of KaiC, which synchronizes different hexamer phosphorylation levels during dephosphorylation. Mehra et al. attributed phosphorylated KaiC hexamers an autocatalytic activity, which induces a

positive feedback on the KaiC phosphorylation process via $KaiC_{12}$ complexes.

However, several experiments contradict an interaction between hexamers. A Blue Native PAGE separation has excluded the existence of stable oligomeric formations of KaiC hexamers (Clodong et al., 2007). Using a negative-stain EM analysis, (Mori et al., 2007) have identified four different KaiABC complexes, excluding oligomeric KaiC complexes. The result is consistent with a detailed BN-PAGE analysis, indicating that KaiC is usually in a hexameric form.

In order to avoid clusters of hexamers, scientists have modeled the switch to dephosphorylation of the individual KaiC by requiring a formation of KaiBC complexes which induces dephosphorylation. In the model of (Kurosawa et al., 2006), active and inactive forms of KaiA and KaiB lead to an activator-inhibitor oscillator which is based on a bistability of phosphorylated KaiC. A negative feedback oscillator has been realized by a depletion of KaiA due to the formation of KaiABC complexes (Mori et al., 2007; van Zon et al., 2007; Clodong et al., 2007; Akiyama et al., 2008). Van Zon et al. have explained the experimentally observed temperature compensation and they have reproduced the response of the oscillator to individually varying levels of the three protein concentrations KaiABC (Kageyama et al., 2006). In the model of (Mori et al., 2007), an additional monomer exchange is needed in order to ensure sustained oscillations. They explain how temperature-dependent conformational changes and dissociation constants of the different Kai complexes cause the observed phase shifts. Yoda et al. (Yoda et al., 2007) have shown that a shuffling mechanism can produce synchronized oscillations. In their approach, shuffling does not only average the phosphorylation level of similar states of KaiC. Shuffling between two

introduced states of KaiC monomers, tensed and relaxed KaiC, actively forces phosphorylated KaiC to dephosphorylate.

These models, however, do not explain the characteristic phosphorylation cycle, $U \rightarrow T \rightarrow D \rightarrow S \rightarrow U$, see Figure (1.5B). The Rust-analysis demonstrates that the two phosphorylation sites have an important function (Rust et al., 2007). A single phosphorylated KaiC phosphorylates if the threonine residue is phosphorylated, it dephosphorylates if the serine residue is phosphorylated. The cycle has been suggested to be the essential oscillatory mechanism for individual KaiC subunits. (Nishiwaki et al., 2007) have strengthen this hypothesis by showing that phosphomimetic mutants do not undergo reverse steps of this cycle. However, the possibility of some reverse steps cannot be ruled out at this stage because phosphomimetic mutant KaiC hexamers are different from native KaiC hexamers. These mutants have six identically phosphorylated monomers and therefore might bind differently to the other Kai proteins (Markson and O'Shea, 2009).

Constraint by the experimental results, (Rust et al., 2007) have set up a mathematical model, which reproduces the period and the distinctive dynamics of the four phosphoforms. In order to investigate the origin of the phosphoform pattern and to determine the basic phosphorylation rates, Rust et al. have decomposed the oscillator into partial reactions, which include dephosphorylating KaiC alone and a phosphorylating KaiAC mixture. (Nagai et al., 2010) also have explicitly taken two phosphorylation sites into account. Similar to previous analyses (Yoda et al., 2007; Eguchi et al., 2008), the molecular synchronization is realized by monomer shuffling of KaiC. Interestingly, they coarse-grained the model by focusing on the most important reaction steps. These two modeling approaches have given great

insight into the function of different phosphorylation states of KaiC as they fulfill several experimental constraints. They show that, in correspondence with the given experiments, the mathematical model of the KaiABC circadian clock has to regulate the amount of free KaiA via conformational changes with a subsequent formation of KaiBC and KaiABC complexes.

However, these models do not predict the dynamics of KaiC phosphorylation quantitatively. Moreover, their oscillations of the total concentration of phosphorylated KaiC only achieve amplitudes of approximately $30\% - 40\%$ of total KaiC, whereas the oscillations in the experiments reach amplitudes of up to 50% of total KaiC. These deficiencies have been my initial motivation to construct an improved mathematical model which quantitatively reproduces the experiments. In order to achieve enhanced oscillations of phosphorylated KaiC, the model must account for sufficient non-linearities and time delays (Novak and Tyson, 2008). In a first analysis, I have successfully tested this proposition using a previous modeling approach from (Clodong et al., 2007), see Appendix 4. Non-linearities and time delays can be assured by introducing additional states (Goodwin, 1965; Griffith, 1968). It has been predicted for the KaiABC system that more than four states of KaiC must be included in a mathematical model (Takigawa-Imamura and Mochizuki, 2006).

The question arises how an enhanced state space is realized biochemically with the three Kai proteins. In my model, the enhancement is achieved by including three biochemical properties of KaiC. First, the identified two phosphorylation sites T432 and S431 lead to four different phosphorylation states of KaiC. Second, the hexamerization of KaiC increases the number of states, as the distribution of differently phosphorylated monomers within

the hexamer is expected to influence the binding properties of KaiC. Third, specific KaiC hexamers bind to KaiA and KaiB, which form three additional protein complexes, KaiAC, KaiBC and KaiABC. All these different states of KaiC and their corresponding transition reactions strongly increase the dimensions of the model, which then becomes difficult to simulate. Therefore, my model focuses on the most important states.

1.5 Questions that will be adressed

The following questions will be adressed in this thesis:

- Which experimental constraints should be included into the mathematical model of the cyanobacterial *in vitro* clock?

The most important property of the KaiABC circadian clock is its exceptional robustness. This can be seen *in vivo* in bacterial colonies. Although there is no cell-to-cell communication between different cells, the different clocks remain synchronous (Mihalcescu et al., 2004). This specific robustness against growth and cell division follows from the following experimental property. The phase and the amplitude of the oscillator do not change when the total protein concentrations are varied concertedly (Kageyama et al., 2006). This property turns out to be the most important modeling constraint for the KaiABC system. Therefore we must ask the following methodological questions:

- How can we model a dynamic invariant system?
- Can we affirm the predictions of the model experimentally?

- Do experiments that measure complex formation provide enough information to support the model?

In order to determine the mechanism of the *in vitro* core oscillator, the following problems have to be analyzed:

- How do KaiC proteins switch between phosphorylation and dephosphorylation?
- How do differently phosphorylated KaiC monomers and hexamers synchronize?
- What are the most important phosphorylation configurations of KaiC hexamers?
- Is the observed monomer exchange essential for the core oscillator? What is the mechanism of the exchange?
- How does the clock fulfill the constraint of dynamic invariance at a molecular level?

Subsequently, the results are used to understand the three defining features. In this sense, the following questions have to be analyzed:

- How does the system fulfill the three defining features (free-running period, temperature compensation and phase entrainment)?
- How do cyanobacteria trade-off the ability for temperature compensation against the ability for temperature entrainment?

In addition to the detailed analysis of the core oscillator, I further investigate the core oscillator from an evolutionary perspective. As the phosphoform distribution displays an ordered pattern (Rust et al., 2007), I follow the

hypothesis that two different phosphorylatable amino acids, which give rise to four phosphorylation states, provide an evolutionary benefit. The following questions are analyzed:

- How did the clock evolve?
- What are the dominating selection pressures?

We can think of more detailed questions to describe the KaiABC circadian clock such as the binding probabilities of specificly phosphorylated KaiC hexamers to KaiA and KaiB. This is related to the levels of free energy of the hexamers. The given experiments, however, do not allow us to identify such detailed properties.

2 Methodology

2.1 Determination of a dynamic invariant oscillator

In this thesis, I construct a quantitative model of the KaiABC circadian clock. The dynamics are described by a system of differential equations

$$\dot{\mathbf{C}} = \mathbf{T} \cdot \mathbf{C}, \tag{2.1}$$

where the concentrations of the phosphoforms $\mathbf{C} = (C_U, C_T, C_S, C_D)$ have been introduced. The transition matrix depends on the total concentration of KaiA and on the phosphoform vector $\mathbf{T} = \mathbf{T}(\mathbf{C}, A^{tot})$. This is the four state model, which has been introduced by (Rust et al., 2007). The four state model, however, is not quantitative. It must fulfill additional constraints. The most important constraint follows from the principle of dynamic invariance. Dynamic invariance refers to the experimentally observed robustness of phase, frequency, and amplitude of the test tube system upon concerted changes of the Kai protein concentrations over one order of magnitude (Kageyama et al., 2006; Rust et al., 2007). I therefore extract some general principles to meet this requirement.

The experimentally observed robustness of phase against concerted changes

in protein concentrations (Kageyama et al., 2006; Rust et al., 2007) is an important principle for the cyanobacterium *Synechococcus elongatus* PCC 7942. In conditions of cell growth or cell division, varying protein expression rates or asymmetric cell divisions likely cause an excess or an underrepresentation of Kai proteins. Osmotic stress may dilute or concentrate the clock proteins of the cell. In these situations, the gene expression noise of KaiABC is correlated, as their genes form a cluster on the DNA. The observed robustness to such variations, dynamic invariance, enables the organism to maintain the phase of its clock throughout many generations.

Over- and underexpression of the concentrations are simulated using the following transformation

$$(\mathbf{C}, A) \rightarrow (\lambda\mathbf{C}, \lambda A) \tag{2.2}$$

The invariance at a hypothetically steady state $\dot{\mathbf{C}} = 0$ can be achieved by demanding homogeneous functions

$$\mathbf{T}(\lambda\mathbf{C}, \lambda A) = \lambda^N \mathbf{T}(\mathbf{C}, A). \tag{2.3}$$

In this case, the term λ^N cancels out and the equations for the steady state remain unchanged (Kollmann et al., 2005).

In the case of dynamic invariance, the transition matrix of the differential equation must satisfy the following condition

$$\mathbf{T}(\lambda\mathbf{C}, \lambda A) = \mathbf{T}(\mathbf{C}, A). \tag{2.4}$$

Four different principles are important to achieve this constraint:

- The transition matrix is independent of $(\mathbf{C}, A)$
- The transition matrix depends on relative concentrations of $(\mathbf{C}, A)$
- Protein inactivation
- Separation of time scales

2.1.1 Transition rates

The simplest case, the function T_{ij}, with $[i, j] \in [U, T, S, D]$, is independent of the variables $(\mathbf{C}, A)$, represents a linear model. The condition 2.4 is fulfilled.

2.1.2 The transition matrix depends on relative protein concentrations

If the model is not linear, the condition 2.4 can only be achieved if T_{ij} is a function of the fraction of two variables, e.g.

$$T_{ij} = f\left(\frac{C_i}{C_j}\right), \; T_{ij} = f\left(\frac{A}{\sum_i k_i C_i}\right). \tag{2.5}$$

This condition is a strong constraint for the underlying model. More interestingly, though, dynamic invariance can be achieved for concerted concentration changes, although the condition (2.4) is only approximately fulfilled.

2.1.3 Inactivation of KaiA

Assume that the dynamics of the C_i depend linearly on the concentration of the enzyme A. Here, the velocity of the reaction depends on the expression level of A and the system is not robust against expression changes. Dynamic invariance, however, can be recovered by an inactivation mechanism.

The inactivation of the free concentration A^f by binding to a specific KaiC phosphorylation state C_i is described in the following

$$A^f + C_i \underset{k_{-1}}{\overset{k_1}{\rightleftharpoons}} [AC_i]. \tag{2.6}$$

The dynamics of free diffusible KaiA are described by an inhomogenous differential equation for the case $C_i \gg A^{tot}$

$$\dot{A}^f(t) = k_{-1} \underbrace{[AC_i]}_{=A^{tot}-A^f(t)} - k_1 A^f(t) C_i = k_{-1} A^{tot} - (k_{-1} + k_1 C_i) A^f(t), \tag{2.7}$$

which can be solved

$$\begin{aligned} A^f(t) = {} & A^f(t_0) e^{-\int_0^t dt'(k_{-1}+k_1 C_i(t'))} \\ & + e^{-\int_0^t dt'(k_{-1}+k_1 C_i(t'))} \int_0^t dt' k_{-1} A^{tot} e^{\int_0^{t'} dt''(k_{-1}+k_1 C_i(t''))}. \end{aligned} \tag{2.8}$$

In the limit $t \to \infty$, $A^f(t)$ does not reach a constant level because $C_i(t)$ is not constant in time. Although it is not possible to calculate the exact trajectory of $A^f(t)$, it can be determined how fast $A^f(t)$ is responding to

changes in C_i by taking constant C_i

$$A^f(t) = A^f(t_0)e^{-(k_{-1}+k_1C_i)t} + \frac{k_{-1}A^{tot}}{k_{-1}+k_1C_i}. \tag{2.9}$$

The response time $T_{1/2} = \frac{\log 2}{k_{-1}+k_1C_i}$ depends on C_i. Therefore, the system is not dynamic invariant. However, a separation of timescales recovers dynamic invariance. Taking large values of k_1, k_{-1}, the steady state value is the only important value for the system

$$\left(A^f\right)^{st} = \frac{A^{tot}}{1+\frac{k_1}{k_{-1}}C_i}. \tag{2.10}$$

For large association constants

$$1 \ll \frac{k_1}{k_{-1}} \equiv K_{CA} \tag{2.11}$$

the condition (2.5) is fulfilled

$$\left(A^f\right)^{st} = \frac{A^{tot}}{K_{CA}C_i}. \tag{2.12}$$

It can be seen that dynamic invariance of the model can be achieved asymptotically for a large range of parameters.

2.1.4 Separation of time scales in the case of multilinear reactions

Here, I assume that the system depends on the formation of oligomers. I therefore introduce oligomeric complexes of n monomers, denoted by $[C_i^n]$ with $[i,j] \in [U,T,S,D]$, that assemble and disassemble. They interact

with the monomer pool, such that

$$[C_i^n] \underset{\gamma_i^-}{\overset{\gamma_i^+}{\rightleftharpoons}} C_i.$$

Moreover, the oligomeric complexes undergo a transition in their phosphorylation state

$$[C_i^n] \overset{\alpha_{ji}}{\rightarrow} [C_j^n]$$

with linear transition rates α_{ji}.

The set of differential equations has the following form

$$\begin{aligned} [\dot{C_i^n}] &= -\gamma_i^- \left[C_i^n\right] + \gamma_i^+ \left(C_i\right)^n + \sum_j \alpha_{ij} \left[C_j^n\right] - \sum_j \alpha_{ji} \left[C_i^n\right], \\ \dot{C}_i &= \gamma^- \left[C_i^n\right] - \gamma^+ \left(C_i\right)^n. \end{aligned} \tag{2.13}$$

When the transformation 2.2 is performed ($C_i \rightarrow \lambda C_i$), the dynamics of C_i and $[C_i^n]$ change with varying expression levels of $\mathbf{C}$. Formally, the system is not dynamic invariant because the transition matrix is homogeneous of degree higher than one.

However, dynamic invariance can be recovered by a separation of timescales. Assembly and disassembly of oligomers is assumed to be a fast process with respect to phosphorylation, $\gamma_i^{\pm} \gg \alpha_{ij}$. The fast variable C_i rapidly reaches an equilibrium and the quasi steady state approximation $\dot{C}_i = 0$ can be applied. The amount of oligomeric complexes is calculated

$$[C_i^n] = \left(\frac{\gamma_i^+}{\gamma_i^-} C_i\right)^n. \tag{2.14}$$

The oligomeric complexes therefore have a scaling factor different from the

monomers

$$[C_i^n] \rightarrow [C_i^n]\,\lambda^n. \tag{2.15}$$

After the transformation 2.2, the differential equation 2.13 has the following form

$$\lambda^n[\dot{C_i^n}] = -\lambda^n\gamma_i^-\,[C_i^n] + \gamma^+\,(\lambda C_i)^n + \sum_j \alpha_{ij}\lambda^n\left[C_j^n\right] - \sum_j \alpha_{ji}\lambda^n\,[C_i^n]\,. \tag{2.16}$$

As all terms of the equation have the same scaling factor λ^n, the factor can be omitted and the dynamics of the slow variable $[C_i^n]$, therefore, do not depend on λ.

2.2 Native mass spectrometry

In collaboration with the Albert Heck laboratory from the university of Utrecht, native mass spectrometry has been employed to confirm the theoretical predictions (Heck, 2008). This is an emerging technology that allows the topological investigation of intact protein complexes with high sensitivity. It also provides complementary information to technologies in structural biology and interactomics studies. The results of this study have been recently published (Brettschneider et al., 2010).

The recombinant Kai proteins from *Synechococcus elongatus* PCC 7942 are produced and purified as described in Iwasaki et al. (2002); Nishiwaki et al. (2004). The reconstitution of the KaiC phosphorylation cycle *in vitro* is performed using the standard concentrations Nakajima et al. (2005). KaiC ($0.2\mu g/\mu l$) is incubated with KaiA ($0.05\mu g/\mu l$) and KaiB ($0.05\mu g/\mu l$) in

the presence of ATP ($1mM$). Samples are collected at selected time points over a 24-hour period. They are loaded by nano-electrospray ionization MS in order to do mass spectral analyses. Representative mass/charge (m/z) spectra are shown in Figure 2.1.

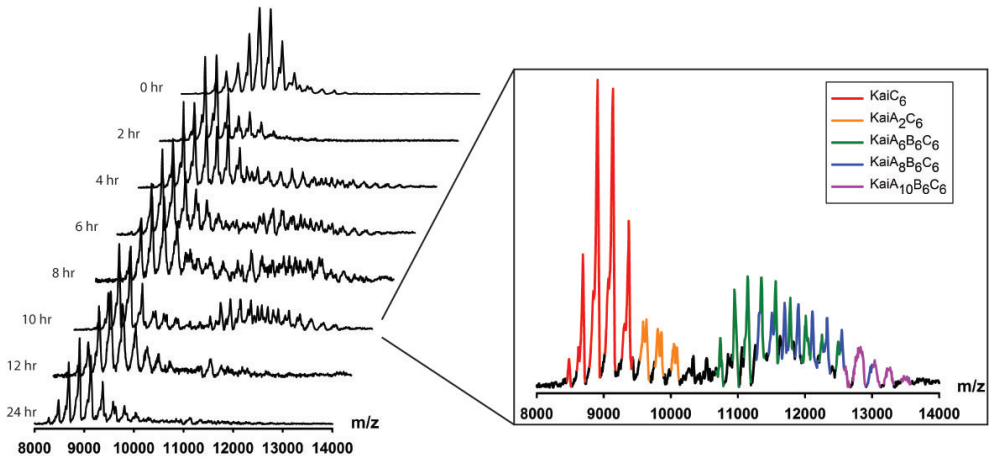

Figure 2.1: Mass spectra showing KaiABC complex formation over a 24 hour period (left). Assignment of m/z peaks to different complexes is shown for the 10 hour time point (right), where $KaiC_6$ (red), $KaiA_2C_6$ (orange), $KaiA_6B_6C_6$ (green), $KaiA_{10}B_6C_6$ (purple) are observed.

The inset in Figure 2.1 shows as an example the spectrum acquired after a 10 hour reaction. The identity of species present was deduced by taking series of m/z peaks, which follow from differently charged states of the same protein complexes. The charges of adjacent peaks only differ by one electron. Then, both the molecular weight and the charge are calculated. The specific complex of the Kai proteins can be deduced from the obtained

mass.

In the spectrum after 10 hours, 5 main complexes are present. $KaiC_6$ is seen to be a dominant species in all spectra (m/z range 8,000 to 9,500), with higher order KaiABC complexes appearing and disappearing with time (observable in the m/z range 10,000 to 14,000). Due to the high complexity of the samples, some minor m/z peaks could not be assigned, and it is possible that lower abundant species may not be observable. Importantly, however, the major m/z peaks in all spectra could unambiguously be assigned to specific KaiABC complexes and the relative abundance was monitored at each time point.

3 Determination of the core oscillator mechanism

In this chapter, the mechanism of the core clock is analyzed as it is a necessary condition for understanding the three defining features of the *in vitro* clock. Therefore, the characteristic phosphorylation cycle of individual KaiC proteins and of KaiC hexamers and the synchronization mechanism of differently phosphorylated KaiC must be discovered.

As also relatively small biological systems can show complex behavior, only a mathematical description enables us to reliably predict the important protein concentrations. I therefore establish a quantitative model which reconstitutes the oscillations of the four phosphorylated states of KaiC (Rust et al., 2007). It must fulfill four essential experimental constraints, see Figure 3.1, which represent strong modeling constraints. They have not been explained in previous approaches. First, the transient behavior of phosphorylated KaiC after addition of KaiB is important, see (Rust et al., 2007, figure 3D). More precisely, the model must give an explanation about the delay between the addition of KaiB and the initiation of dephosphorylation. Second, the KaiC phosphorylation levels are dynamically invariant, which refers to the experimentally observed robustness of phase, frequency, and amplitude of the test tube system upon concerted changes of the Kai protein concentrations over one order of magnitude (Kageyama et al., 2006; Rust

et al., 2007). Consequently, the individual Kai concentrations do not determine the clock but their relation is decisive. Third, the oscillator displays no transient behavior but instantaneously initiates with the dephosphorylation phase when mixing six different circadian phases (Ito et al., 2007). Fourth, the shape of totally phosphorylated KaiC oscillations is crucial, in particular the observed asymmetry between phosphorylation and dephosphorylation.

3.1 A four state model describes the phosphorylation dynamics of KaiC

In a first approach, I set up a model for the phosphorylation dynamics between the four monomer states of KaiC. The transition rate from the state j to the state i is described by the rate α_{ij}, $[i,j] \in [U,T,S,D]$. The two residues (serine, threonine) further do not change their phosphorylation state simultaneously, see Figure 3.2. The corresponding transition rates are set to zero, $\alpha_{UD}, \alpha_{TS}, \alpha_{ST}, \alpha_{DU} = 0$. This is the four state model introduced by (Rust et al., 2007) that describes quantitatively the basic phosphorylation/dephosphorylation dynamics of the four monomer concentrations.

For a quantitative approach to phosphorylation kinetics in presence of KaiA, the transition rates α_{ij} must have both a constant basal term $\alpha_{ij}^0 > 0$ and a KaiA-dependent term $\tilde{\alpha}_{ij}^A > 0, \quad i,j \in \{U,T,S,D\}$. In contrast to previous approaches (Mori et al., 2007; van Zon et al., 2007; Clodong et al., 2007; Akiyama et al., 2008), I resume the idea that the phosphorylation dynamics of each KaiC monomer depend on the concentration of free KaiA.

$$\begin{aligned}\dot{C}_i = \alpha_{ij} C_j = \alpha^0_{ij} C_j + \tilde{\alpha}^A_{ij}[A_2 C_j] = \left(\alpha^0_{ij} + \frac{\tilde{\alpha}^A_{ij}}{K^M_j} A^f_2\right) C_j \\ \Leftrightarrow \alpha_{ij} = \alpha^0_{ij} + \alpha^A_{ij} A^f_2.\end{aligned} \tag{3.1}$$

where the replacement $\alpha^A_{ij} = \frac{\tilde{\alpha}^A_{ij}}{K^M_j}$ has been done for simplicity. The Michaelis-Menten constant K^M_j defines the catalytic binding site properties of KaiC. Note that the transition matrix α^0_{ij} does not depend on the phosphoforms C_i, so the transition function fulfills the requirement of dynamic invariance, see section 2.1.1. The transition rate $\alpha^A_{ij} A^f_2$ is dynamic invariant if the amount of free KaiA dimers do not vary with changing expression levels. Initially, I have modeled KaiA inactivation by including a sufficiently small Michaelis-Menten constant similar to section 2.1.3 $A^f_2 = \frac{A^{tot}_2}{1+\frac{C_{tot}}{K^M_j}}, \quad K^M_j \ll C_{tot}$. However, the constant K^M_j is constraint by the experiments and the dynamic invariant property is lost. In order to fulfill this constraint, I introduce a second KaiA binding site at KaiC hexamers, $[A_2 C_6]_s$. This $[A_2 C_6]_s$ complex represents a constant sequestration of KaiA dimers to KaiC. It depends on the dissociation constant K^D_{AC}. As this complex is present throughout the circadian cycle, free KaiC hexamers C^f_6

bind to KaiA dimers independently of its phosphoform distribution.

$$\begin{aligned} &A_2^f + C_6^f \rightleftharpoons [A_2C_6]_s \\ &[A_2C_6]_s = \frac{1}{K_{AC}^D} A_2^f C_6^f = \frac{1}{K_{AC}^D} \left(A_2^{tot} - [A_2C_6]_s\right)\left(C_6^{tot} - [A_2C_6]_s\right) \\ \Leftrightarrow &[A_2C_6]_s = \frac{A_2^{tot} + C_6^{tot} + K_{AC}^D}{2} - \sqrt{\left(\frac{A_2^{tot} + C_6^{tot} + K_{AC}^D}{2}\right)^2 - A_2^{tot} C_6^{tot}}. \end{aligned} \tag{3.2}$$

Besides the constant sequestration of KaiA by KaiC, the C_6A_4 complex illustrates the second binding site of KaiC, which has different properties. KaiA dimers bind to specifically phosphorylated or unphosphorylated KaiC with a smaller affinity for catalyzing phosphorylation at an early circadian time. In the equations of the model, this complex is represented by $[A_2C_j]$, see Equation 3.1. Its concentration can be calculated with the Michaelis-Menten constant K_j^M

$$\begin{aligned} A_2^f + C_j^f &\underset{k_{-1}}{\overset{k_1}{\rightleftharpoons}} [A_2C_j] \overset{k^{cat}}{\rightarrow} A_2^f + C_j^f \\ [A_2C_j] &= \frac{1}{K_j^M} A_2^f C_j^f \approx \frac{1}{K_j^M} A_2^f C_j. \end{aligned} \tag{3.3}$$

As a large amount of free KaiA dimers is constantly sequestrated, the concentration of free KaiA dimers is small with respect to KaiC monomers $A_2^f \ll C_j^f$. Therefore, the approximation $C_j^f \approx C_j$ holds.

The amount of free KaiA dimers A_2^f can be calculated to give

$$\begin{aligned} A_2^{tot} &= A_2^f + [A_2C_6]_s + \sum_j [A_2C_j] \\ A_2^{tot} - [A_2C_6]_s &= A_2^f + \sum_j \frac{1}{K_j^M} A_2^f C_j \\ \Leftrightarrow \quad A_2^f &= \frac{A_2^{tot} - [A_2C_6]_s}{1 + \frac{C_{tot}}{K_j^M}}. \end{aligned} \tag{3.4}$$

These binding properties of KaiA assure that the amount of free KaiA only varies little upon concerted over- and underexpression, which is represented by the expression level λ, see Figure 3.3.

In a first global optimization, the transient dynamics of the KaiC phospho-forms in absence of KaiA and KaiB is used to identify the 8 basic phosphorylation and dephosphorylation rates α_{ij}^0 for all KaiC phospho-forms by a least squares fit, Figure 3.4. The 8 KaiA-dependent rates α_{ij}^A are determined by a least square fit to the KaiA-dependent phosphorylation data.

3.2 An enhanced model fulfills the experimental constraints

In order to set up a quantitative model for the oscillatory long-term behavior of the system, the four state model is not sufficient. The four constraints I introduced at the beginning of the chapter cannot be reproduced, see (Rust et al., 2007). The model has to be completed by two well studied binding mechanisms of KaiABC which strongly regulate the circadian rhythm:

- The majority of KaiC monomers aggregate to hexamers (Clodong et al., 2007; Mori et al., 2002).
- Approximately $10-20\%$ of KaiC are bound to KaiB dimers during the dephosphorylation phase (Kageyama et al., 2006; Mori et al., 2007).

According to (Pattanayek et al., 2008), KaiB tetramers form a ring on top of the KaiC hexamers. On the contrary, (Clodong et al., 2007) have measured 5-6 KaiB dimers binding one hexamer. These KaiB proteins form stable KaiBC complexes, as they do not vary with changing concentrations of KaiB (Clodong et al., 2007; Kageyama et al., 2006). Therefore, two different states of KaiC must be introduced, see Figure 3.5. KaiC monomers that are part of a hexamer belong to the $\mathbf{C}^H$ pool. If they are part of a KaiBC complex, they belong to the $\mathbf{C}^B$ pool. KaiB behaves like a switch between phosphorylating and dephosphorylating KaiC. A third pool $\mathbf{C}^P$ describes the fraction of KaiC that is present as free monomers (Clodong et al., 2007; Mori et al., 2002). I assume that the assembly and disassembly of hexamers via free KaiC monomers is the molecular origin of the experimentally observed KaiC-hexamer shuffling mechanism (Kageyama et al., 2006). The three pools are defined in the following

$$\begin{aligned}\mathbf{C}^H &= (C_U^H, C_T^H, C_S^H, C_D^H)^T \\ \mathbf{C}^B &= (C_U^B, C_T^B, C_S^B, C_D^B)^T \\ \mathbf{C}^P &= (C_U^P, C_T^P, C_S^P, C_D^P)^T.\end{aligned} \tag{3.5}$$

The experimental constraint of KaiB-induced dephosphorylation shows an abrupt switch from phosphorylation, which can only be described by

introducing nonlinear terms in the mathematical model. Therefore, I follow the hypothesis that the formation of KaiBC and KaiABC complexes strongly depends on the phosphorylated state of KaiC hexamers. A phosphorylation state (U, T, S, D) is assigend to every subcomponent of the hexamer, see Figure 3.6. This extends the number of potential hexameric phosphorylation configurations to $4^6 = 4096$. To decrease the amount of configurations, the symmetry of the hexamer must be taken into consideration. The free energy of the hexamer is approximated by the sum of the contributions from its constituent monomers (van Zon et al., 2007). Hence, the position of one monomer within the hexamer is not important and many different configurations are equivalent. The remaining number of different hexameric states can be calculated by standard combinatorics. Given $k = 6$ draws with replacement in an urn with $n = 4$ balls (U, T, S, D), the total number of different results in which the sequence is not important is given by

$$\binom{n+k-1}{k} = 84. \tag{3.6}$$

Consequently, the model consists of 84 states for both the KaiC hexamer pool $\mathbf{C}^H$ and the KaiBC hexamer complexes of the pool $\mathbf{C}^B$ and four additional monomer states of the monomer pool $\mathbf{C}^P$. This leads to a $2 \times 84 + 4 = 172$-dimensional model, which is difficult to calculate.

In order to reduce computational work and to keep the model simple, I assume that the monomer exchange rates via free KaiC monomers are sufficiently fast. As this shuffling process assures a well shuffled ensemble, the corresponding hexamer concentrations can be approximated by multinomial distributions of the state vectors $\mathbf{C}^H, \mathbf{C}^B, \mathbf{C}^P$. The concentration

of the specific hexamer $H(\mathbf{n})$ can be calculated as follows

$$H\left[\mathbf{C}^H\right] = \frac{6!}{n_U!n_T!n_S!n_D!}\left(\frac{C_U^H}{C_{tot}^H}\right)^{n_U}\left(\frac{C_T^H}{C_{tot}^H}\right)^{n_T}\left(\frac{C_S^H}{C_{tot}^H}\right)^{n_S}\left(\frac{C_D^H}{C_{tot}^H}\right)^{n_D}\frac{C_{tot}^H}{6}, \tag{3.7}$$

The total monomer concentration is described by $C_{tot}^H = C_U^H + C_T^H + C_S^H + C_D^H$ and $\mathbf{n}$ must satisfy the boundary condition $n_U + n_T + n_S + n_D = 6$. The probability of finding a single monomer in the $\mathbf{C}^H$ pool is $C_i^H/C_{tot}^H, i \in \{U, T, S, D\}$. The total concentration of hexamers is $C_{tot}^H/6$.

Analogously, the concentration of a specific KaiBC hexamer complex is

$$H\left[\mathbf{C}^B\right] = \frac{6!}{n_U!n_T!n_S!n_D!}\left(\frac{C_U^B}{C_{tot}^B}\right)^{n_U}\left(\frac{C_T^B}{C_{tot}^B}\right)^{n_T}\left(\frac{C_S^B}{C_{tot}^B}\right)^{n_S}\left(\frac{C_D^B}{C_{tot}^B}\right)^{n_D}\frac{C_{tot}^B}{6}. \tag{3.8}$$

Consequently, the assumption of a well shuffled ensemble has reduced the 172-dimensional model to 12 dimensions at the cost of introducing a transition matrix that depends nonlinearly on the phosphoforms.

3.3 Hexamer-dependent reactions assure oscillations of high amplitudes

It is known that KaiB rapidly inhibits the enzymatic activity of KaiA (Kitayama et al., 2003; Rust et al., 2007). Consequently, both inactivation of KaiA as well as formation of KaiBC complexes lead to dephosphorylation of KaiC. It is a challenging problem to find the exact hexamer phosphorylation

configurations for these two fundamental reactions. Recent analyses of that problem have not explicitly taken into consideration both the two phosphorylation sites of KaiC (serine, threonine) and the hexameric structure of KaiC.

It has been considered (van Zon et al., 2007) that the binding of KaiB to KaiC depends on the hexameric level of free energy which in turn depends strongly on the phosphorylation of KaiC. They conclude that hexamers flip to KaiBC hexamer complexes with a higher probability when all monomers are phosphorylated. This is reasonable as a conformational change to dephosphorylation at only highly phosphorylated KaiC levels represents an accumulation of phosphorylated KaiC monomers. This provides larger amplitudes for the oscillations. Since KaiC displays three phosphorylated states, all hexamer configurations assembled from T-, S- and D-KaiC monomers represent a fully phosphorylated hexamer. A priori, it is not clear which hexamer configurations have the highest affinity for KaiB. Rust et al. have shown that the assembly of the KaiBC complexes must strongly depend on the concentration of S-KaiC (Rust et al., 2007, Fig. 3C). However, as one can see that the concentration of KaiBC complexes is slightly shifted towards the peak of maximal D-KaiC, the KaiBC complexes might contain both serine and double phosphorylated monomers.

Consequently, I suppose that seven configurations $S^{6-i}D^i, 0 \leq i \leq 6$ catalyze the assembly of KaiBC complexes. In order to keep the parameter space small, a clear distinction between $S-$ and $D-$induced binding

reactions is implemented. Only the following transitions are included

$$\begin{aligned} \left(C_S^H\right)^6 &\rightarrow \left(C_S^B\right)^6, \\ \left(C_D^H\right)^6 &\rightarrow \left(C_D^B\right)^6. \end{aligned} \tag{3.9}$$

On the other hand, KaiB dissociates with a larger probability when the hexamer is completely dephosphorylated (van Zon et al., 2007). In my model, this is represented formally by the following transition

$$\left(C_U^B\right)^6 \rightarrow \left(C_U^H\right)^6. \tag{3.10}$$

Note, however, that KaiB dissociation also occurs by the decay of hexamers into monomers.

Rust et al. assume that KaiA is mainly inactivated by S-KaiC. I further specify that KaiA is inactivated by a sixfold serine-phosphorylated hexamer complex $\left(C_S^B\right)^6$. A third KaiC binding site for KaiA additionally has to be introduced

$$\begin{aligned} A_2^{tot} &= A_2^f + [A_2C_6]_s + \sum_i [A_2C_i] + \left[A_2\left(C_S^B\right)^6\right] \\ A_2^f &= \frac{A_2^{tot} - [A_2C_6]_s}{1 + \frac{C_{tot}^H}{K_j^M} + \frac{\left(C_S^B\right)^6}{K_{AS}^D}}. \end{aligned} \tag{3.11}$$

Again, it is assumed that $\left[\left(C_S^B\right)^6\right]^{free} \approx \left(C_S^B\right)^6$.

The concentrations of the complexes which have been introduced in (3.9,3.10)

and (3.11) are determined by using 3.7 and 3.8

$$\begin{aligned}\left[\left(C_S^H\right)^6\right] &= \frac{C_S^H}{6}\left(\frac{C_S^H}{C_{tot}^H}\right)^5, \left[\left(C_D^H\right)^6\right] = \frac{C_D^H}{6}\left(\frac{C_D^H}{C_{tot}^H}\right)^5, \\ \left[\left(C_S^B\right)^6\right] &= \frac{C_S^B}{6}\left(\frac{C_S^B}{C_{tot}^B}\right)^5, \left[\left(C_U^B\right)^6\right] = \frac{C_U^B}{6}\left(\frac{C_U^B}{C_{tot}^B}\right)^5.\end{aligned} \tag{3.12}$$

The transition rates between the three pools can be formulated with these expressions. The negative feedback is given by an inactivation of KaiA, equation (3.11). The resulting amount of free KaiA is given by

$$A_2^f = \frac{A_2^{tot} - [A_2C_6]_s}{1 + \frac{C_{tot}^H}{K_j^M} + \frac{C_S^B}{6K_{AS}^D}\left(\frac{C_S^B}{C_{tot}^B}\right)^5}, \tag{3.13}$$

where the total concentration of KaiC monomers being part of a hexameric KaiBC complex is denoted by $C_{tot}^B = C_U^B + C_T^B + C_S^B + C_D^B$.

The reaction rates that describe the conformational changes between the pools $\mathbf{C}^H$ and $\mathbf{C}^B$ are given by

$$\beta_i^+ = \frac{c_S}{6}\left(\frac{C_S^H}{C_{tot}^H}\right)^5 \delta_{iS} + \frac{c_D}{6}\left(\frac{C_D^H}{C_{tot}^H}\right)^5 \delta_{iD} \tag{3.14}$$

$$\beta_i^- = \frac{c_U}{6}\left(\frac{C_U^B}{C_{tot}^B}\right)^5 \delta_{iU}. \tag{3.15}$$

Here, the Kronecker delta is denoted by δ_{ij}.

An explicit exchange of monomers between different KaiC hexamers is not included because the model describes the time evolution of the monomer

concentration, which is not modified by the exchange. However, a monomer exchange between KaiC hexamers and KaiBC complexes has to be included. The molecular origin of the shuffling process can be twofold. First, an interaction between two hexamers could cause an exchange of monomers, see Figure 3.7. In this case, two monomers exchange with the rate $\gamma_{ij} C_i^H C_j^B$ (Yoda et al., 2007) and the rate γ_{ij} is constrained by the velocity of monomer exchange. The monomer concentrations C_i, C_j are constrained by the phosphorylation dynamics. Secondly, KaiC hexamers and KaiBC complexes could disassemble into a pool of monomers with rate γ^- and, as in the mathematical model, subsequently reassemble with a rate $\gamma^+ (C^P)^5$. Again, the disassembly rate γ^- is constrained by the exchange velocity.

Both mechanisms stay in contrast to the constraint of dynamic invariance. In the monomer pool approach however, the remaining degree of freedom γ^+ can be adjusted in order to enhance robustness against concerted protein changes.

KaiC hexamers and KaiBC complexes both decompose into the monomer pool $\mathbf{C}^P$, which is quantified by the concentration $C_{tot}^P = C_U^P + C_T^P + C_S^P + C_D^P$. In the model, this is described by a constant disassembly reaction with rate γ^-. Inversely, monomers of the $\mathbf{C}^P$ pool assemble to KaiC hexamers $\mathbf{C}^P \rightarrow \mathbf{C}^H$. The rate depends on the probability that five other monomers of $\mathbf{C}^P$ have aggregated to the monomer as well

$$\gamma^+ = \kappa \left(\frac{C_{tot}^P}{K^P} \right)^5 . \tag{3.16}$$

The amount C_{tot}^P has to be small, as has been pointed out in section 2.1.4. It has been fixed to an amount of $C_{tot}^P \approx 5\% C_{tot}$. The hexamer assembly

is characterized by the Michaelis-Menten constant K^P. With the total concentrations of the three KaiC pools, the total concentration of KaiC can be written as $C_{tot} = C^H_{tot} + C^B_{tot} + C^P_{tot} = 3.5\mu M$.

The rates $\gamma^{\pm}$ determine the extent of the monomer exchange. Note that the monomer exchange only has a significant effect on the phosphorylation dynamics whenever [S-KaiC]$_6$ or [S-KaiBC]$_6$ is sufficiently large. Thus, the constant monomer exchange rates could be substituted by temporal active exchange rates that only contribute during the dephosphorylation phase.

Consequently, the model is described by a set of 12 differential equations

$$\dot{\mathbf{C}} = \mathbf{T} \cdot \mathbf{C}, \quad \mathbf{C} = (\mathbf{C^H}, \mathbf{C^B}, \mathbf{C^P})^T, \tag{3.17}$$

where the three pools are determined by

$$\begin{aligned} \mathbf{C^H} &= (C^H_U, C^H_T, C^H_S, C^H_D)^T, \\ \mathbf{C^B} &= (C^B_U, C^B_T, C^B_S, C^B_D)^T, \\ \mathbf{C^P} &= (C^P_U, C^P_T, C^P_S, C^P_D)^T. \end{aligned} \tag{3.18}$$

The transition matrix $\mathbf{T}$ depends on 23 open parameters. From the above assumptions and constraints, effective rate equations for the phosphorylation and complex formation dynamics are given by

$$\partial_t \mathbf{C}^H = \mathbf{T}^H \cdot \mathbf{C}^H + \boldsymbol{\beta}^- \cdot \mathbf{C}^B + \gamma^+ \mathbf{C}^P \tag{3.19}$$

$$\partial_t \mathbf{C}^B = \mathbf{T}^B \cdot \mathbf{C}^B + \boldsymbol{\beta}^+ \cdot \mathbf{C}^H \tag{3.20}$$

$$\partial_t \mathbf{C}^P = \gamma^- \left(\mathbf{C}^H + \mathbf{C}^B \right) - \gamma^+ \mathbf{C}^P. \tag{3.21}$$

The transition matrices $\mathbf{T}^H$ and $\mathbf{T}^B$ include the hexamer decay rate, γ^-, to

the free monomer pool, $\mathbf{C}^P$

$$T_{ij}^H = \alpha_{ij}^0 + \frac{\tilde{\alpha}_{ij}^A}{K_j^M} A_2^f - \beta_i^+ \delta_{ij} - \gamma^- \tag{3.22}$$

$$T_{ij}^B = \alpha_{ij}^0 - \beta_i^- \delta_{ij} - \gamma^-. \tag{3.23}$$

In a second least square fit, the remaining parameters are determined, see Appendix 1.

3.4 The experimental constraints lead to biochemical predictions

The model, see Equations (3.19-3.21), fulfills the four experimental constraints, Figure 3.1. The transient behavior of phospho-KaiC with KaiB added at different times (Figure 3.8) turned out to be crucial for identifying the mechanism by which individual KaiC hexamers can be synchronized in their phosphorylation dynamics. A sudden addition of KaiB two hours after incubation of KaiC with KaiA and ATP did not lead to an immediate effect on phosphorylation kinetics. Instead, the dephosphorylation phase was entered after a time delay of several hours by an abrupt change from the phosphorylation phase to the dephosphorylation phase. This can only be explained by a strong nonlinear dependency of the KaiBC complex formation on the actual phosphorylation state. A simple way to recover this strongly nonlinear transient behavior quantitatively is to allow only KaiBC complexes with exclusively serine phosphorylated KaiC, $[\text{S-KaiBC}]_6$, to inactivate KaiA with a high efficiency.

To test the hypothesis of an $[\text{S-KaiBC}]_6$-mediated feedback, I have assumed that KaiA is inactivated by KaiBC complexes that have less serine phosphorylated monomers, see Appendix 2. However, a high value of χ^2 for the least square fit is in contrast to that assumption. This has strengthened the hypothesis that KaiA is inactivated exlusively by $[\text{S-KaiBC}]_6$.

Having determined the parameters, the two specific experiments that have constrained the modeling approach are simulated. The concept of dynamic invariance, Figure 3.9, has constrained the binding properties of KaiAC complexes. The experimental observation of instantaneous oscillations after mixing Kai proteins of different phases, Figure 3.10, requires the introduction of a monomer pool.

Although no direct constraints are used to arrive at the characteristic shape of the oscillations in phospho-KaiC, the model excellently predicts the experimentally found dynamic behavior, Figure 3.11. Besides reproduction of the correct peak-to-peak time distances of the four phospho-forms, the asymmetry of the amplitude peak of phospho-KaiC has been recovered, resulting in phosphorylation and dephosphorylation phases of approximately 9.5 h and 18.5 h, respectively. Here, the *in vitro* experiments of Rust et al. showed a period of 28 h, whereas other *in vitro* experiments recover the circadian 24 h rhythm (Ito et al., 2007). In the model, the different periods can be adjusted by changing the transition rates to KaiBC complexes, c_S and c_D, see Appendix.

In conclusion, the two experimental constraints (see Figures 3.9 and 3.10) have directly lead us to two biochemical predictions:

- In order to fulfill the constraint of dynamic invariance, KaiC must have

two different KaiA binding sites. Besides a catalytic binding site to enhance the autophosphorylation activity, KaiC constantly sequestrates KaiA, irrespective of its phosphorylation state.

- In order to meet the requirements of KaiB-induced dephosphorylation, KaiA is inactivated by exclusively serine phosphorylated KaiBC complexes.

These biochemical properties have not yet been observed experimentally and therefore are analyzed by native mass spectrometry.

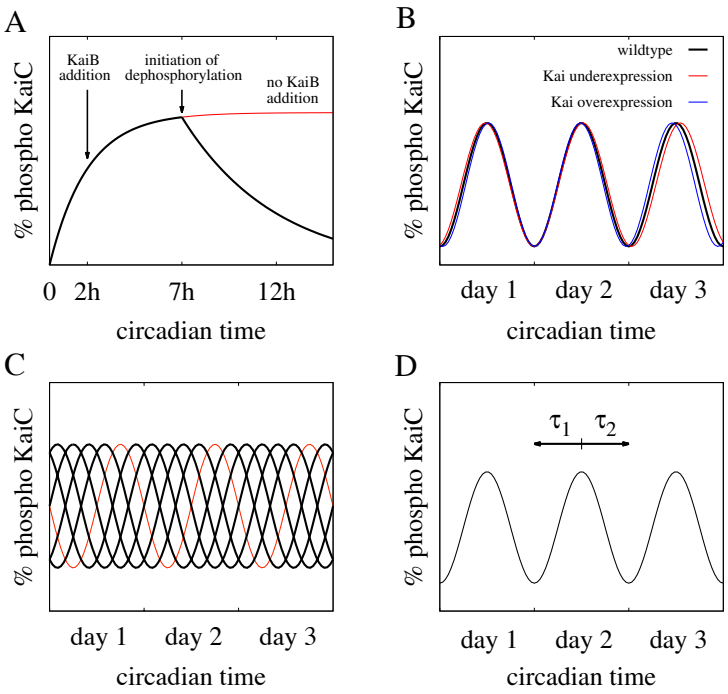

Figure 3.1: The model must explain four basic experimental facts. A) The dephosphorylation initiates with a delay after the addition of KaiB. B) The KaiC phosphorylation dynamics remain invariant when equally over- or underexpressing the Kai proteins. C) When putting together six KaiABC mixtures in six different phases, the new mixture diplays no transient behavior but immediately initiates dephosphorylation. D) The shape of the oscillations is asymmetric, showing different times of phosphorylation (τ_1) and dephosphorylation (τ_2).

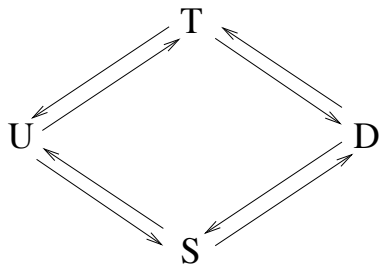

Figure 3.2: Schematic model of the basic phosphorylation dynamics. Due to cooperativity effects, the phosphorylation/dephosphorylation of threonine depends on the phosphorylation state of serine and vice versa. Therefore, eight different rates α_{XY}, described by the arrows, have to be introduced.

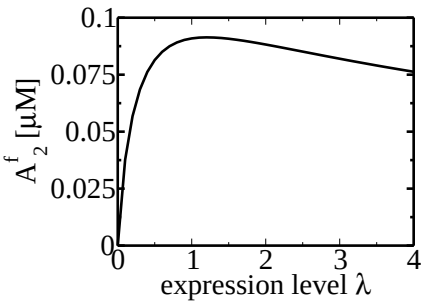

Figure 3.3: The concentration of free KaiA varies only slightly in the interval $\lambda \in [0.5, 4]$. This ensures the preservation of dynamic invariance when varying the expression level.

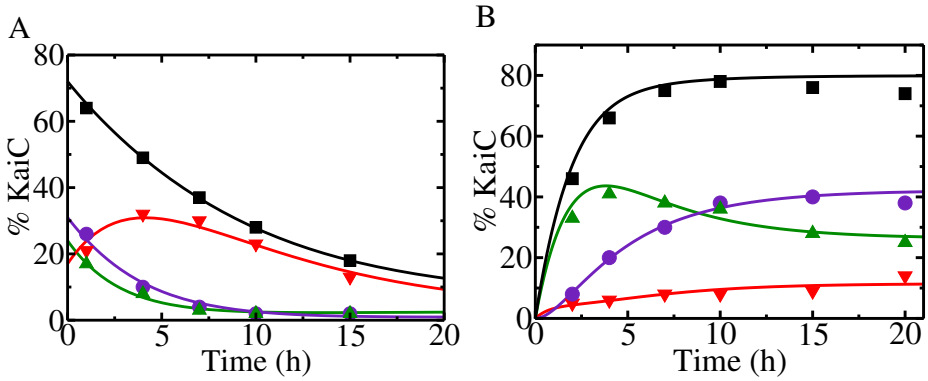

Figure 3.4: Phosphorylation dynamics of KaiC in absence of KaiB. The symbols represent experimental data from (Rust et al., 2007) and the solid lines result from a least square fit to the mathematical model. Shown are the fraction of the different KaiC phospho-forms, threonine phosphorylated (green upward triangles), serine phosphorylated (red downward triangles), double phosphorylated (violet circles), and the total amount of phosphorylated KaiC (black squares). (A) Autonomous dephosphorylation of KaiC in absence of KaiA. (B) KaiC phosphorylation in the presence of KaiA.

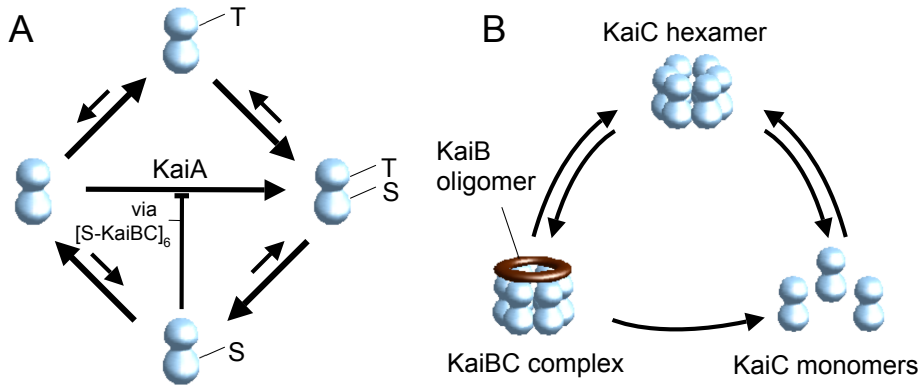

Figure 3.5: Essential states of the KaiABC system included in our modeling approach. (A) Simplified picture of the major transitions between the four phosphorylation states of the KaiC protein, unphosphorylated (U), serine phosphorylated (S), threonine phosphorylated (T) and both residues phosphorylated (D). Autophosphorylation of KaiC is enhanced by KaiA whose activity is inhibited by only serine phosphorylated KaiBC complexes $[\text{S-KaiBC}]_6$. (B) Rapid assembly and disassembly of KaiC hexamers and KaiBC complexes.

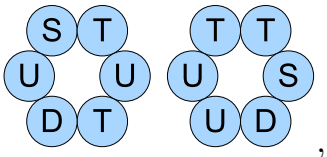

,

Figure 3.6: Two different phosphorylation configurations that are equivalent

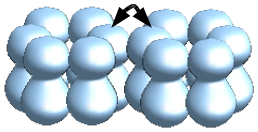

Figure 3.7: Two hexamers interact to exchange a monomer.

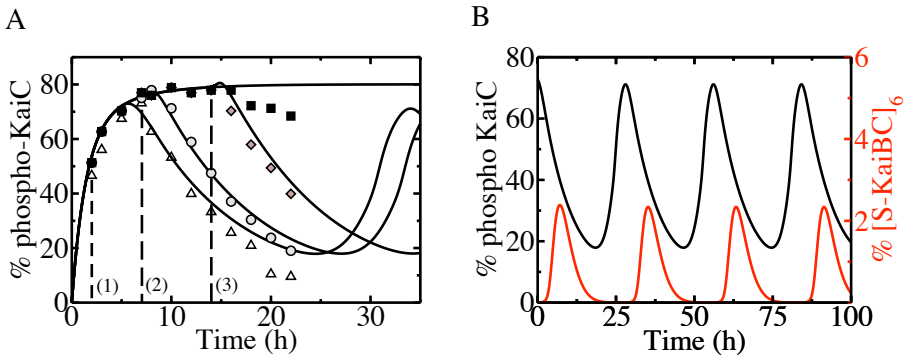

Figure 3.8: (A) Transient KaiC phosphorylation dynamics in presence of KaiA and ATP. Experimental data are taken from (Rust et al., 2007). KaiB is added at times, 2 h ((1), triangles), 7 h ((2), circles) and 14 h ((3), diamonds) after incubation, indicated by dashed lines. Phosphorylation dynamics in absence of KaiB is shown by black squares. Solid lines are the corresponding predictions of the mathematical model. (B) Oscillations in the abundance of only serine phosphorylated KaiBC complexes, $[\text{S-KaiBC}]_6$, (red line), can explain the delayed sudden dephosphorylation dynamics of total phospho-KaiC (black line).

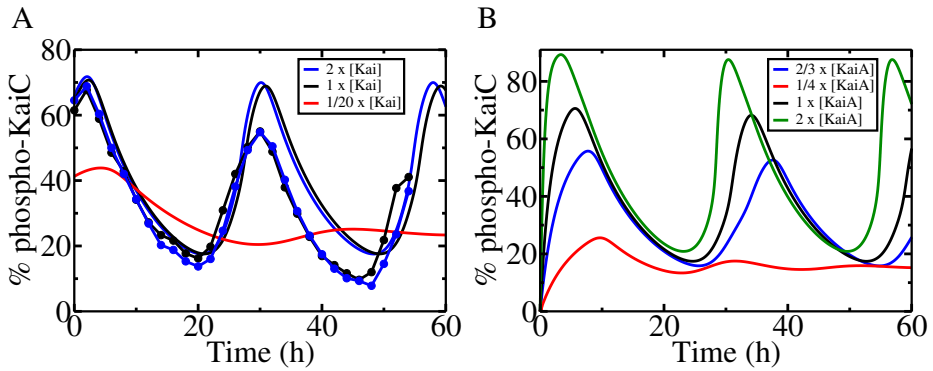

Figure 3.9: Behavior of KaiC phosphorylation dynamics against concentration changes of all Kai proteins. (A) Dynamic invariance of phospho-KaiC against a two-fold concentration change of all proteins as measured by Rust et al, 2007 (filled circles) and the predictions of the mathematical model (solid lines). Loss of oscillatory behavior is found after a 20-fold decrease in Kai concentrations. (B) Sensitivity of KaiC phosphorylation dynamics against changes in KaiA concentrations as predicted from the mathematical model with KaiB and KaiC kept at their standard values.

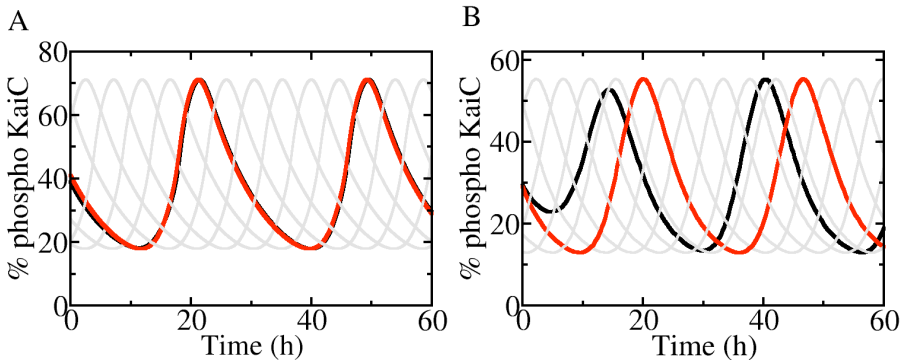

Figure 3.10: Transient KaiC phosphorylation dynamics (black line) resulting from mixing six oscillating samples with equidistant phases that differ by 4 h (gray lines). (A) The phosphorylation dynamics of the mathematical model presented in this work are similar to the experiment by (Ito et al., 2007). (B) An alternative model where KaiBC complexes are stable until they reach a low phosphorylated state ($\beta_i^{\pm} = 0$).

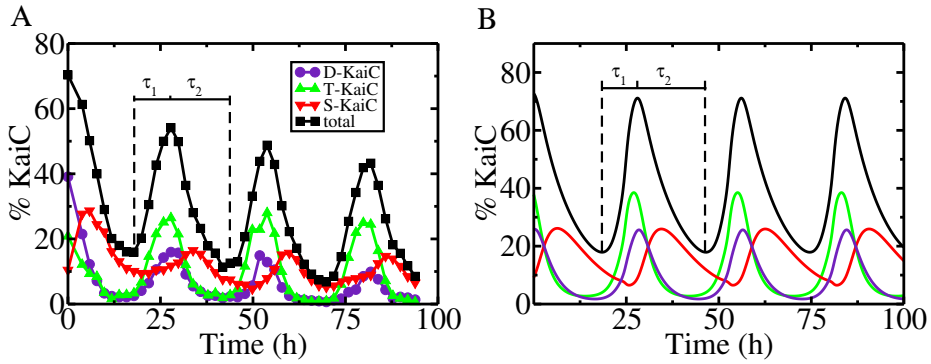

Figure 3.11: Oscillations of the KaiC phospho-forms, threonine phosphorylated (green upward triangles), serine phosphorylated (red downward triangles), double phosphorylated (violet circles), and the total amount of phosphorylated KaiC (black squares). The different durations of the phosphorylation phase ($\tau_1 \approx 9.5$ h) and dephosphorylation phase ($\tau_2 \approx 18.5$ h) lead to an asymmetric position of the peak maximum. (A) Experimental data taken from (Rust et al., 2007). (B) Corresponding phosphorylation dynamics from the mathematical model.

3.5 Native mass spectrometry confirms the theoretical predictions

In this section, the two biochemical prediction from the mathematical model are analyzed by experiments. Thereby, the Kai complexes are measured using native mass spectrometry. The spectra are generated as described in section 2.2.

3.5.1 KaiC has two KaiA binding sites

From the measured spectra, see Figure 2.1, I calculate the intensity of the signal for KaiC and the KaiAC complexes in relation to the total intensity of the spectrum, see Figure 3.12. The experiments show the existence of a significant amount of both free KaiC hexamers ($KaiC_6$) and $KaiA_2C_6$ complexes at every stage of the circadian cycle, with the observed signal for $KaiA_2C_6$ only exceeding that for $KaiC_6$ in the initial phosphorylation phase. The constant sequestration of free KaiA by the $KaiA_2C_6$ complexes is interpreted as the molecular realization of the dynamic invariance condition that requires most of the KaiA to be inactive at every instant of time, regardless of the phosphorylation state. As theoretically predicted, the experiments indicate the existence of two different binding sites for KaiA dimers on a KaiC hexamer, which is supported by both the observation of $KaiA_4C_6$ complexes and the absence of higher order complexes, $KaiA_{2n}C_6$, with $n > 2$. The second binding site would then reflect the KaiA binding domain at the catalytic active center of the KaiC hexamer. Thus, the concentration relation of the low abundance complex

$KaiA_4C_6$ to the total amount of KaiC estimates the relative enhancement of the KaiC autophosphorylation activity. The semi-quantitative time course of the $KaiA_4C_6$ species shows great similarities with the theoretical time course of free KaiA, see Figure (3.14A,B).

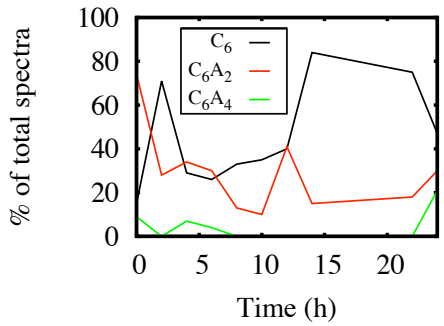

Figure 3.12: The relative mass spectrometry signal of protein complexes as a percentage of the total spectral signal. There is a constant basal amount of KaiA dimers which are sequestrated by KaiC hexamers $[C_6A_2]$ (red line). The $[C_6A_4]$ complexes (green line) indicate the initiation of phosphorylation. The relative amount of KaiC hexamers (black line) is shown for comparison.

3.5.2 Serine phosphorylated KaiBC complexes inactivate KaiA

The relative intensities also show the transient KaiABC complexes $KaiA_6B_2C_6$ and $KaiA_6B_4C_6$, Figure 3.13. However, higher KaiABC complexes are particularly important because they are present throughout the whole dephosphorylation phase, the $KaiA_6B_6C_6$ complex, or because they represent the peak of sequestration, the $KaiA_{10}B_6C_6$ complex.

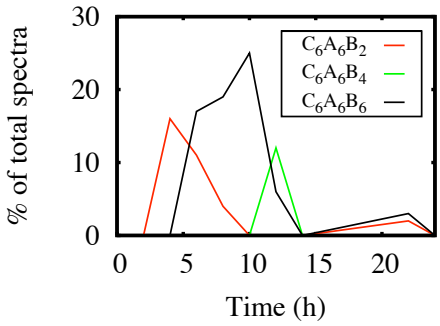

Figure 3.13: Only $[C_6A_6B_6]$ complexes (black line) remain present throughout the dephosphorylation phase. $[C_6A_6B_2]$ (red line) and $[C_6A_6B_6]$ (green line) appear transiently.

The semi-quantitative time courses of the KaiABC complex formation dynamics are compared with the theoretically predicted time courses, Figure 3.14. Comparison of 3.14C with 3.14A shows that the amount of KaiA bound with low affinity to the active center, $KaiA_4C_6$, decreases abruptly if the amount of $KaiA_6B_6C_6$ is raised, thereby confirming the sequestration hypothesis. The time of maximum sequestration - as defined by the appearance of the largest observed sequestration complex $KaiA_{10}B_6C_6$ (Fig. 3.14E) - agrees with the theoretical expected sequestration maximum (Figure 3.14F) where $[S - KaiBC]_6$ is maximal. I speculate that each KaiB within a hexameric KaiBC complex can sequester one KaiA dimer. The abrupt inactivation of KaiA supports the hypothesis that a nonlinear sequestration mechanism is the key driving force of the KaiABC circadian clock.

Moreover, the presence of the largest complex $KaiA_{10}B_6C_6$ shows that there is no oligomerization between different KaiC hexamers, which has been suggested in previous modeling approaches (Emberly and Wingreen, 2006; Mehra et al., 2006).

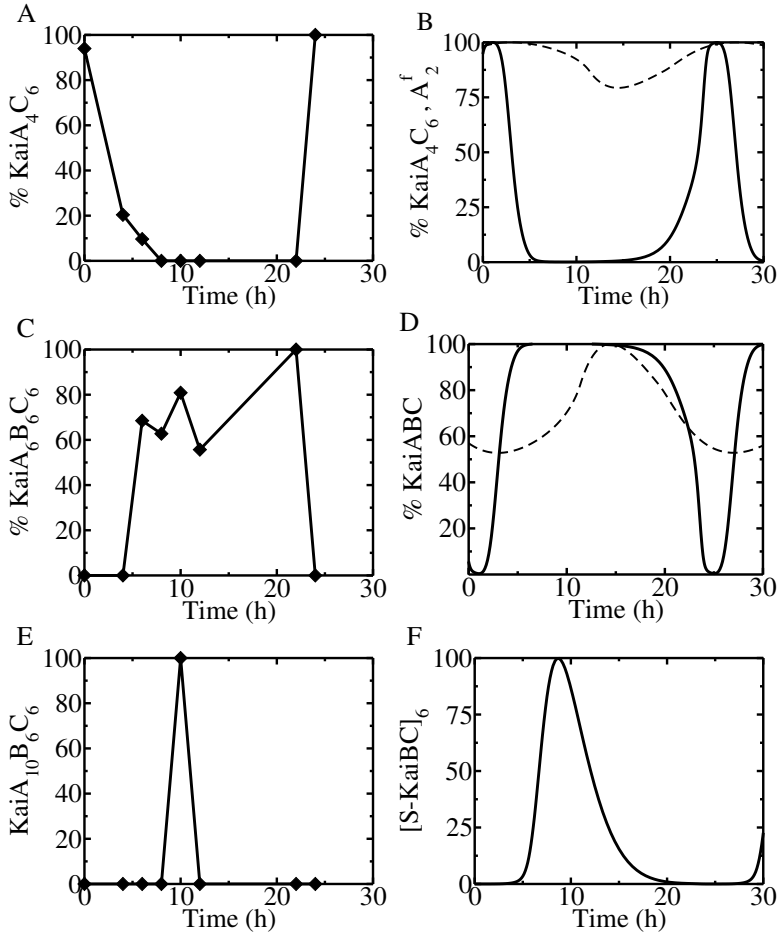

Figure 3.14: Trends of KaiABC complex formation over a circadian period derived from semi-quantitative native mass spectrometry measurements (left panels) in comparison with theoretical predictions (right panels). Results from the mathematical model presented in this work (solid line) and an alternative model of Rust et al, 2007 (dashed line) are shown. The abundances of complexes are drawn relative to their maxima within the circadian cycle. (A) and (B): The phosphorylation phase is determined by the occupancy of the catalytic active site of KaiC hexamers with KaiA as measured by the abundance of $KaiA_4C_6$, which scales linearly with the amount of freely diffusible KaiA. (C) and (D): The dephosphorylation phase is determined by KaiA sequestration due to KaiABC complexes. (E) Time of the KaiA sequestration maximum as indicated by the complex of highest mass, $KaiA_{10}B_6C_6$. (F) Theoretical prediction of the KaiA sequestration maximum by the peak position of $[S\text{-}KaiBC]_6$ at ~ 9.5 h. In (A), (C), (E), the fractional abundance of complexes relates to the relative mass spectrometry signal.

4 The quantitative model explains the defining features of the clock

Both the mathematical and the experimental approach have given strong insight into the mechanism of the cyanobacterial clock. Therefore, the three defining features can be explained in great detail. In this chapter, I explain the biochemical basis of the free-running circadian period. Moreover, the model can be applied to elucidate the trade-off between temperature compensation and temperature entrainment.

4.1 Free-running period

Two different mechanisms assure the free-running phosphorylation cycle of the KaiABC circadian clock. Besides the inherent phosphorylation cycle of KaiC, KaiA and KaiB bind to KaiC in order to switch between phosphorylation and dephosphorylation. Although the phosphorylation reactions themselves are slow (turnover of approximately one phosphor-group per hour per hexamer), fluctuations of the net phosphorylation rates can be expected to be low. Therefore, the phosphorylation punctually reaches a certain threshold level after a given time. The nonlinear feedback

by exclusively serine phosphorylated KaiBC complexes then induces a switch to dephosphorylation of KaiC. This mechanism assures a precise period of approximately 24 hours of the free-running oscillator.

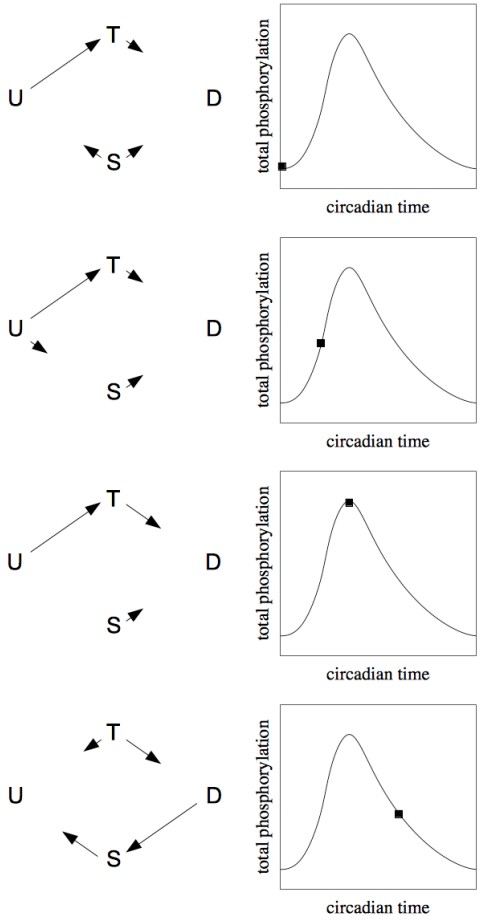

Figure 4.1: The fluxes are drafted at four time points within the circadian cycle. Within each chart, the arrows lengths represent the fluxes semi-quantitatively. Remarkably, synchronization of differently phosphorylated KaiC occurs in every stage, as the fluxes either point to double phosphorylated or unphosphorylated KaiC.

In the model, synchronization of different phosphorylation levels occurs in two steps. First, the abundance of KaiA within the phosphorylation phase yields an accumulation of double phosphorylated KaiC, a lack of KaiA during dephosphorylation leads to an accumulation of unphosphorylated KaiC, see Figure 4.1. Secondly, an exchange of monomers in the dephosphorylation phase synchronizes differently phosphorylated KaiC hexamers.

The given characteristic phosphorylation cycle and the determined synchronization between hexamers in turn implies that the phosphoform distribution completely determines the current state and the subsequent dynamics. This has been shown experimentally (Rust et al., 2007, Figure 1c). The proposed model exactly reproduces the experimental observations, Figure 4.2.

4.2 Temperature compensation

Here, I show that a molecular explanation of temperature compensation and of phase entrainment arises from the previously determined quantitative model. As phosphorylation and dephosphorylation dynamics of KaiC alone and incubated with KaiA do not show significant temperature dependence (Tomita et al., 2005), phase entrainment is likely a consequence of temperature-induced changes in binding constants associated with the various KaiABC complexes. Thermodynamic arguments imply that an increasing temperature will enhance dissociation of KaiA and KaiB from KaiC. Indeed, a reduction in the net complex formation rate for KaiBC and KaiAC upon temperature increase results in the experimentally observed differences in phase response, Figure 4.3. Here, a sudden temperature increase at

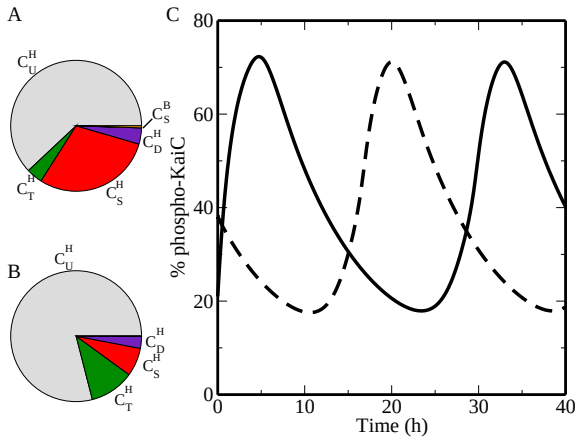

Figure 4.2: The initial condition determines the subsequent behavior (Rust et al., 2007). Serine phosphorylated enriched KaiC, 4% T-KaiC, 4% D-KaiC and 30% serine phosphorylated KaiC (condition A), has been achieved by phosphorylating KaiC with KaiA (18h) and by autodephosphorylating KaiC without KaiA (5.5h). The amount of serine phosphorylated KaiC has to be divided into S-KaiC (29.5%) and S-KaiBC (0.5%). Subsequent dynamics are predicted by the mathematical model (dashed line, C). As has been measured for threonine phosphorylated enriched KaiC, 11% T-KaiC, 3% D-KaiC, 7% S-KaiC (condition B), subsequent phosphorylation is predicted (solid line, C).

the end of the phosphorylation phase leads to a negative phase shift, whereas a temperature increase within the dephosphorylation phase leads to a positive phase shift, as shown by the corresponding phase response curve for positive temperature steps, see Figure 4.3C. This difference leads to phase synchronization of the circadian oscillations that agree excellently with the experimental observations (Yoshida et al., 2009), where the maximum KaiC phosphorylation level aligns with the end of the high temperature phase, Figure 4.4.

To understand the underlying molecular mechanisms in detail, the time evolution equation of the KaiC phospho-form distribution, equation (3.17), is expanded to first order in changes in effective binding constants for KaiBC and KaiAC complexes

$$\partial_t \delta\mathbf{C}(t) = \mathbf{J}(t)\cdot\delta\mathbf{C}(t)+\mathbf{h}_A(t)\delta K_{AC}^D+\mathbf{h}_S(t)\delta c_S+\mathbf{h}_D(t)\delta c_D. \quad (4.1)$$

Here, $\delta\mathbf{C}(t)$, denotes the resulting change of KaiC phosphorylation states upon a temperature-mediated change in the effective KaiA sequestration constant, δK_{AC}^D, and a change in the rates to enter KaiBC complexes, δc_S and δc_D, of serine and double phosphorylated KaiC. The corresponding time-dependent expansion coefficients result in the Jacobi matrix $\mathbf{J}(t)$ and the flux vectors $\mathbf{h}_A(t)$, $\mathbf{h}_S(t)$, and $\mathbf{h}_D(t)$. The formal solution of Eq.(4.1) is given by

$$\delta\mathbf{C}(t) = \int_{t_0}^{t} \mathbf{G}(t,t')\cdot\left\{\mathbf{h}_A(t')\delta K_{AC}^D + \mathbf{h}_S(t')\delta c_S + \mathbf{h}_D(t')\delta c_D\right\} dt' \quad (4.2)$$

with t_0 the time when the temperature step has occurred. In equation (4.2), effects of changes in δK_{AC}^D, δc_S and δc_D at time t' on the current deviation in phospho-form distribution, $\delta\mathbf{C}(t)$, are determined by the time ordered matrix propagator $\mathbf{G}(t,t') := \exp\left[\int_{t'}^{t}\mathbf{J}(t'')dt''\right]$. If temperature changes would affect only one of the three rate constants then a change in period would be the consequence, as the time integral in equation (4.2) shifts the phase by the same distance for any subsequent circadian cycle. For example, a temperature induced reduction in the amount of only serine phosphorylated KaiBC complexes, $\delta c_S < 0$, shortens the dephosphorylation phase as KaiA

inactivation terminates earlier and thereby reduces the circadian period, see Figure 4.3A.

As the circadian period is temperature-compensated, $\delta\mathbf{C}$ must satisfy the relation $\delta\mathbf{C}(t_1) = \delta\mathbf{C}(t_1 + nT_C)$ for all cycles $n \in \{1, 2, ..\}$. Here t_1 denotes the time when the resulting transients from a temperature change have declined and T_C denotes the circadian period. This relation demands that upon temperature increase the shortened circadian period resulting from both dissociation of KaiA from KaiC, $\delta K_{AC}^D > 0$, and from the reduction in serine phosphorylated KaiBC complexes, $\delta c_S < 0$, must be precisely compensated by the prolonged circadian period resulting from a reduction of double phosphorylated KaiBC complexes, $\delta c_D < 0$. The prolonged phase can be explained by the fact that KaiBC complexes can only dephosphorylate and a reduced transition to double phosphorylated KaiBC complexes results in a reduced amount of only serine phosphorylated KaiC and thus transition to the dephosphorylation phase is delayed. The determined values of δK_{AC}^D, δc_S and δc_D are described in the Appendix 3.

It is interesting to see that the rate c_D that had to be introduced into the mathematical model to arrive at a quantitative description of the experimental data now turns out to be essential to explain the observed temperature independence of the circadian period. I emphasize that the temperature dependence of the three rates, K_{AC}^D, c_S, and c_D are fixed by the experimentally determined maximum and minimum phase shifts and the temperature invariance of the period. Thus, the temperature compensation of the KaiABC circadian clock follows one of the earliest proposed mechanisms – the cancellation of opposing effects on the circadian period (Hastings and Sweeney, 1957).

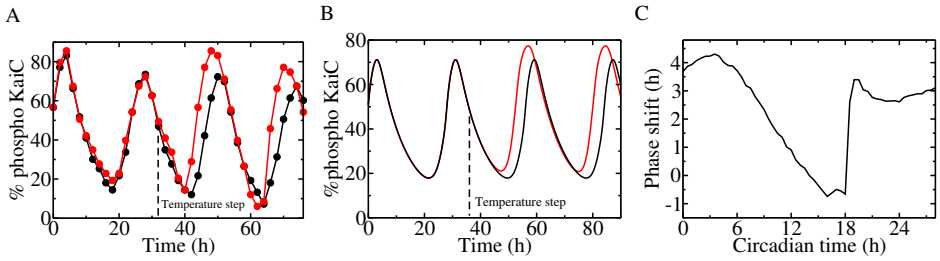

Figure 4.3: Phase shift of the KaiC phosphorylation dynamics after a sudden temperature increase from 30°C to 45°C within the dephosphorylation phase as indicated by the dashed line. (A) Experimental data (Yoshida et al., 2009) for 30°C (black line) and 45°C (red line). (B) Corresponding phosphorylation dynamics of panel (A) as predicted by the mathematical model. (C) Theoretically predicted phase response curve, calculated from phase shifts in the peak maxima for a 28 h period. The peaks of phospho-KaiC can be found on the circadian time scale at 18.5h for a 28h period (Rust et al., 2007) and 16 h for a 24 h period (Yoshida et al., 2009).

Strikingly, the rapid phase shift observed in experiments and theory around the circadian time 18 h (Figure 4.3C) has the same origin as the sudden switching from the phosphorylation phase to the dephosphorylation phase after KaiB addition, see Figure 3.8A. In both cases the nonlinear feedback of KaiA inactivation results in an all-or-none behavior that in my model is attributed to only serine phosphorylated KaiBC complexes. Thus, the existence of a nonlinear feedback follows also from Figure 4.3A and Figure 4.3B, where a sudden temperature increase leads to an abrupt change in phosphorylation dynamics after a time delay of several hours.

4.3 Phase entrainment

The anticipation to cyclic changes in the environment such as light or temperature has been observed to be a fundamental characteristic of circadian clocks. Due to time shifts, the internal clock has to be entrained by external zeitgebers. Even the *in vitro* KaiABC clockwork adapts to environmental cues by entrainment of the KaiC phosphorylation kinetics to temperature cycles (Yoshida et al., 2009).

The entrainment to a shifted external phase can be explained by the response of phosphorylated KaiC to rhythmic temperature changes. An increase in temperature leads to three different phase perturbations of phosphorylated KaiC, according to the three perturbed parameters $\delta K_{AC}^D, \delta c_S, \delta c_D$. However, a clock within a shifted external rhythm of high and low temperature only senses one or two perturbations during the day. These fewer perturbations do not compensate, but induce a positive or a negative phase shift within one day. Continuing phase shifts then lead to phase entrainment. I have performed a simulation of phase entrainment, see Figure 4.4, using the temperature perturbations from the Appendix 3. This simulation corresponds to the experimental observations (Yoshida et al., 2009).

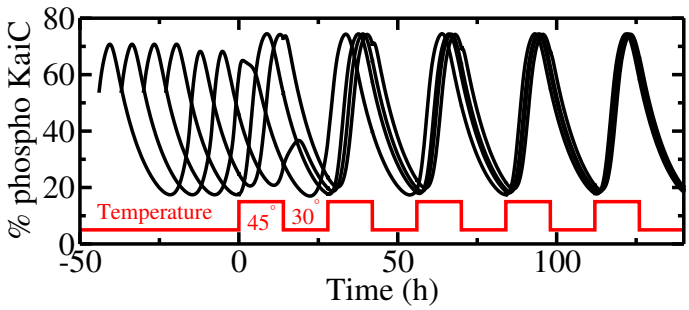

Figure 4.4: Phase synchronization dynamics of the KaiC phosphorylation level due to rhythmic temperature changes given by 12h phases of low temperature (30°C) and high temperature (45°C), respectively. Shown are the trajectories as predicted by the mathematical model for four different initial phases.

5 Evolutionary constraints have shaped the KaiABC clock

Cyanobacteria are ideally suitable for studying the evolution of circadian clocks because they are among the simplest and earliest organisms that have evolved daily rhythms. It has been shown, that this clock has evolved independently from eucaryotic circadian clocks (Rosbash, 2009). The most probable scenario for the development of the cyanobacterial circadian clock is an evolution in gradual steps (Simons, 2009). A light induced chromosome compaction, protecting the DNA from damaging effects of ultraviolet radiation, represents a simple masking mechanism, which likely came first. In succession, the anticipation of light in the morning, allowing to prepare for photosynthesis, provided another benefit which has led to the evolution of an hourglass mechanism. This mechanism enables KaiC to switch between slow phosphorylation and slow dephosphorylation in the presence and absence of ATP (Hayashi et al., 2006; Kageyama et al., 2006). According to Simons, it became important to temporally separate between nitrogen fixation and photosynthesis after the oxygenation of the atmosphere. This additional selection pressure has contributed to the evolution of the circadian oscillator in phototrophic organisms.

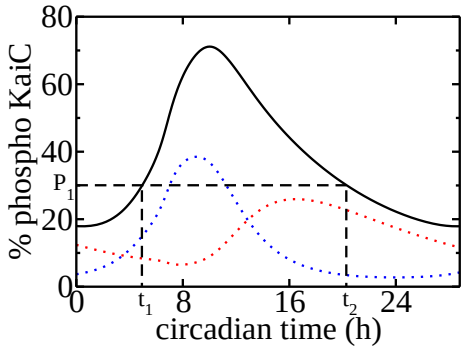

Figure 5.1: The clock cannot anticipate a specific circadian time, if the total phosphorylation is the only physiologically important variable. One phosphorylation concentration P_1 may refer to two time points t_1, t_2. However, all times can be distinguished if two phosphorylated states are included, e.g. T (blue dots) and S (red dots).

In this chapter, I follow the hypothesis that the reaction parameters can be determined deductively by applying one simple evolutionary constraint: The KaiABC circadian clock has evolved in order to correctly predict the time throughout the day. This hypothesis implies that the circadian time must be represented by two protein concentrations because the concentration of a single oscillating protein may refer to two different time points, see Figure 5.1. I therefore assume that KaiC phosphorylates at the two residues serine 431 and threonine 432, in order to correctly distinguish between the phosphorylation and the dephosphorylation phase.

These assumptions have been analyzed by *in silico* evolution. For modeling the evolution of the KaiABC circadian clock, I have resumed the previously developed mathematical equations (3.19-3.21) as they represent all experimentally observed Kai complexes. This time, the parameters have not been fitted to the data, but an objective function has been optimized. This function

includes several biochemical constraints which all assure that the bacterium correctly anticipates the time. The clock thereby achieves a well-defined output, which is robust against internal and external noise.

The outlined method of obtaining a quantitative model has been split into three parts according to three different experiments, in order to determine all parameters of the differential equations.

5.1 Basic phosphorylation dynamics

First, the phosphorylation and dephosphorylation dynamics have to be reproduced according to the basic experiments of the O'Shea lab (Rust et al., 2007, fig. 2). These experiments have been reproduced by using the four state model, see Figure 5.2. The phosphorylation rates are composed of a basal and a KaiA-dependent term

$$\alpha_{ij} = \alpha_{ij}^0 + \alpha_{ij}^A A_2^f \tag{5.1}$$

The amount of free KaiA dimers depends on the Michaelis-Menten constant K_j^M and the dissociation constant K_{AC}^D

$$A_2^{free} = \frac{A_2^{tot} - [A_2C_6]_s}{1 + \frac{C_{tot}}{K_j^M}}. \tag{5.2}$$

The constants K_j^M and K_{AC}^D are constraint by the concept of dynamic invariance and therefore can be determined without experimental data.

In order to correctly deduce the phosphorylation dynamics of KaiC, a

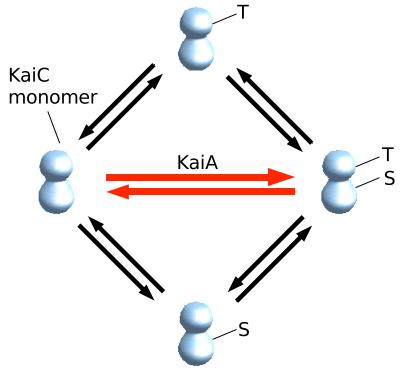

Figure 5.2: On the level of monomers, two different phosphorylation sites of KaiC determine the four states U - unphosphorylated, T - threonine phosphorylated, S - serine phosphorylated, D - double phosphorylated. Due to its enzymatic activity, addition or privation of KaiA alters phosphorylation dynamics.

previous optimization approach has maximized the amplitude $P_{max} - P_{min}$ (Clodong et al., 2007). This constraint is based on the assumption that only one molecule concentration represents the time. In this case, the bacterium would only anticipate circadian times of maximal and minimal phosphorylation because the total concentration is not a unique readout, i.e. an intermediate phosphorylation value P_1 of KaiC may refer to two circadian time points, see Figure 5.1. Consequently, a reliable prediction of phosphorylation and dephosphorylation phases demands the circadian time to be represented by two protein concentrations that distinctively differ. Therefore, the following specific constraints are required:

- During phosphorylation (5 h) T-KaiC must be larger than S-KaiC, $S - T \ll 0$.
- At the time of maximal phosphorylation (10 h) D-KaiC must be larger

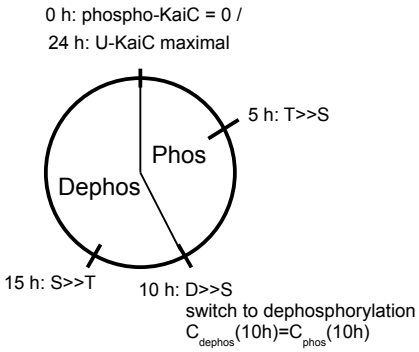

Figure 5.3: The evolutionary constraints are illustrated according to the circadian cycle. Dephosphorylation initiates after $10h$ with the current phosphoform distribution $\mathbf{C}_{dephos}(10h) = \mathbf{C}_{phos}(10h)$.

than S-KaiC, $S - D \ll 0$.

- During dephosphorylation (15 h) S-KaiC must be larger than T-KaiC, $T - S \ll 0$.
- After one circadian cycle (24 h) U-KaiC must be maximal, $-U \ll 0$.

In order to receive parameters that are physiologically reasonable, I introduce the following side conditions:

- The differences $S-T$, $S-D$ and $T-S$ must have all a negative value. In order to avoid that one has such a large value that it compensates a positive value of the other, the differences must have the same value.
- The ATP consumption rate on the phosphorylation binding site is limited. The phoshporylation rates α_{ij}^0 and α_{ij}^A both contribute to the ATP consumption.

The following side conditions are added according to the experimental setup

(Rust et al., 2007, Fig. 2):

- KaiC must start in the unphosphorylated state before inducing KaiA.
- The dephosphorylation must start with the phosphoform distribution after the phosphorylation process at 10 h.

In order to assure that these constraints appropriately contribute to the *in silico* evolution analysis, the weights w_i are introduced. The costfunction can be written as follows

$$\begin{aligned} cost =& w_1(S-T)_{5h} + w_2(S-D)_{10h} + w_3(T-S)_{15h} - w_4 U_{26h} \\ &+ w_5|(S-T)_{5h} - (S-D)_{10h}| + |(S-T)_{5h} - (T-S)_{15h}| \\ &+ \sum_{ij}(w_6)_{ij}\alpha^0_{ij} + \sum_{ij}(w_7)_{ij}\alpha^A_{ij}. \end{aligned} \tag{5.3}$$

The first four constraints are assumed to equally contribute to the fitness of the bacterium $w_1 = w_2 = w_3 = w_4 = 1$ because they all assure a well defined output of the clock. The weight $w_5 = 1$ assures that the three differences have the same value according to the side condition. The constants w_6, w_7 must have a value < 1 because the corresponding cost functions represent minor constraints. They have been set to $w_6 = w_7 = 0.02$.

The minimization of the costfunction reproduces the time courses of both phosphorylating KaiC $\mathbf{C}_{phos}$ and dephosphorylating KaiC $\mathbf{C}_{dephos}$, see

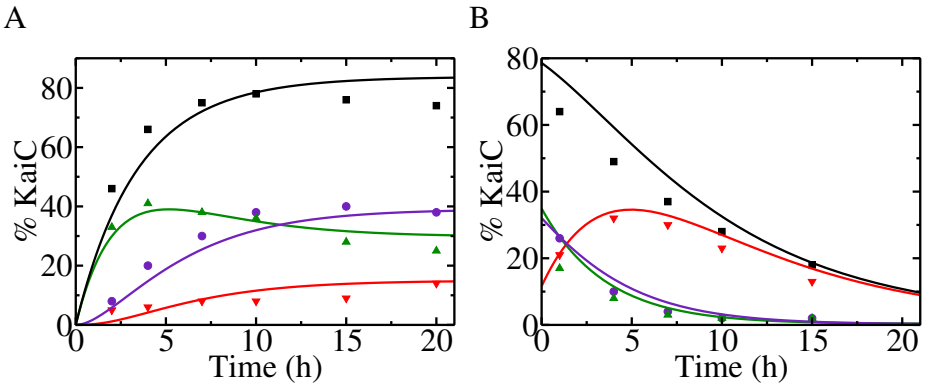

Figure 5.4: Evolutionary constraints elucidate the basic phosphorylation dynamics of (Rust et al., 2007).

Figure 5.4. The following phosphorylation rates have been obtained:

$$\begin{aligned} \alpha^0_{TU} &= 0 & \alpha^0_{UT} &= 0.23h^{-1} \\ \alpha^0_{DT} &= 0.19h^{-1} & \alpha^0_{TD} &= 0 \\ \alpha^0_{DS} &= 0 & \alpha^0_{SD} &= 0.29h^{-1} \\ \alpha^0_{SU} &= 0 & \alpha^0_{US} &= 0.16h^{-1}. \end{aligned}$$

$$\begin{aligned} \alpha^A_{TU} &= 5.15h^{-1}\mu M^{-1} & \alpha^A_{UT} &= 0 \\ \alpha^A_{DT} &= 0 & \alpha^A_{TD} &= 0.83h^{-1}\mu M^{-1} \\ \alpha^A_{DS} &= 6.68h^{-1}\mu M^{-1} & \alpha^A_{SD} &= 0 \\ \alpha^A_{SU} &= 0 & \alpha^A_{US} &= 0. \end{aligned}$$

5.2 The dynamics of hexamer assembly

Second, the dynamics of hexamer assembly and disassembly must be determined, as free KaiC monomers have been detected.

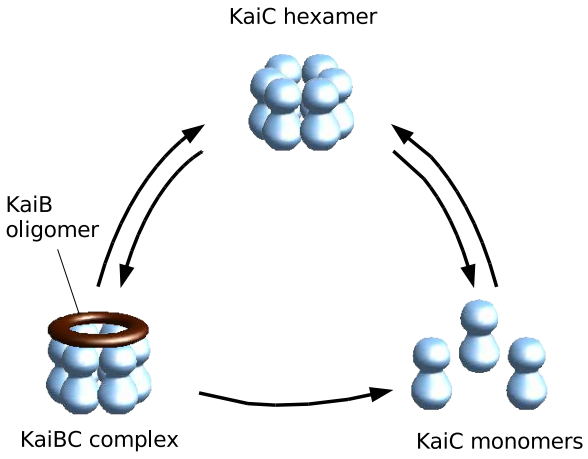

Figure 5.5: Both KaiC hexamers and KaiBC complexes disassemble into monomers with a constant rate γ^{-}. Monomers assemble into KaiC hexamers.

It has been shown in section 2.1 that the concept of dynamic invariance is important. It demands a second KaiA binding site of KaiC and it demands the monomer pool to be small. The KaiC monomer pool has been introduced in order to recover oscillations when mixing different phases *in vitro* (Ito et al., 2007, experiment 1b). This is the observed shuffling mechanism (Kageyama et al., 2006).

Two opposing constraints regulate the assembly and disassembly rates:

- The hexamers must disassemble in a short time such that mixing phosphorylated KaiC with a burst of newly synthesized KaiC does not introduce transient behavior. The transient behavior is represented by $T_{\frac{1}{2}} = \frac{-1}{\gamma^-} \log\left(\frac{1}{2}\right)$. $T_{\frac{1}{2}}$ is the time when 50% of the hexamers are disassembled. The disassembly rate γ^- must be large such that the time $T_{\frac{1}{2}}$ is minimal.
- A large disassembly rate and thus a high turnover rate of KaiC hexamers in turn demands a high reassembly rate γ^+ of hexamers. This reassembly, however, consumes energy. The assembly and disassembly rates $\gamma^\pm$, therefore must be small.

The time of transient behavior $T_{\frac{1}{2}}$ must be short in comparison to the times of phosphorylation $T_{phos} \approx 10h$ and dephosphorylation $T_{dephos} \approx 16h$. The transient behavior is therefore estimated by $T_{\frac{1}{2}} \approx 1h$. The disassembly rate is calculated to give

$$\gamma^- = 0.69h^{-1}$$

The total amount of monomers C^P_{tot} can be described according to Figure

5.5 by the following differential equation

$$\dot{C}_{tot}^{P} = \gamma^{-} \underbrace{\left(C_{tot}^{H} + C_{tot}^{B}\right)}_{=C_{tot}-C_{tot}^{P}} - \gamma^{+} \left(C_{tot}^{P}\right)^{6}. \tag{5.4}$$

Assuming that the amount of monomers C_{tot}^{P} reaches the steady state value of $\left(C_{tot}^{P}\right)_{st}$ the relation $\gamma^{+}(\gamma^{-})$ can be determined

$$\gamma^{+} = \gamma^{-} \left(\frac{C_{tot}}{\left(C_{tot}^{P}\right)_{st}^{6}} - \frac{1}{\left(C_{tot}^{P}\right)_{st}^{5}} \right). \tag{5.5}$$

In comparison to section 3.3, I approximate the total concentration of the monomer pool by $\left(C_{tot}^{P}\right) \approx 5\% C_{tot}$.

Therefore, the value of γ^{+} can be calculated

$$\gamma^{+} = 8.0 \times 10^{4}.$$

Here, the determination of the parameters depends to a large extent on the approximation $T_{\frac{1}{2}} \approx 1h$. The parameters, therefore, cannot be determined with a greater precision.

5.3 Oscillatory dynamics

Third, the monomer dynamics and the hexamer dynamics must be merged to a quantitative model of the circadian clock. In order to reproduce the experimentally observed oscillations, the inactivation mechanism must be deduced. The observed switch to dephosphorylation is caused by KaiA

sequestration of exclusively serine phosphorylated KaiBC complexes $\left(C_S^B\right)^6$. The optimal maximal amount of complexes is assumed to be $\left(C_S^B\right)^6_{max} = 0.03\mu M$, in order to sequestrate the remaining amount of free KaiA dimers $A_2^f = 0.09\mu M$.

During dephosphorylation, the concentration of free KaiA dimers is decreased such that the phosphorylation dynamics are only determined by the basal rates. The following inequality must hold for each $(i,j) \in (U,T,S,D)$

$$\alpha_{ij}^0 \gg \alpha_{ij}^A \left(A_2^f\right)_{min} \tag{5.6}$$

The smallest basic rate is of order $\alpha^0 = 10^{-2}$, the largest KaiA dependent rate is of order $\alpha^A = 10^1$. The minimal amount of free KaiA dimers can be estimated as

$$\left(A_2^f\right)_{min} \ll 10^{-3}. \tag{5.7}$$

This enables us to determine the sequestration constant K_{AS}^D

$$\left(A_2^f\right)_{min} = \frac{A_2^{tot} - [A_2C_6]_s}{1 + \frac{C_{tot}^H}{K_j^M} + \frac{\left(C_S^B\right)^6_{max}}{K_{AS}^D}} \ll 10^{-3} \quad \Leftrightarrow \quad K_{AS}^D \ll 10^{-4}. \tag{5.8}$$

As an infinitely strong binding of KaiA is not realistic, the dissociation constant is set to

$$K_{AS}^D = 10^{-5}. \tag{5.9}$$

In order to determine the remaining transition rates c, the following additional constraints are included:

- The period of the *in vivo* clock must be circadian. The *in vitro* clock

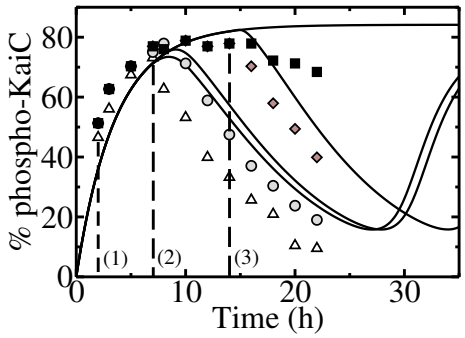

Figure 5.6: The response to KaiB addition of the evolved system is compared to the experimental observations after an addition of KaiB at 2h (triangles), 7h (circles), 14h (diamonds) and no KaiB addition (boxes) (Rust et al., 2007).

shows a period of approximately 26 h (Rust et al., 2007).

- The concentration of $\left(C_S^B\right)^6$ must be maximal, such that they can inactivate a significant amount of A^{free}.

These constraints have been translated into the costfunction

$$cost = |T - 26\text{h}| + 100 \times \left|\left(C_S^B\right)^6_{max} - 0.03\mu M\right|. \qquad (5.10)$$

The following remaining parameters have been determined

$$c_S = 680, c_D = 200, c_U = 0.$$

The transition rate c_U is unidentifiable and therefore has been set to zero.

By applying these general optimization constraints, I reproduced the experimentally observed response to KaiB addition, Figure 5.6, and the final oscillations, Figure 5.7.

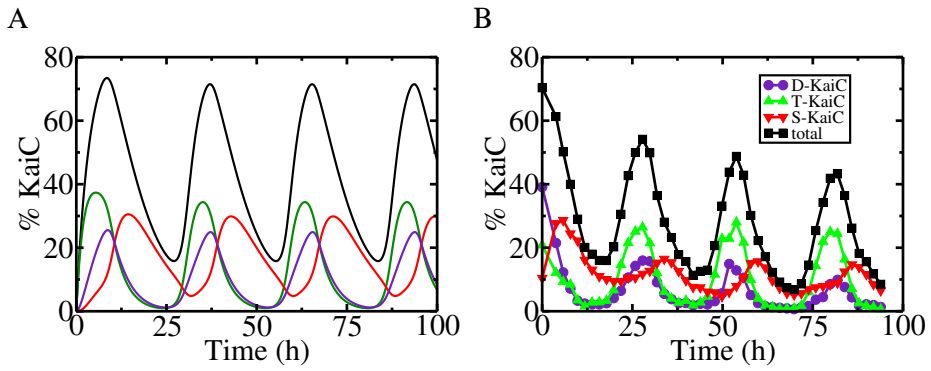

Figure 5.7: Oscillations obtained by the evolutionary constraints (A) are compared to the corresponding experimental result (B) (Rust et al., 2007).

The consistent reproduction of the experiments strongly supports the initial assumption. The two phosphorylatable amino acids serine 431 and threonine 432 have evolved in order to uniquely predict the circadian time. Moreover, the analysis affirms the importance of the constraints I used to select the objective function. The *in silico* evolution shows that a rapid synchronization of differently phosphorylated KaiC and a small pool of KaiC monomers increase robustness and precision of the KaiABC circadian clock and thus provide an advantage for the cyanobacterium.

6 Conclusions and discussion

6.1 Conclusions

The cyanobacterial circadian clock is composed of coupled oscillators. The KaiABC oscillator is the simplest circadian oscillator of living systems, which displays the three defining principles (free-running period of 24 hours, temperature compensation and phase entrainment). This core oscillator originates from the interaction of only three proteins, KaiA, KaiB and KaiC and, therefore, is subject of numerous experimental and computational studies. In my thesis, I investigated the mechanism of the KaiABC oscillator by analyzing the synchronization of KaiC phosphorylation using mathematical modeling in combination with experimental data from native mass spectrometry. Building on these results, the molecular mechanism of the three defining principles becomes comprehensible. Moreover, the modelling results give an insight into the dominating evolutionary selection pressures. This thesis emphasizes the importance of the four phosphorylated states of KaiC, as they assure the performance of the core oscillator and represent an important evolutionary advantage for cyanobacteria.

In order to investigate the KaiABC circadian clock, I developed an appropriate

mathematical abstraction level. The most important constraint of the mathematical model is the observed robustness of KaiC phosphorylation to varying total protein consentrations of KaiABC (dynamic invariance). Therefore, the transition rates of the mathematical model must fulfill simple rules I have deduced in section 2.1. The mathematical equations predict molecular properties of the Kai proteins. In order to confirm these predictions experimentally, I have analyzed time courses of the KaiABC complexes, which have been generated using native mass spectrometry. This novel methodology allows us to investigate the stoichiometry of intact protein complexes. A deficiency arises as the phosphorylated state of KaiC (serine or threonine phosphorylated) could not be determined directly in the experiments. Moreover, the time courses of the Kai species, which have been deduced from the spectra, are only semi-quantitative because it is not possible to characterize all peaks of the spectra. However, the semi-quantitative curves of the Kai complexes indicates the circadian time of maximal concentration changes. This circadian time can be linked to the phosphorylated state of KaiC.

Using these computational and experimental methodologies, I determined the mechanism of the core oscillator of cyanobacteria. In order to fulfill the experimental constraints, the model must include two biochemical properties. First, the circadian clock is based on rhythms of phosphorylation and dephosphorylation of KaiC. Free KaiA increases the activity of autophosphorylation and autodephosphorylation. The amount of free diffusible KaiA dimers must remain constant when varying the total Kai concentrations concertedly, such that the principle of dynamic invariance is fulfilled. At the molecular level, the constant level of free KaiA is assured by two KaiA

binding sites of KaiC. Besides a KaiA binding site, which is responsible for increasing the autophosphorylation activity, KaiC constantly binds a large fraction of KaiA at a second binding site. This second binding site is an important theoretical prediction I concluded from the model. Second, to meet the requirement of KaiB induced dephosphorylation, the model must include a highly non-linear feedback loop. The feedback originates from an accumulation of exclusively serine phosphorylated KaiBC complexes, which sequestrate KaiA. This sequestration feedback represents another theoretical prediction. Both predictions have been affirmed in the experiments of native mass spectrometry.

The mathematical model I determined answers further questions that are addressed in this thesis. In the presence of KaiA, KaiC phosphorylates. An accumulation of double phosphorylated KaiC occurs and a formation of KaiBC complexes occurs. The following KaiA inactivation induces dephosphorylation, which leads to an accumulation of unphosphorylated KaiC. Therefore, the nonlinear sequestration feedback represents the key synchronization mechanism, because it induces the system to switch between rapid phosphorylation and dephosphorylation. The observed monomer exchange follows from a disassembly and a rapid reassembly of KaiC hexamers. A direct exchange of monomers between two interacting hexamers can be excluded as complexes of two hexamers have not been observed. A shuffling process of KaiC is necessary, in order for the circadian clock to meet the experimental constraint of short transient oscillations when six probes with different phases are mixed (Ito et al., 2007). The model indicates the most important phosphorylation configurations of KaiC hexamers. From the analysis I conclude that hexamers which are exclusively serine or dou-

ble phosphorylated are important, because they promote the formation of KaiBC complexes and therefore induce dephosphorylation. For simplicity, I focused on the two most extreme configurations ($[S^6 - KaiC]$ and $[D^6 - KaiC]$) in the mathematical model. They strongly regulate the concentration of the KaiA-inactivating complex.

Moreover, the model elucidates the mechanism by which the three defining principles are satisfied. The free running rhythm with a precise period of approximately 24 hours originates from constant and stable phosphorylation and dephosphorylation rates and from a punctual switch between these two processes. This precise phosphorylation switch follows from the nonlinear sequestration feedback. The phosphorylation process, therefore, does not switch until phosphorylated KaiC reaches a certain threshold. Temperature compensation follows from different temperature-induced phase shifts I determined. As phosphorylation rates are temperature-compensated (Tomita et al., 2005), I concluded that three dissociation constants for KaiAC and KaiBC complexes must depend on the temperature. The two dissociation constants of KaiBC complexes, representing the binding processes $\left(C_S^H\right)^6 \rightarrow \left(C_S^B\right)^6$ and $\left(C_D^H\right)^6 \rightarrow \left(C_D^B\right)^6$ are crucial for temperature compensation, as they induce opposing phase shifts. The three phase shifts, which follow from the temperature-induced increase of the three dissociation constants, exactly compensate each other. It is interesting to note that the two dissociation constants of KaiBC complexes have not been introduced to achieve temperature compensation but to quantitatively describe the dynamics of the clock. As an increase in temperature leads to three different phase perturbations, a clock within a shifted external rhythm of high and low temperature only senses a part of these three daily phase

perturbations. These fewer perturbations do not compensate but induce a positive or a negative phase shift. Continuing phase shifts then lead to phase entrainment, which has been observed experimentally (Yoshida et al., 2009).

The obtained computational methods have limitations as the equations are simplified to reduce the computational time. It is, therefore, possible that essential biochemical properties of the system have been ignored. In particular, experimental results that contradict the computational analyses have been observed. From the least squares fit to the data, it follows that KaiA increases the autophosphorylation rate from S-KaiC to double phosphorylated KaiC. This is a strong contrast to experiments involving phosphomimetic mutants (Nishiwaki et al., 2007). In these experiments, however, the corresponding KaiC monomers of the KaiC mutants are all constantly phosphorylated at their serine residues within the hexamer, which does not correspond to the native state. Moreover, in this thesis I give evidence that these exclusively serine phosphorylated hexamers have specific binding properties. It is therefore questionable whether phosphomimetic mutants reproduce the phosphorylation kinetics of the heterogeneously phosphorylated hexamers.

In chapter 5, I have shown that the evolutionary constraint of correctly anticipating the circadian time explains important biochemical properties of the oscillator. This is an important step to understand the evolution of the cyanobacterial KaiABC circadian clock. The *in silico* evolution analysis has shown that two phosphorylatable residues within the monomer provide an evolutionary benefit in comparison to a single phosphor binding site and that a simple phosphorylation chain from unphosphorylated to sixfold

phosphorylated hexamers does not fully determine the time. Therefore, two different concentrations must be compared in order for the organism to uniquely determine the time. The *in silico* evolution analysis has reconstituted the model that has been determined in chapter 3, by minimizing an objective function instead of performing a least squares fit. It demonstrates that the distribution of differently phosphorylated KaiC is optimized for clearly indicating the circadian time.

6.2 Outlook

We can think of multiple questions which have not been analyzed in this thesis. They are important for further understanding the cyanobacterial circadian clock.

In order to explain the trade-off between temperature compensation and temperature entrainment, temperature-dependent changes of the Kai complexes have been predicted by thermodynamical considerations. A direct experimental proof of the proposed temperature dependence of the Kai complexes, however, remains to be analyzed.

In addition to the evolutionary analysis, I further assume that the duration of phase entrainment represents an evolutionary optimum, which could be calculated in an extended study of *in silico* evolution. If cyanobacteria are frequently carried over large distances by ocean currents, bacteria rapidly have to adapt to the shifted circadian rhythm. Simultaneously, they have to retain their original rhythm if the environmental changes only represent temporary random fluctuations of the external zeitgeber, e.g. light and temperature. More fundamentally, it is not clear if a clock provides a

benefit for the species of cyanobacteria. A clockless bacterium, which simply measures the light intensity to rapidly approximate the circadian time, might have a benefit as it saves the costs of a circadian clock. In contrast to the unicellular freshwater cyanobacterium *Synechococcus elongatus*, it has been shown that marine cyanobacteria of the genus *Prochlorococcus* have lost the protein KaiA. Here, KaiC is phosphorylated due to an increased autophosphorylation activity, dephosphorylation is induced by KaiB. Due to the loss of KaiA, the bacteria have lost a free-running circadian clock. Instead, they possess an hourglass mechanism (Axmann et al., 2009). Consequently, the trade-off between the benefit and the costs of a circadian clock may vary within different species of cyanobacteria.

In order to elucidate this question for each species, the evolutionary step from an hourglass mechanism to the emergence of the clock must be reconsidered, which in the future might lead to further experimental and computational efforts. According to (Simons, 2009) the emergence of the clock coincides with the oxygenation of the atmosphere, when nitrogen fixation became important. Nitrogenase must be protected from damage by photosynthetically produced oxygen by a temporal and spatial segragation of nitrogen fixation and photosynthesis (Berman-Frank et al., 2001). To effectively coordinate the experimentally observed temporal segragation, the circadian clock provides an important benefit. More generally, multiple metabolic activities have been hypothesized to favor the generation of a circadian clock (Tu and McKnight, 2006).

As the cyanobacterial circadian clock coordinates gene expression, the mechanism of this coordination represents another interesting problem. It is particularly interesting to investigate how the circadian clock coordinates

metabolic activities. As cyanobacteria are used to produce organic compounds such as toxins and ethanol, an optimization of the metabolism is important for future applications.

Currently, investigations of the cyanobacterial circadian clock focus on the coupling mechanism of the core oscillator to the *kaiBC* promoter and on the origin of the transcription-translation-oscillator (Zwicker et al., 2010). It is particularly interesting to investigate the phosphorylated state of KaiC, which feeds back to the gene expression. The origin of this feedback could be reavealed by comparing the phases of the two oscillators.

The results in this thesis are significant, as novel methodologies have been used to understand the molecular mechanism. Both the mathematical concept of dynamic invariance and the experiments of native mass spectrometry are important for various applications. The principle of dynamic invariance is an essential modeling constraint (section 2.1) and an important evolutionary constraint (chapter 5) for the KaiABC circadian clock. Therefore, I raise the additional hypothesis that this principle is important for a multitude of organisms. It follows that biological clocks and signaling pathways could be determined to a greater extent by searching for invariant properties. Moreover, the mathematical principles could represent an outline to construct invariant modules in synthetic biology. In one of the recent developments, scientists have constructed synthetic model oscillatory systems such as the repressilator (Elowitz and Leibler, 2000). In order to find oscillatory regimes, the research group has complemented the experimental methods by computational analyses. Delayed negative feedback oscillators, in which the period is tunable, have been constructed both in *Escherichia coli* (Stricker et al., 2008; Atkinson et al., 2003) and in mammalian cells (Tigges et al.,

2009).

Recently, more circadian rhythms have been discovered, which deserve closer attention. Using genome-wide expression profiling experiments, (van der Linden et al., 2010) identified oscillating transcripts in worms *Caenorhabditis elegans*, which also fulfill the three defining features of a biological clock. *C. elegans* is regarded as an organism of little complexity, because it has a small genome ($\sim 10^8$ base pairs) in comparison to other eukaryotes. Further studies will therefore elucidate the mechanism and the evolution of this particular biological clock. Another interesting circadian rhythm has been observed in human red blood cells (O'Neill and Reddy, 2011). The rhythms are temperature-compensated and entrainable. Analyses of such clocks of little complexity will facilitate modeling approaches of biological clocks in eukaryotic cells. They will therefore provide insight into the interdependency between circadian clocks and the physiology of various organisms.

Appendix

1 Quantitative model of the KaiABC clock

The standard *in vitro* mixture ($A_{tot} = 1.2\mu M, C_{tot} = 3.5\mu M$) implies that the total amount of KaiA dimers ($(A_2)_{tot} = 0.6\mu M$) is comparable to the amount of KaiC hexamers ($(C_6)_{tot} = 0.58\mu M$).

The dynamic of the circadian clock is described by a system of differential equations

$$\dot{\mathbf{C}} = \mathbf{T} \cdot \mathbf{C}, \tag{1}$$

where the concentrations of the phosphoforms $\mathbf{C} = (C_U, C_T, C_S, C_D)$ have been introduced. The phosphorylation dynamics between the four monomer states of KaiC are described by eight transition rates, see Figure 1, which consist of a basal and a KaiA dependent rate

$$\alpha_{ij} = \alpha_{ij}^0 + \alpha_{ij}^A A_2^f, \quad \alpha_{ij}^A = \frac{\tilde{\alpha}_{ij}^A}{K_j^M}. \tag{2}$$

The amount of free KaiA is decribed by the two binding constants K_j^M and

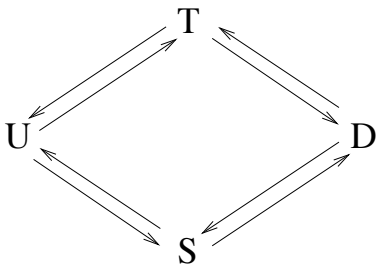

Figure 1: Schematic model of the basic phosphorylation dynamics. Due to cooperativity effects, the phosphorylation/dephosphorylation of threonine is dependent on the phosphorylation state of serine and vice versa. Therefore eight different rates α_{XY}, described by the arrows, have to be introduced.

K_{AC}^{D}.

$$[A_2C_6]_s = \frac{A_2^{tot} + C_6^{tot} + K_{AC}^{D}}{2} - \sqrt{\left(\frac{A_2^{tot} + C_6^{tot} + K_{AC}^{D}}{2}\right)^2 - A_2^{tot}C_6^{tot}}. \tag{3}$$

$$A_2^f = \frac{A_2^{tot} - [A_2C_6]_s}{1 + \frac{C_{tot}}{K_j^M}}. \tag{4}$$

As no quantitative data is available for A_2^f, the amount is determined by looking for dynamic invariant properties of the system. There is experimental evidence that amplitude and frequency do not change for a concerted over- and underexpression of the total amounts of KaiABC $(A^{tot}, B^{tot}, C^{tot}) \rightarrow \lambda(A^{tot}, B^{tot}, C^{tot})$ within a large interval of $\lambda \in [0.5, 4]$ (Rust et al., 2007). Lowering the concentrations of both KaiA and KaiC tenfold, the phosphorylation maxima of the oscillations reduce (Kageyama et al., 2006).

This property demands the concentration of A_2^f to remain constant when varying the expression level $\lambda \in [0.5, 4]$, because the KaiA-dependent phosphorylation rates depend linearly on the amount of A_2^f. This property of free KaiA dimers, see Figure 3.3, is assured by small dissociation constants

$$K_{AC}^D = 0.1\mu M \quad K_j^M = 3\mu M.$$

The dissociation constants determine the amount of $[A_2C_6]_s$ complexes and of free KaiA dimers for the wildtype $(\lambda = 1)$ in the KaiAC system

$$[A_2C_6]_s = 0.39\mu M, \tag{5}$$

$$A_2^f = 0.09\mu M = 15\% A_2^{tot}. \tag{6}$$

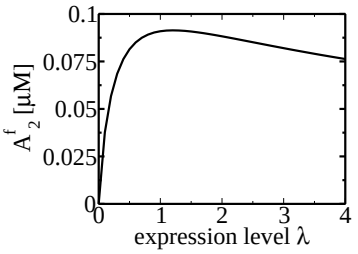

Figure 2: The concentration of free KaiA varies only slightly in the interval $\lambda \in [0.5, 4]$. This ensures the preservation of dynamic invariance when varying the expression level.

In the *in vivo* system, the concentration of free KaiA would be calculated

differently because the total number of KaiA molecules $\tilde{A} \approx 500$ is small against the total number of KaiC molecules $\tilde{C} \approx 10000$ (Kitayama et al., 2003). By assuming $C_6^f \approx C_6^{tot}$ in Eq. 3, the concentration of free KaiA dimers is $A_2^f = \frac{A_2^{tot}}{1+C_{tot}\left(1/K_j^M+1/K_{AC}^D\right)}$. Similarly to the *in vitro* system, dynamic invariance is assured by small dissociation constants.

The data from time course experiments of the O'Shea laboratory (Rust et al., 2007) is employed to determine the unknown parameters of the KaiABC *in vitro* system. To this end, an orders of magnitude range of the parameter values is scanned with a global optimization algorithm. To ensure that the found optimum is not local, the parameter search is repeated from different initial conditions. As for each initial condition the same set of parameters is obtained up to the default tolerance, I confirm that the algorithm has found the global optimum. This advancement enables to explain the results that have been measured, especially the above described four experimental constraints.

Incubation of KaiC together with ATP, Figure (3.4A) in section 3.1, shows the dephosphorylation kinetics of the relative amounts of KaiC monomers that occupy a specific phosphorylated state, i.e. $C_T/C_{tot}, C_S/C_{tot}, C_D/C_{tot}$. I have used a simulated annealing algorithm in order to determine the autophosphorylation rates of the four states model α_{ij}^0. The objective function to be optimized is the sum of the least squares

$$\chi_D^2 = \sum_{\substack{i=U,T,S,D \\ t_n=(1h,4h,7h,10h,15h)}} \left(\frac{C_i(t_n) - C_i^{exp}(t_n)}{\sigma_i} \right)^2 . \qquad (7)$$

The errors σ_i are approximately $0.1 \times C_i(t_n)$. As some of the parameters

are poorly constrained by the data, the sum of the parameters is added to the objective function using a low weight

$$E = \chi_D^2 + 0.1 \times \sum_{ij} \alpha_{ij}^0. \tag{8}$$

This implies that the lowest possible reaction rates are chosen. Low phosphorylation rates can be biologically important because they imply a lower ATP consumption.

In the parameter space $\alpha_{ij} > 0$, the following rates have been determined

$$\begin{aligned} \alpha_{TU}^0 &= 0.01h^{-1} & \alpha_{UT}^0 &= 0.22h^{-1} \\ \alpha_{DT}^0 &= 0.13h^{-1} & \alpha_{TD}^0 &= 0 \\ \alpha_{DS}^0 &= 0 & \alpha_{SD}^0 &= 0.34h^{-1} \\ \alpha_{SU}^0 &= 0 & \alpha_{US}^0 &= 0.12h^{-1}. \end{aligned}$$

For the dephosphorylation experiment, these rates lead to a value of $\chi_D^2 = 0.23$. They agree with the previously published values (Rust et al., 2007).

For modeling the phosphorylation experiment of the KaiAC system (Rust et al., 2007, Figure 2A), again the value of χ^2 is minimized, see Figure (3.4B) in section 3.1

$$\chi_P^2 = \sum_{\substack{i=U,T,S,D \\ t_n=(2h,4h,7h,10h,15h,20h)}} \left(\frac{C_i(t_n) - C_i^{exp}(t_n)}{\sigma_i} \right)^2. \tag{9}$$

In the experiments of the O'Shea lab (Rust et al., 2007, Fig. 2A, 3D), it can be seen that phosphorylation dynamics seem to interfere with protein degradation. This effect leads to a non-constant asymptotic behavior of the

phosphorylation dynamics, which is not included in our modeling approach. In addition to the objective function (8), the total phosphorylation is reqired to reach a maximum of 80% phosphorylated KaiC

$$E = \chi_P^2 + 10 \times \left| \frac{(C_T + C_S + C_D)^{max}}{C_{tot}} - 0.8 \right| + 0.1 \times \sum_{ij} \alpha_{ij}^A. \quad (10)$$

The following parameters have been determined

$$\begin{aligned} \alpha_{TU}^A &= 3.9 h^{-1}\mu M^{-1} & \alpha_{UT}^A &= 0 \\ \alpha_{DT}^A &= 0 & \alpha_{TD}^A &= 0.5 h^{-1}\mu M^{-1} \\ \alpha_{DS}^A &= 10.9 h^{-1}\mu M^{-1} & \alpha_{SD}^A &= 0 \\ \alpha_{SU}^A &= 0.6 h^{-1}\mu M^{-1} & \alpha_{US}^A &= 0.6 h^{-1}\mu M^{-1}. \end{aligned}$$

For the dephosphorylation experiment, these rates lead to a value of $\chi_P^2 = 0.51$.

In the model, KaiA effectively increases dephosphorylation by the values $\alpha_{US}^A = 0.6 h^{-1}\mu M^{-1}$ and $\alpha_{TD}^A = 0.5 h^{-1}\mu M^{-1}$. On the one hand, this value could indicate a bifunctional behavior of KaiA. On the other hand, this might reflect unknown cooperative interactions in the dephosphorylation of hexamers that is not included in our monomer based reaction model. If all dephosphorylation enhancing rates are set to zero, a value of $\chi_P^2 = 1.84$ is achieved.

The analysis of phosphomimetic mutants (Nishiwaki et al., 2007) has suggested that the KaiA-dependent parameters $\alpha_{SU}^A, \alpha_{TD}^A$ and α_{DS}^A must be set to zero. If the rates $\alpha_{SU}^A, \alpha_{TD}^A$ are set to zero, the model is still able to explain the phosphorylation experiment, which is illustrated by the value $\chi_P^2 = 1.13$. However, with a rate $\alpha_{DS}^A = 0$, it is not possible

to recover the observed phosphorylation dynamics, which is illustrated by the value $\chi^2_P = 5.47$. As in the analysis of (Rust et al., 2007), the KaiA-mediated rephosphorylation of S-KaiC to D-KaiC $\alpha^A_{DS} = 10.9$ is essential for describing the experiments. I believe, and more scientists agree (Markson and O'Shea, 2009), that phosphomimetic KaiC-DT mutants (Nishiwaki et al., 2007) might not correctly imitate the true phosphoforms because they form hexamers in which all subunits constantly have the same phosphorylation state, i.e. S-KaiC. This is an indication that a sixfold serine phosphorylated KaiC hexamer must have different binding affinities to KaiA than S-KaiC monomers.

With the description of every transition rate as a function of the corresponding monomers, the KaiABC clock can be modeled by a set of nonlinear differential equations

$$\dot{\mathbf{C}}(t) = \mathbf{T} \cdot \mathbf{C}(t). \tag{11}$$

The twelve-dimensional state vector is given by the three pools

$$\mathbf{C} = \left(\mathbf{C}^H, \mathbf{C}^B, \mathbf{C}^P\right). \tag{12}$$

The matrix elements of the transition matrix $\mathbf{T}$ can be subdivided according to the three pools

$$\mathbf{T} = \begin{pmatrix} \mathbf{T}^{HH} & \mathbf{T}^{HB} & \mathbf{T}^{HP} \\ \mathbf{T}^{BH} & \mathbf{T}^{BB} & \mathbf{T}^{BP} \\ \mathbf{T}^{PH} & \mathbf{T}^{PB} & \mathbf{T}^{PP} \end{pmatrix}. \tag{13}$$

The matrices $\mathbf{T}^{kl}$ specify the rates between the pools $\mathbf{C}^l \to \mathbf{C}^k,\ \{k,l\} \in$

$\{H, B, P\}$. The matrices $\mathbf{T}^{kk}$ include the phosphorylation dynamics of the corresponding four state model α_{ij} and the rates that are responsible for the outfluxes of the corresponding pool. The inner dynamics of the $\mathbf{C}^B$ pool are determined by the four states model with $\alpha_{ij}^A = 0$ because KaiB antagonizes the enzymatic effect of KaiA.

$$\mathbf{T}^{HH} = \alpha_{ij} - c_S \left(\frac{C_S^H}{C_{tot}^H}\right)^5 \delta_{SS} - c_D \left(\frac{C_D^H}{C_{tot}^H}\right)^5 \delta_{DD} - \gamma^- \delta_{ii} \tag{14}$$

The transition rate from the $\mathbf{C}^B$-pool to the $\mathbf{C}^H$-pool is similar

$$\mathbf{T}^{HB} = c_U \left(\frac{C_U^B}{C_{tot}^B}\right)^5 \delta_{UU}. \tag{15}$$

$$\mathbf{T}^{HP} = \kappa \left(\frac{C_{tot}^P}{K^P}\right)^5 \delta_{ii} \tag{16}$$

$$\mathbf{T}^{BH} = \frac{c_S}{6} \left(\frac{C_S^H}{C_{tot}^H}\right)^5 \delta_{SS} + \frac{c_D}{6} \left(\frac{C_D^H}{C_{tot}^H}\right)^5 \delta_{DD} \tag{17}$$

$$\mathbf{T}^{BB} = \alpha_{ij}^0 - \frac{c_U}{6} \left(\frac{C_U^B}{C_{tot}^B}\right)^5 \delta_{UU} - \gamma^- \delta_{ii} \tag{18}$$

$$\mathbf{T}^{BP} = 0 \tag{19}$$

$$\mathbf{T}^{PH} = \gamma^- \delta_{ii} \tag{20}$$

$$\mathbf{T}^{PB} = \gamma^{-}\delta_{ii} \tag{21}$$

$$\mathbf{T}^{PP} = -\kappa \left(\frac{C^P_{tot}}{K^P}\right)^5 \delta_{ii} \tag{22}$$

This notation is equivalent to the equations 3.17 which have been introduced in section 3.3.

In the following, the reaction rates between the different pools are determined. The rapid degradation rate of KaiC hexamers can be seen in (Mori et al., 2007, fig. 5B). In this experiment, the time-dependent fraction of KaiC which is part of non-shuffled hexamers C^H_{NS} decays exponentially $C^H_{NS} = e^{-\gamma^- t}$. The hexamer degradation rate is fixed to the experimentally measured value

$$\gamma^- = 0.4h^{-1}.$$

The final parameters $K^D_{AS}, c_U, c_S, c_D, \frac{\kappa}{(K^P)^5}$ determine the period and the amount of the C^B and C^P pool and of the KaiABC complexes. It is difficult to fit the rates to the experiments because few quantitative data of these concentrations exist. A wide range of the parameter space is consistent with the previous experiments because the period is between 24 h (Kondo) and 28 h (Rust) and the response when adding KaiB is within the expected errors.

In order to fully determine the parameters, the following concentrations have to be estimated

- The optimal concentration of $\left(C^B_S\right)^6$ can be estimated by calculating the amount of free KaiA that is sequestrated during dephosphoryla-

tion. The basic level of free diffusible KaiA dimers is approximately $0.09\mu M$, see Equation 6. The experiment of native mass spectrometry, see Figure 3.14C, shows that every $\left(C_S^B\right)^6$ complex sequestrates 3 KaiA dimers on average. Consequently, the maximal concentration of $\left(C_S^B\right)^6$ complexes must be close to $0.03\mu M$.

- On the one hand, the amount of free KaiC monomers C^P must be small because a large monomer pool violates the principle of dynamic invariance. On the other hand, the shuffling mechanism is essential for the molecular clock, so a significant amount of C^P must be present. Here, the value is arbitrarily fixed to $C_{tot}^P = 5\% C_{tot} = 0.175\mu M$.

Obviously, the model has to be consistent with the response of the system when adding KaiB at different times (Rust et al., 2007, fig. 3D). This strongly determines the dissociation constant K_{AS}^D. It is also a test for our initial assumption of a $\left(C_S^B\right)^6$-mediated feedback. The data had to be multiplied by a scaling factor of 0.95 because the phosphorylation is higher than in experiment (Rust et al., 2007, fig. 2A). Analogously to the Eq. (23), the consistency is represented by the value of χ_B^2

$$\chi_B^2 = \sum_{i,t_n} \left(\frac{C_{Phos}^i(t_n) - \left(C_{Phos}^i\right)^{exp}(t_n)}{\sigma_i} \right)^2 , \qquad (23)$$

where $C_{Phos}^i(t_n)$ represents the total phosphorylation at time $t_n = (2h, 7h, 8h, 14h)$ with an addition of KaiB at time $i = (2h, 7h, 14h)$. Again, the errors are approximated by $\sigma_i = 0.1 \times C_{Phos}^i(t_n)$.

Analyzing the phosphorylation and dephosphorylation times of the Kondo lab (Nakajima et al., 2005) and the O'Shea lab (Rust et al., 2007), it can be

seen that the shape of the curves is similar to the individual measurements (Rust et al., 2007, Fig. 2). Hence, a modification of the dissociation constants must result in a changing period. In the following, I illustrate two optimization runs. First, the required period T is close to $T_1 = 24h$ (Kondo lab), secondly it is close to $T_2 = 28h$ (O'Shea lab). The objective function for the simulated annealing algorithm can be written down

$$E = |T - T_{1,2}| + \chi_B^2 + \left|C_{tot}^P - 0.175\right| + \left|\left(C_S^B\right)_{max}^6 - 0.03\right|. \quad (24)$$

For $T, T_1, T_2, C_{tot}^P, \left(C_S^B\right)_{max}^6$ absolute values without the corresponding units $h, \mu M$ have been taken because the costfunction is nondimensional. Due to the stochasticity of the simulated annealing algorithm, the individual components of the costfunction vary during the optimization. Heuristic weights are assigned to these components according to the importance of the corresponding constraints. For the optimization equal weights are assumed.

It turns out that the parameter c_U is not identifiable. Variations of c_U have no effect on the oscillations because unbinding of KaiB occurs via the hexamer disassembly γ^-. Therefore, the transition rate has been set to zero $c_U = 0$. However, the other paramaters are identifiable.

Applying the objective function with a period of $T_1 = 24h$ the following parameters have been obtained

$$\begin{array}{lll} K_{AS}^D = 8 \times 10^{-6}\mu M & \frac{\kappa}{(K^P)^5} = 5 \times 10^4 h^{-1}\mu M^{-5} & \\ c_U = 0 & c_S = 300h^{-1} & c_D = 5400h^{-1}. \end{array} \quad (25)$$

With the rates (25) the following values have been achieved

$$T = 24.01, \quad \chi^2_B = 0.36, \quad \left(C^B_S\right)^6_{max} = 0.005\mu M, \quad C^P_{tot} = 0.05 C_{tot}.$$

Applying the objective function with a period of $T_2 = 28h$ the following parameters have been obtained

$$\begin{array}{lll} K^D_{AS} = 8 \times 10^{-6}\mu M & \frac{\kappa}{(K^P)^5} = 5 \times 10^4 h^{-1}\mu M^{-5} & \\ c_U = 0 & c_S = 1380h^{-1} & c_D = 2420h^{-1}. \end{array} \tag{26}$$

With the rates (26) the following values have been achieved

$$T = 28.02, \quad \chi^2_B = 0.32, \quad \left(C^B_S\right)^6_{max} = 0.013\mu M, \quad C^P_{tot} = 0.05 C_{tot},$$

note that $C_{tot} = C^H_{tot} + C^B_{tot} + C^P_{tot}$.

These two optimizations illustrate the crucial parameters for tuning the period. A larger value of c_S increases the period whereas a larger value of c_D decreases the period. The parameters c_S and c_D are therefore determined by the costs $|T - T_{1,2}|$ and $\left|C^P_{tot} - 0.175\right|$. The large values of c_S, c_D do not lead to a depletion of the substrate because only a few hexamers are able to assemble into KaiBC complexes. They are a consequence of our simplifying assumption of only two transition reactions (3.9), which was necessary in order to assure the identifiablity of the parameters.

The two remaining parameters $\frac{\kappa}{(K^P)^5}$ and K^D_{AS} are strongly determined by the data. The value $\frac{\kappa}{(K^P)^5}$ is determined by the magnitude of the monomer pool. K^D_{AS} is determined by a minimization of χ^2_B because it determines the time delay between the addition of KaiB and the phosphorylation response.

The small value of K_{AS}^D implies that the binding of KaiA to the $\left(C_S^B\right)^6$ hexamer complex is very strong. KaiA only unbinds when a monomer of the complex dephosphorylates or a KaiC-hexamer decays into the monomer pool.

The assumed equal weights have assured that the period T and the amount of KaiC monomers C_{tot}^P are fixed to the assumed value after optimization. The final values of $\chi_B^2 = 0.32$ and $\left|\left(C_S^B\right)_{max}^6 - 0.03\right| = 0.017$ (with the parameters (26)) show that the equal weights in fact have assigned a tenfold larger weight on the minimization of χ_B^2. This is reasonable because the optimal value of $\left(C_S^B\right)_{max}^6$ is only an estimation.

Several fold changes in the weights with similar strengths for the minimization of χ_B^2 as well as different initial parameter estimations lead to the same results (25, 26).

With the parameters (25, 26), the quantitative model of the circadian KaiABC clock is complete. In Figure (3), the dynamics of the three pools are illustrated.

2 A strong nonlinearity assures a perfect phosphorylation switch

In order to reproduce the experimentally observed response to KaiB addition, see Figure 3, the amount of the sequestrating $[S-KaiBC]_6$ concentration must rapidly rise from zero to its maximum, before coming back to zero, see Figure 4. To strengthen the hypothesis of an exclusively $[S-KaiBC]_6$ mediated feedback, I have weakened this constraint by allowing more KaiBC

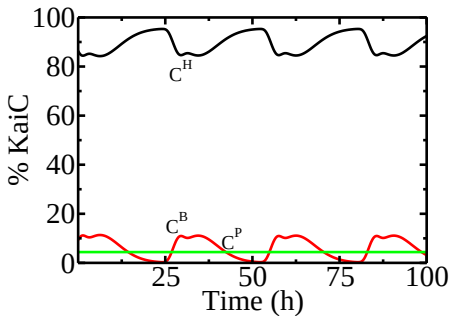

Figure 3: Our model reproduces the experimental values of the three pools. The black line represents the C^H-pool, the red line represents the C^B-pool. The monomer pool C^P (green line) has been fixed to $C^P = 5\% C_{tot}$.

complexes involving S-KaiC to sequestrate KaiA

$$A_2^f = \frac{A_2^{tot} - [A_2C_6]_s}{1 + \frac{C_{tot}^H}{K_j^M} + \frac{C_S^B}{K_{AS}^D}\left(\frac{C_S^B}{C_{tot}^B}\right)^{n-1}}. \tag{27}$$

An optimization with the objective function (24) for $n = 1$ gives us an oscillatory solution, see Figure 4 and the following parameters

$$\begin{array}{lll} K_{AS}^D = 3 * 10^{-5}\mu M & \frac{\kappa}{(K^P)^5} = 10^4 h^{-1}\mu M^{-5} & \\ c_U = 0 & c_S = 105h^{-1} & c_D = 0. \end{array} \tag{28}$$

The values of c_S, c_D are crucial for correctly tuning the oscillator, see section 1. The optimized parameters (28) have revealed that the D-KaiC-mediated binding rate of KaiB must be set to zero $c_D = 0$ in order to obtain oscillations. By allowing only $(C_S^H)^6 \rightarrow (C_S^B)^6$ transitions, the nonlinear behavior of sequestrating concentration C_S^B can be recovered,

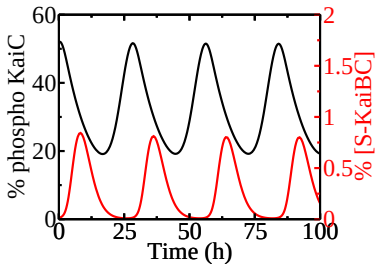

Figure 4: A KaiA sequestration of every S-KaiBC monomer C_S^B (red line) provides an oscillation with an amplitude of $\sim 30\%$ (black line).

i.e. a sharp increase and decrease of the concentration. One can observe that C_{tot}^B has the same nonlinear behavior. However, a strong selectivity of S-KaiC hexamers to KaiB has not been observed in experiments (Rust et al., 2007, Fig. 3C). Therefore, the transition parameters have been set to the constant values (26) while varying the nonlinearity n. As $\frac{\kappa}{(K^P)^5}$ is strongly constrained by $C_{tot}^P = 5\% C_{tot}$ and the value of c_U is not important for the system, we have optimized only K_{AS}^D for any given value of n, see table (29).

$$\begin{array}{lll} n & K_{AS}^D & \chi^2 \\ 6 & 8 \times 10^{-6} \mu M & 0.32 \\ 5 & 1.0 \times 10^{-5} \mu M & 0.41 \\ 4 & 1.5 \times 10^{-5} \mu M & 0.78 \\ 3 & 6.6 \times 10^{-5} \mu M & 0.81 \\ 2 & 2.4 \times 10^{-4} \mu M & 0.92 \\ 1 & 1.3 \times 10^{-3} \mu M & 1.20 \end{array} \tag{29}$$

These results clearly show the importance of a highly nonlinear feedback.

Only a high value of n explains the correct response after KaiB addition (Rust et al., 2007, Fig. 3D). Values of $n \leq 3$ cannot recover oscillations as have been observed in the experiments. This is a strong indication for a $[S - KaiBC]_6$-mediated feedback, although a sequestration by four- or fivefold serine phosphorylated KaiBC hexamers cannot be fully excluded.

3 Simulation of temperature changes

As mentioned in section 4.2, the constants K_{AC}^D, c_S, c_D must be temperature-dependent. For modeling the system at $30°C$, the parameters (26) have been chosen.

Thermodynamic arguments imply that the experimentally analyzed temperature step of $30°C \rightarrow 45°C$ reduces the binding of KaiA and KaiB to KaiC. The corresponding parameters change largely because they depend exponentially on the temperature, given the Arrhenius law. At $45°C$, the system has been modeled with the following parameters

$$\begin{aligned} (c_S)_{45°C} &= \frac{1}{5}\,(c_S)_{30°C}\,, \\ (c_D)_{45°C} &= \frac{1}{20}\,(c_D)_{30°C}\,, \\ \left(K_{AC}^D\right)_{45°C} &= 1.2\left(K_{AC}^D\right)_{30°C}\,. \end{aligned} \tag{30}$$

By introducing the parameter changes

$$\begin{aligned} \delta c_S = (c_S)_{45°C} - (c_S)_{30°C}\,, \delta c_D = (c_D)_{45°C} - (c_D)_{30°C}\,, \\ \delta K_{AC}^D = \left(K_{AC}^D\right)_{45°C} - \left(K_{AC}^D\right)_{30°C}\,, \end{aligned} \tag{31}$$

the time dependent parameters are simulated using the heaviside function $\theta(t)$ for a temperature step at time t_0

$$c_S(t) = (c_S)_{30^\circ C} + \delta c_S \times \theta(t - t_0). \tag{32}$$

The rates $c_D(t)$ and $K_{AC}^D(t)$ have been simulated analogously.

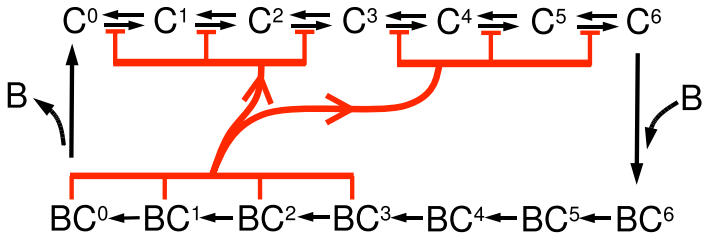

Figure 5: Schematic model of the circadian clock according to Clodong et al.

4 An optimization for large amplitudes

Based on the previous model of the KaiABC circadian clock by (Clodong et al., 2007), see Figure 5, I have determined general principles for achieving high and robust amplitudes.

Here, H_n describes the concentration of the n-fold phosphorylated KaiC hexamer, C_n represents n-fold phosphorylated KaiBC complexes.

The dynamics of the circadian clock are described on the basis of differential equations. The rates $k^+(t), k^-$ denote phosphorylation and dephosphorylation probabilities. $k^+(t)$ is given by the concentration of free KaiA $A^{free}(t)$

$$k^+(t) = \frac{k_A}{K_A} A^{free}(t). \tag{33}$$

The transition to a KaiBC complex, represented by c^+, occurs at the highest phosphorylation state, the inverse transition, represented by c^-, at the lowest phosphorylation state. The transition rates $c^\pm$ are KaiB independent.

The time dependence of the hexamers can be written down

$$\begin{aligned}
\dot{H}_0(t) &= k^- H_1(t) + c^- C_0(t) - k^+(t) H_0(t) \\
\dot{H}_n(t) &= k^+(t) H_{n-1}(t) + k^- H_{n+1}(t) - (k^+(t) + k^-) H_n(t) \quad \forall 0 < n < N \\
\dot{H}_N(t) &= k^+(t) H_{N-1}(t) - (k^- + c^+) H_N(t).
\end{aligned} \tag{34}$$

The dephosphorylation of the complexes is described by equal rates $\tilde{k}^-$

$$\begin{aligned}
\dot{C}_0(t) &= \tilde{k}^- C_1(t) - c^- C_0(t) \\
\dot{C}_n(t) &= \tilde{k}^- C_{n+1}(t) - \tilde{k}^- C_n(t) \\
\dot{C}_N(t) &= c^+ H_N(t) - \tilde{k}^- C_N(t).
\end{aligned} \tag{35}$$

The total concentration of KaiA monomers is the sum of free monomers and of monomers sequestrated by the complexes $C_i, i \in (0, 1, 2, 3)$. The amount of free KaiA is then given by

$$A^{free}(t) = \frac{A^{tot}}{1 + \frac{1}{K} \Sigma_{i=0}^{3} C_i}. \tag{36}$$

Analytical and computational results reveal that several mechanisms contribute to high amplitudes.

4.1 The rate of the conformational change has to be small

Using a global optimization for big amplitudes, it has been found out that the rates of conformational changes have to be small. This can be explained by an intuitive argument. Big amplitudes require that there must be an

accumulation at high phosphorylation states. This accumulation can only be achieved with small rates of conformational changes.

4.2 Multiple phosphorylation sites assure a non-linear behavior

In the following, a maximal difference between highest and lowest phosphorylation level is assumed to be an advantage for the clock. This level can be determined by the amplitude of H_N or equivalently of the weighted sum $\sum_i iH_i/(NH^{tot})$. Therefore, an accumulation at a well-defined state has to be established.

$$\tilde{k}^-, c^\pm \ll k^\pm. \tag{37}$$

This separation of time scales assures that every hexamer is in a highly phosphorylated state before forming KaiBC complexes. The slower rates $\tilde{k}^-, c^\pm$ cause a time delay in the system, which sets the period length of the clock.

The small transition rate c^+ causes high amounts of hexamers and low amounts of complexes which has been proved experimentally

$$C^{tot} \ll H^{tot}, \;\; C_n \ll H_n \tag{38}$$

The assumption (37) is confirmed by the results of an optimization routine for high phosphorylation amplitudes of the dynamical system. In this case a quasi-steady-state approximation can be applied. Setting $\dot{H}_i(t) = 0$ we get

$$H_n(t) = H_0(t) \left(\frac{k^+(t)}{k^-} \right)^n. \tag{39}$$

The normalisation $\sum_{n=0}^{N} H_n(t) = H^{tot}$ has to be required

$$\begin{aligned} H^{tot} &= \sum_{n=0}^{N} H_n(t) = \sum_{n=0}^{N} H_0(t) \left(\frac{k^+(t)}{k^-}\right)^n = H_0(t) \frac{\left(\frac{k^+(t)}{k^-}\right)^{N+1} - 1}{\frac{k^+(t)}{k^-} - 1} \\ &= H_0(t) F[k^+(t)] \end{aligned} \tag{40}$$

where the normalization function $F[k^+(t)]$ has been introduced. Taking equation (39) and replacing $H_0(t)$ as in (40), a sigmoidal function for H_N is obtained

$$\frac{H_N[k^+(t)]}{H^{tot}} = \frac{1}{F[k^+(t)]} \left(\frac{k^+(t)}{k^-}\right)^N. \tag{41}$$

In order to describe recent measurements one has to introduce the total phosphorylation level of KaiC that can be approximated by (38)

$$\frac{\sum_n n(H_n[k^+(t)] + C_n(t))}{N(H^{tot} + C^{tot})} = \frac{\sum_n n H_n[k^+(t)]}{N H^{tot}}. \tag{42}$$

Inserting (39) and (40) into (42) we have a sigmoidal function as well

$$\frac{\sum_n n H_n[k^+(t)]}{N H^{tot}} = \frac{\sum_{n=1}^{N} n \left(\frac{k^+(t)}{k^-}\right)^n}{N F[k^+(t)]}. \tag{43}$$

The switch-like behavior of the equations (41) and (43) are important ingredients of a good oscillator. Their switch-like behavior can be sharpened by increasing N. The parameter k^- varies the switching-point of maximal slope.

The slope is calculated at $k^+(t) = k^-$. Taking the derivative of H_N and

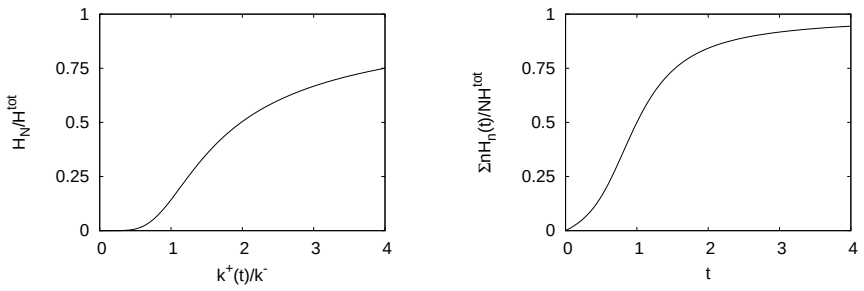

Figure 6: The sigmoidal behavior of $H_N[k^+(t)]$

$\frac{\sum_n nH_n}{NH^{tot}}$, respectively, with respect to $k^+(t)$ and the limit $k^+ \to k^-$ I get

$$\lim_{k^+ \to k^-} \frac{\partial H_N[k^+(t)]}{\partial k^+} = \frac{H^{tot}}{k^-} \left(\frac{N}{N+1} \right). \tag{44}$$

Taking equation (43), the switching-point is at $k^+ = k^-$ in the limit $N \to \infty$. The derivative at this point is

$$\lim_{k^+ \to k^-} \frac{\partial}{\partial k^+(t)} \frac{\sum_n nH_n}{NF[k^+(t)]} = \frac{1}{6k^-} \left[\frac{N}{2} + 1 \right]. \tag{45}$$

Taking arbitrary values of $c^\pm$ with the same order of magnitude as $k^\pm$ it can be shown that the switch-like behavior of $H_N[k^+(t)]$ is maintained at a lower level. The accumulation occurs one step later at C_N. In this case, the switch has a small effect on the oscillations.

4.3 Strong sequestration and multiple phosphorylation steps cause large amplitudes

The time evolution of the complexes follows a poisson process, the explicit solution can be calculated by Laplace Transform of (35)

$$\begin{aligned}\mathcal{L}\{C_0\}(s) &= \tfrac{\tilde{k}^-}{s+c^-}\mathcal{L}\{C_1\}(s)\\ \mathcal{L}\{C_n\}(s) &= \tfrac{\tilde{k}^-}{s+\tilde{k}^-}\mathcal{L}\{C_{n+1}\}(s)\\ \mathcal{L}\{C_N\}(s) &= \tfrac{c^+}{s+\tilde{k}^-}\mathcal{L}\{H_N\}(s)\end{aligned} \tag{46}$$

By succesive insertion we have

$$\begin{aligned}\mathcal{L}\{C_0\}(s) &= \tfrac{\tilde{k}^-}{s+c^-}\left(\tfrac{\tilde{k}^-}{s+\tilde{k}^-}\right)^{N-1}\tfrac{c^+}{s+\tilde{k}^-}\mathcal{L}\{H_N\}(s)\\ \mathcal{L}\{C_n\}(s) &= \left(\tfrac{\tilde{k}^-}{s+\tilde{k}^-}\right)^{N-n}\tfrac{c^+}{s+\tilde{k}^-}\mathcal{L}\{H_N\}(s).\end{aligned} \tag{47}$$

The solution for the complexes is the convolution

$$C_n = G_n * \frac{H_N}{H^{tot}} = \int_{t_0}^{t} G_n(t-t')\frac{H_N(t')}{H^{tot}}dt' \tag{48}$$

with G_n given by

$$G_n(t) = \mathcal{L}^{-1}\left\{\left(\frac{\tilde{k}^-}{s+\tilde{k}^-}\right)^{N-n}\frac{c^+}{s+\tilde{k}^-}\right\}(t) = \frac{1}{(N-n)!}c^+e^{-\tilde{k}t}(\tilde{k}t)^{N-n} \tag{49}$$

and

$$
\begin{aligned}
G_0(t) &= \mathcal{L}^{-1}\left\{\frac{\tilde{k}^-}{s+c^-}\left(\frac{\tilde{k}^-}{s+\tilde{k}^-}\right)^{N-1}\frac{c^+}{s+\tilde{k}^-}\right\}(t) \\
&= \frac{c^+(\tilde{k}^-)^N}{(\tilde{k}^- - c^-)^N}\left[e^{-c^-t} - e^{-\tilde{k}^-t}\sum_{l=0}^{N-1}\frac{(\tilde{k}^- - c^-)^l t^l}{l!}\right].
\end{aligned}
\tag{50}
$$

For a given set of parameters that were found by global optimization for large amplitudes, $G_0(t)$ is plotted.

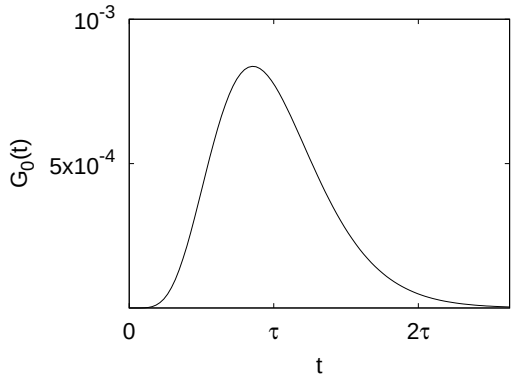

Figure 7: The function $G_0(t)$

Given the assumption (37), the solution for hexamers and complexes (39, 48) with the rate $k^+(t)$ (33, 36) describes exactly the dynamics for the set of differential equations.

4.4 Properties of G_0

In order to find optimal values for $N, \tilde{K}$, the function (48) with the integrand (49) has to be simplified. $G_0(t)$ represents the distribution of the time delay for the complex running from H_N to C_0. This distribution is not normalized $\int_0^\infty dt G_0(t) \neq 1$ because not every H_N is transformed into a complex. The normalized distribution is

$$\hat{G}_0(t) = \frac{G_0(t)}{\int_0^\infty dt G_0(t)} = \frac{G_0(t)}{M_0}, \tag{51}$$

where the zeroth moment M_0 has been introduced. This distribution is the inverse Fouriertransform of the corresponding characteristic function, that in turn can be expressed by the cumulants

$$\hat{G}_0(t) = \int \frac{dk}{2\pi} e^{-ikt}\phi(k) = \int \frac{dk}{2\pi} e^{-ikt} e^{ikK_1 - \frac{k^2}{2}K_2 + \dots}. \tag{52}$$

The first cumulant K_1 is the average time delay τ, that can be calculated stepwise. The average time delay for the first step is

$$\tau = \frac{\int_0^\infty dt\, t G_N(t)}{\int_0^\infty dt G_N(t)} = \frac{c^+ \int_0^\infty dt t e^{-\tilde{k}^- t}}{c^+ \int_0^\infty dt e^{-\tilde{k}^- t}} = \frac{1}{\tilde{k}^-} \tag{53}$$

where the following approximation has been used

$$\int_0^\infty dt e^{-at} t^n = \frac{n!}{a^{n+1}}. \tag{54}$$

According to this the average time-delay is the inverse of the degradation rate of the arrival point. Adding the delay times of every step from H_N to

C_0, the time delay is calculated

$$\tau = \frac{N}{\tilde{k}^-} + \frac{1}{c^-}. \tag{55}$$

The average time delay can also be calculated by the expression

$$\tau = \frac{\int_0^\infty dt\, tG_0(t)}{\int_0^\infty dt G_0(t)}. \tag{56}$$

The calculation of the integrals gives

$$\tau = \frac{\frac{1}{(c^-)^2} - \frac{1}{(\tilde{k}^-)^2} \sum_{l=0}^{N-1} (l+1) \left(1 - \frac{c^-}{\tilde{k}^-}\right)^l}{\frac{1}{c^-} - \frac{1}{\tilde{k}^-} \sum_{l=0}^{N-1} \left(1 - \frac{c^-}{\tilde{k}^-}\right)^l}. \tag{57}$$

With $q = 1 - \frac{c^-}{\tilde{k}^-}$ we can write for equation (57)

$$\tau = \frac{\frac{1}{(c^-)^2} - \frac{1}{(\tilde{k}^-)^2} \partial_q q \sum_{l=0}^{N-1} q^l}{\frac{1}{c^-} - \frac{1}{\tilde{k}^-} \sum_{l=0}^{N-1} q^l} = \frac{\frac{1}{(c^-)^2} - \frac{1}{(\tilde{k}^-)^2} \partial_q q \frac{1-q^N}{1-q}}{\frac{1}{c^-} - \frac{1}{\tilde{k}^-} \frac{1-q^N}{1-q}} \tag{58}$$

where the geometric row has been applied. Calculating the derivative, simplifying the expression and inserting again $q = 1 - \frac{c^-}{\tilde{k}^-}$ we get

$$\tau = \frac{N}{\tilde{k}^-} + \frac{1}{c^-}. \tag{59}$$

Secondly, M_0 is calculated

$$\begin{aligned} M_0 = \int_0^\infty dt G_0(t) &= \frac{c^+(\tilde{k}^-)^N}{(\tilde{k}^- - c^-)^N}\left[\frac{1}{c^-} - \frac{1}{\tilde{k}^-}\sum_{l=0}^{N-1}\left(1-\frac{c^-}{\tilde{k}^-}\right)^l\right] \\ &= \frac{c^+(\tilde{k}^-)^N}{(\tilde{k}^- - c^-)^N}\left[\frac{1}{c^-} - \frac{1}{\tilde{k}^-}\frac{1-\left(1-\frac{c^-}{\tilde{k}^-}\right)^N}{1-(1-\frac{c^-}{\tilde{k}^-})}\right] \\ &= \frac{c^+(\tilde{k}^-)^N}{(\tilde{k}^- - c^-)^N}\left[\frac{\left(1-\frac{c^-}{\tilde{k}^-}\right)^N}{c^-}\right] = \frac{c^+}{c^-} \end{aligned} \tag{60}$$

4.5 A simplified model allows for analytical results

$\hat{G}_0(t)$ is approximated by the first cumulant

$$G_0(t) = M_0\hat{G}_0(t) = M_0\int \frac{dk}{2\pi}e^{-ik(t-K_1)} = \frac{c^+}{c^-}\delta(t-\tau). \tag{61}$$

The non-phosphorylated complex can be formulated

$$C_0(t) = \int_{t_0}^t G_0(t-t')\frac{H_N(t')}{H^{tot}}dt' \approx \frac{c^+}{c^-}\frac{H_N(t-\tau)}{H^{tot}}. \tag{62}$$

The simplified equations represent oscillations with a period of $T = 2\tau$, Figure 8.

With this closed set of equations (39, 62) and the rate $k^+(t)$ (33, 36), the

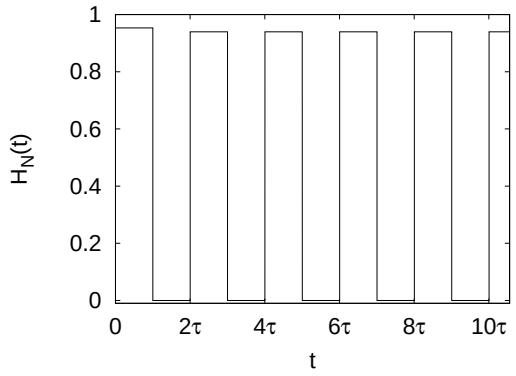

Figure 8: Oscillations of the simplified system

extrema are approximated

$$\begin{aligned} \frac{H_N[k^+(t)]}{H^{tot}} &= \frac{1}{F[k^+(t)]}\left(\frac{k^+(t)}{k^-}\right)^N \\ k^+(t) &= \frac{k_A}{K_A}\frac{A^{tot}}{1+\frac{C_0}{\tilde{K}}} \\ C_0(t) &= \int_{t_0}^{t} G_0(t-t')\frac{H_N(t')}{H^{tot}}dt' \approx \frac{c^+}{c^-}\frac{H_N(t-\tau)}{H^{tot}}. \end{aligned} \tag{63}$$

Since τ is the only time scale of the system, only the discrete time is of interest

$$t_i = i\tau. \tag{64}$$

Given an initial condition, e.g. $H_N(t_i)$ the equations (63) enable to calculate the following values of $H_N(t_j)$ and $C_0(t_j)$. Because of the period $T = 2\tau$, the time step $t_i \rightarrow t_{i+1}$ is a transition $H_N^{max} \rightarrow H_N^{min}$ or conversely

$H_N^{min} \to H_N^{max}$

$$\begin{aligned} \ldots \to \; & (H_N^{max})_i \quad \to \; (C_0^{max})_{i+1} \\ \to \; & \left(H_N^{min}\right)_{i+1} \to \left(C_0^{min}\right)_{i+2} \to (H_N^{max})_{i+2} \to \ldots \end{aligned} \tag{65}$$

A relation $H_N(t_{i+1})[H_N(t_i)]$ can be set up

$$\begin{aligned} H_N(t_{i+1}) \sim \left(\frac{k^+(t)}{k^-}\right)^N &\approx \left(1 + \frac{C_0(t_{i+1})}{\tilde{K}}\right)^{-N} \\ &\approx \left(1 + \frac{C^{tot} H_N(t_i)}{\tilde{K}}\right)^{-N} = F(H_N(t_i)). \end{aligned} \tag{66}$$

with $F(x)$ given by

$$F(x) = \left[1 + \frac{x}{\tilde{K}}\right]^{-N}. \tag{67}$$

A row for the successive maxima and minima are calculated

$$H_N(t_{i+2})[H_N(t_i)] = F\left[F\left[H_N(t_i)\right]\right]. \tag{68}$$

For fixed N and $\tilde{K}$, respectively, steady state values of the amplitude can be found with root finding algorithms.

The function $H^{max}(\tilde{K})$ is decreasing, i.e. smaller values of $\tilde{K}$, $\tilde{K} \ll C_0$, cause larger oscillations, see Figure 9. Of course the condition (37) still has to be valid, $\tilde{k}^- \ll k^+(t)$

$$\Rightarrow \quad C_0 \gg \tilde{K} \gg \frac{C_0}{\frac{k_A A^{tot}}{k^- K \tilde{k}^-} - 1}, \tag{69}$$

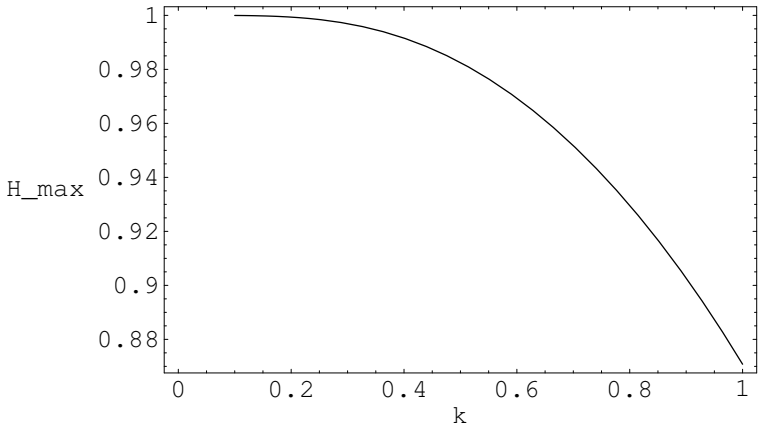

Figure 9: The amplitude depends on the sequestration strength.

where C_0 is of order $\frac{c^+}{c^-}$, see Equation 60.

Similarly, the amplitude of $H_N[k^+(t)]$ is increasing when N increases, see Figure 10.

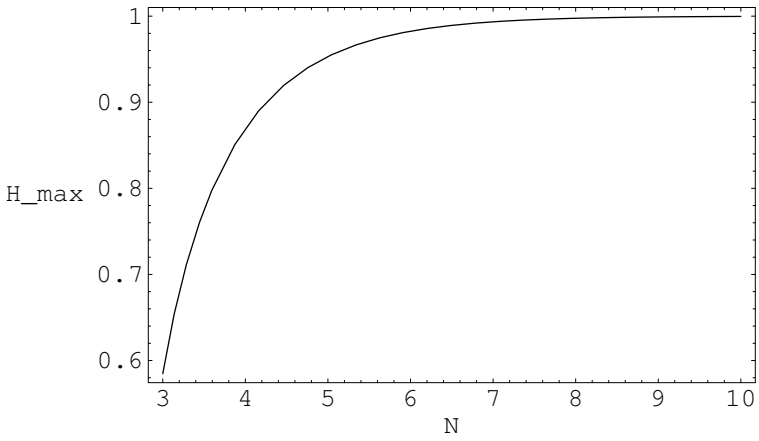

Figure 10: The amplitude depends on the number of phosphorylation sites.

Bibliography

Akiyama, S., Nohara, A., Ito, K., and Maeda, Y. (2008). Assembly and disassembly dynamics of the cyanobacterial periodosome. *Molecular Cell*, 29(6):703--716.

Albrecht, U. (2003). The mammalian circadian clock. *Current Opinion in Genetics & Development*, 13(3):271--277.

Aschoff, J. (1969). Desynchronization and resynchronization of human circadian rhythms. *Aerospace medicine*, 40(8):844--9.

Aschoff, J., Gerecke, U., and Wever, R. (1967). Desynchronization of human circadian rhythms. *The Japanese journal of physiology*, 17(4):450--7.

Aschoff, J. and Pohl, H. (1978). Phase relations between a circadian rhythm and its zeitgeber within the range of entrainment. *Naturwissenschaften*, 65:80--84.

Aschoff, J. and Wever, R. (1976). Human circadian rhythms: a multioscillatory system. *Federation proceedings*, 35(12):236--32.

Atkinson, M. R., Savageau, M. A., Myers, J. T., and Ninfa, A. J. (2003). Development of genetic circuitry exhibiting toggle switch or oscillatory behavior in Escherichia coli. *Cell*, 113(5):597--607.

Axmann, I. M., Dühring, U., Seeliger, L., Arnold, A., Vanselow, J. T., Kramer, A., and Wilde, A. (2009). Biochemical evidence for a timing mechanism in prochlorococcus. *Journal of Bacteriology*, 191(17):5342--5347.

Berman-Frank, I., Lundgren, P., Chen, Y. B., Küpper, H., Kolber, Z., Bergman, B., and Falkowski, P. (2001). Segregation of nitrogen fixation and oxygenic photosynthesis in the marine cyanobacterium Trichodesmium. *Science (New York, N.Y.)*, 294(5546):1534--7.

Brettschneider, C., Rose, R. J., Hertel, S., Axmann, I. M., Heck, A. J. R., and Kollmann, M. (2010). A sequestration feedback determines dynamics and temperature entrainment of the KaiABC circadian clock. *Molecular Systems Biology*, 6:389.

Brown, F. A. and Webb, H. M. (1948). Temperature relations of an endogenous daily rhythmicity in the fiddler crab, Uca. *Physiological zoology*, 21(4):371--381.

Clodong, S., Dühring, U., Kronk, L., Wilde, A., Axmann, I., Herzel, H., and Kollmann, M. (2007). Functioning and robustness of a bacterial circadian clock. *Molecular systems biology*, 3:90.

Dunlap, J. C., Loros, J. J., DeCoursey, P. J., et al. (2004). *Chronobiology: biological timekeeping*. Sinauer Associates Sunderland:.

Eguchi, K., Yoda, M., Terada, T., and Sasai, M. (2008). Mechanism of robust circadian oscillation of KaiC phosphorylation in vitro. *Biophysical Journal*, 95(4):1773--1784.

Elowitz, M. B. and Leibler, S. (2000). A synthetic oscillatory network of transcriptional regulators. *Nature*, 403(6767):335--8.

Emberly, E. and Wingreen, N. S. (2006). Hourglass model for a protein-based circadian oscillator. *Physical review letters*, 96(3):038303.

Goodwin, B. C. (1965). Oscillatory behavior in enzymatic control processes. *Advances in Enzyme Regulation*, 3:425--428, IN1--IN2, 429--430, IN3--IN6, 431--437.

Griffith, J. S. (1968). Mathematics of cellular control processes II. positive feedback to one gene. *Journal of Theoretical Biology*, 20(2):209--216.

Grobbelaar, N., Huang, T., Lin, H., and Chow, T. (1986). Dinitrogen-fixing endogenous rhythm in Synechococcus RF-1. *FEMS Microbiology Letters*, 37(2):173--177.

Gwinner, E. (1977). Circannual rhythms in bird migration. *Annual Review of Ecology and Systematics*, 8:381--405.

Gwinner, E. and Dittami, J. (1990). Endogenous reproductive rhythms in a tropical bird. *Science (New York, N.Y.)*, 249(4971):906--8.

Harmer, S. L., Panda, S., and Kay, S. A. (2001). Molecular bases of circadian rhythms. *Annual review of cell and developmental biology*, 17:215--53.

Hastings, J. W. and Sweeney, B. M. (1957). On the mechanism of temperature independence in a biological clock. *Proceedings of the National Academy of Sciences of the United States of America*, 43(9):804--11.

Hayashi, F., Iwase, R., Uzumaki, T., and Ishiura, M. (2006). Hexamerization by the n-terminal domain and intersubunit phosphorylation by the

c-terminal domain of cyanobacterial circadian clock protein KaiC. *Biochemical and biophysical research communications*, 348(3):864--72.

Heck, A. J. (2008). Native mass spectrometry: a bridge between interactomics and structural biology. *Nat. Methods*, 5:927--933.

Ishiura, M., Kutsuna, S., Aoki, S., Iwasaki, H., Andersson, C. R., Tanabe, A., Golden, S. S., Johnson, C. H., and Kondo, T. (1998). Expression of a gene cluster kaiABC as a circadian feedback process in cyanobacteria. *Science (New York, N.Y.)*, 281(5382):1519--23.

Ito, H., Kageyama, H., Mutsuda, M., Nakajima, M., Oyama, T., and Kondo, T. (2007). Autonomous synchronization of the circadian KaiC phosphorylation rhythm. *Nature structural & molecular biology*, 14(11):1084--8.

Iwasaki, H., Nishiwaki, T., Kitayama, Y., Nakajima, M., and Kondo, T. (2002). KaiA-stimulated KaiC phosphorylation in circadian timing loops in cyanobacteria. *Proceedings of the National Academy of Sciences of the United States of America*, 99(24):15788--93.

Kageyama, H., Kondo, T., and Iwasaki, H. (2003). Circadian formation of clock protein complexes by KaiA, KaiB, KaiC, and SasA in cyanobacteria. *The Journal of biological chemistry*, 278(4):2388--95.

Kageyama, H., Nishiwaki, T., Nakajima, M., Iwasaki, H., Oyama, T., and Kondo, T. (2006). Cyanobacterial circadian pacemaker: Kai protein complex dynamics in the KaiC phosphorylation cycle in vitro. *Molecular cell*, 23(2):161--71.

Kim, Y., Dong, G., Carruthers, C. W., Golden, S. S., and LiWang, A. (2008). The day/night switch in KaiC, a central oscillator component of the circadian clock of cyanobacteria. *Proceedings of the National Academy of Sciences of the United States of America*, 105(35):12825--12830.

Kitayama, Y., Iwasaki, H., Nishiwaki, T., and Kondo, T. (2003). KaiB functions as an attenuator of KaiC phosphorylation in the cyanobacterial circadian clock system. *The EMBO journal*, 22(9):2127--34.

Kitayama, Y., Nishiwaki, T., Terauchi, K., and Kondo, T. (2008). Dual KaiC-based oscillations constitute the circadian system of cyanobacteria. *Genes & Development*, 22(11):1513--21.

Kollmann, M., Lovdok, L., Bartholome, K., Timmer, J., and Sourjik, V. (2005). Design principles of a bacterial signalling network. *Nature*, 438(7067):504--7.

Kondo, T., Strayer, C. A., Kulkarni, R. D., Taylor, W., Ishiura, M., Golden, S. S., and Johnson, C. H. (1993). Circadian rhythms in prokaryotes: luciferase as a reporter of circadian gene expression in cyanobacteria. *Proceedings of the National Academy of Sciences of the United States of America*, 90(12):5672--5676.

Konopka, R. J. and Benzer, S. (1971). Clock mutants of Drosophila melanogaster. *Proceedings of the National Academy of Sciences of the United States of America*, 68(9):2112--6.

Kurosawa, G., Aihara, K., and Iwasa, Y. (2006). A model for the circadian rhythm of cyanobacteria that maintains oscillation without gene expression. *Biophysical journal*, 91(6):2015--23.

Liu, Y., Tsinoremas, N. F., Johnson, C. H., Lebedeva, N. V., Golden, S. S., Ishiura, M., and Kondo, T. (1995). Circadian orchestration of gene expression in cyanobacteria. *Genes Dev.*, 9:1469--1478.

Markson, J. S. and O'Shea, E. K. (2009). The molecular clockwork of a protein-based circadian oscillator. *FEBS Letters*, 583(24):3938--3947.

Mehra, A., Hong, C. I., Shi, M., Loros, J. J., Dunlap, J. C., and Ruoff, P. (2006). Circadian rhythmicity by autocatalysis. *PLoS computational biology*, 2(7):e96.

Mihalcescu, I., Hsing, W., and Leibler, S. (2004). Resilient circadian oscillator revealed in individual cyanobacteria. *Nature*, 430(6995):81--85.

Mori, T., Saveliev, S. V., Xu, Y., Stafford, W. F., Cox, M. M., Inman, R. B., and Johnson, C. H. (2002). Circadian clock protein KaiC forms ATP-dependent hexameric rings and binds DNA. *Proceedings of the National Academy of Sciences*, 99(26):17203--17208.

Mori, T., Williams, D. R., Byrne, M. O., Qin, X., Egli, M., Mchaourab, H. S., Stewart, P. L., and Johnson, C. H. (2007). Elucidating the ticking of an in vitro circadian clockwork. *PLoS biology*, 5(4):e93.

Murakami, R., Miyake, A., Iwase, R., Hayashi, F., Uzumaki, T., and Ishiura, M. (2008). ATPase activity and its temperature compensation of the cyanobacterial clock protein KaiC. *Genes to Cells: Devoted to Molecular & Cellular Mechanisms*, 13(4):387--395.

Nagai, T., Terada, T. P., and Sasai, M. (2010). Synchronization of circadian oscillation of phosphorylation level of KaiC inÂ vitro. *Biophysical Journal*, 98(11):2469--2477.

Nakajima, M., Imai, K., Ito, H., Nishiwaki, T., Murayama, Y., Iwasaki, H., Oyama, T., and Kondo, T. (2005). Reconstitution of circadian oscillation of cyanobacterial KaiC phosphorylation in vitro. *Science*, 308(5720):414--415.

Nishiwaki, T., Iwasaki, H., Ishiura, M., and Kondo, T. (2000). Nucleotide binding and autophosphorylation of the clock protein KaiC as a circadian timing process of cyanobacteria. *Proceedings of the National Academy of Sciences*, 97(1):495--499.

Nishiwaki, T., Satomi, Y., Kitayama, Y., Terauchi, K., Kiyohara, R., Takao, T., and Kondo, T. (2007). A sequential program of dual phosphorylation of KaiC as a basis for circadian rhythm in cyanobacteria. *The EMBO journal*, 26(17):4029--37.

Nishiwaki, T., Satomi, Y., Nakajima, M., Lee, C., Kiyohara, R., Kageyama, H., Kitayama, Y., Temamoto, M., Yamaguchi, A., Hijikata, A., Go, M., Iwasaki, H., Takao, T., and Kondo, T. (2004). Role of KaiC phosphorylation in the circadian clock system of synechococcus elongatus PCC 7942. *Proceedings of the National Academy of Sciences of the United States of America*, 101(38):13927--32.

Novak, B. and Tyson, J. J. (2008). Design principles of biochemical oscillators. *Nature Reviews. Molecular Cell Biology*, 9(12):981--991.

O'Neill, J. S. and Reddy, A. B. (2011). Circadian clocks in human red blood cells. *Nature*, 469(7331):498--503.

Pattanayek, R., Williams, D. R., Pattanayek, S., Mori, T., Johnson, C. H., Stewart, P. L., and Egli, M. (2008). Structural model of the circadian clock

KaiB-KaiC complex and mechanism for modulation of KaiC phosphorylation. *The EMBO Journal*, 27(12):1767--78.

Pattanayek, R., Williams, D. R., Pattanayek, S., Xu, Y., Mori, T., Johnson, C. H., Stewart, P. L., and Egli, M. (2006). Analysis of KaiA-KaiC protein interactions in the cyano-bacterial circadian clock using hybrid structural methods. *The EMBO journal*, 25(9):2017--28.

Pittendrigh, C. S. (1954). On temperature independence in the clock system controlling emergence time in drosophila. *Proceedings of the National Academy of Sciences of the United States of America*, 40:1018--1029.

Qin, X., Byrne, M., Xu, Y., Mori, T., and Johnson, C. H. (2010). Coupling of a core post-translational pacemaker to a slave transcription/translation feedback loop in a circadian system. *PLoS Biol.*, 8:e1000394.

Rosbash, M. (2009). The implications of multiple circadian clock origins. *PLoS biology*, 7(3):e62.

Rust, M. J., Markson, J. S., Lane, W. S., Fisher, D. S., and O'Shea, E. K. (2007). Ordered phosphorylation governs oscillation of a three-protein circadian clock. *Science (New York, N.Y.)*, 318(5851):809--812.

Simons, M. J. P. (2009). The evolution of the cyanobacterial posttranslational clock from a primitive "phoscillator". *Journal of Biological Rhythms*, 24(3):175--182.

Stricker, J., Cookson, S., Bennett, M. R., Mather, W. H., Tsimring, L. S., and Hasty, J. (2008). A fast, robust and tunable synthetic gene oscillator. *Nature*, 456(7221):516--9.

Takigawa-Imamura, H. and Mochizuki, A. (2006). Predicting regulation of the phosphorylation cycle of KaiC clock protein using mathematical analysis. *Journal of biological rhythms*, 21(5):405--16.

Terauchi, K., Kitayama, Y., Nishiwaki, T., Miwa, K., Murayama, Y., Oyama, T., and Kondo, T. (2007). ATPase activity of KaiC determines the basic timing for circadian clock of cyanobacteria. *Proceedings of the National Academy of Sciences*, 104(41):16377--16381.

Tigges, M., Marquez-Lago, T. T., Stelling, J., and Fussenegger, M. (2009). A tunable synthetic mammalian oscillator. *Nature*, 457(7227):309--12.

Tomita, J., Nakajima, M., Kondo, T., and Iwasaki, H. (2005). No transcription-translation feedback in circadian rhythm of KaiC phosphorylation. *Science (New York, N.Y.)*, 307(5707):251--4.

Tu, B. P. and McKnight, S. L. (2006). Metabolic cycles as an underlying basis of biological oscillations. *Nature reviews. Molecular cell biology*, 7(9):696--701.

Uzumaki, T., Fujita, M., Nakatsu, T., Hayashi, F., Shibata, H., Itoh, N., Kato, H., and Ishiura, M. (2004). Crystal structure of the c-terminal clock-oscillator domain of the cyanobacterial KaiA protein. *Nature structural & molecular biology*, 11(7):623--31.

van der Linden, A. M., Beverly, M., Kadener, S., Rodriguez, J., Wasserman, S., Rosbash, M., and Sengupta, P. (2010). Genome-Wide Analysis of Light- and Temperature-Entrained Circadian Transcripts in Caenorhabditis elegans. *PLoS Biology*, 8(10):e1000503.

van Zon, J. S., Lubensky, D. K., Altena, P. R. H., and ten Wolde, P. R. (2007).

An allosteric model of circadian KaiC phosphorylation. *Proceedings of the National Academy of Sciences*, 104(18):7420--7425.

Wahl, O. (1931). Neue Unteruchungen über das Zeitgedächtnis der Bienen. *Z. f. vergl. Physiologie*, 16(1):529--589.

Xu, Y., Mori, T., and Johnson, C. H. (2000). Circadian clock-protein expression in cyanobacteria: rhythms and phase setting. *EMBO J*, 19(13):3349--3357.

Xu, Y., Mori, T., and Johnson, C. H. (2003). Cyanobacterial circadian clockwork: roles of KaiA, KaiB and the kaiBC promoter in regulating KaiC. *The EMBO journal*, 22(9):2117--26.

Xu, Y., Mori, T., Pattanayek, R., Pattanayek, S., Egli, M., and Johnson, C. H. (2004). Identification of key phosphorylation sites in the circadian clock protein KaiC by crystallographic and mutagenetic analyses. *Proceedings of the National Academy of Sciences of the United States of America*, 101(38):13933--13938.

Ye, S., Vakonakis, I., Ioerger, T. R., LiWang, A. C., and Sacchettini, J. C. (2004). Crystal structure of circadian clock protein KaiA from synechococcus elongatus. *The Journal of biological chemistry*, 279(19):20511--8.

Yoda, M., Eguchi, K., Terada, T. P., and Sasai, M. (2007). Monomer-Shuffling and allosteric transition in KaiC circadian oscillation. *PLoS ONE*, 2:e408.

Yoshida, T., Murayama, Y., Ito, H., Kageyama, H., and Kondo, T. (2009). Nonparametric entrainment of the in vitro circadian phosphorylation rhythm of cyanobacterial KaiC by temperature cycle. *Proceedings of the*

National Academy of Sciences of the United States of America, 106(5):1648--1653.

Zwicker, D., Lubensky, D. K., and ten Wolde, P. R. (2010). Robust circadian clocks from coupled protein-modification and transcription-translation cycles. *Proceedings of the National Academy of Sciences*, pages 1--6.

List of Figures

Acknowledgements

During my PhD studies I enjoyed the support of the Institute for Theoretical Biology (ITB) at the Humboldt Universität zu Berlin.

Foremost, I would like to thank my advisor Markus Kollmann for guiding my research. I am grateful for his scientific support, and for giving me the opportunity to work in his group.

In addition, I would like to thank my research group Kajetan Bentele, Johannes Meisig and Robert Lehmann for critical discussions and their encouragement.

I thank Stefanie Hertel, Ilka Axmann and Rebecca Rose for the kind collaboration.

Selbständigkeitserklärung

Ich erkläre, dass ich die vorliegende Arbeit selbständig und nur unter Verwendung der angegebenen Literatur und Hilfsmittel angefertigt habe.

Berlin, den 23. März 2011 Christian Brettschneider